JOURNAL OF PETROLOGY

Journal of Petrology, 2016, Vol. 57, No. 9, 1775–1810
doi: 10.1093/petrology/egw060
Original Article

OXFORD

TTG and Potassic Granitoids in the Eastern North China Craton: Making Neoarchean Upper Continental Crust during Micro-continental Collision and Post-collisional Extension

Chao Wang[1], Shuguang Song[1]*, Yaoling Niu[2,3], Chunjing Wei[1] and Li Su[4]

[1]MOE Key Laboratory of Orogenic Belts and Crustal Evolution, School of Earth and Space Sciences, Peking University, Beijing 100871, China; [2]Department of Earth Sciences, Durham University, Durham DH1 3LE, UK; [3]Institute of Oceanology, Chinese Academy of Science, Qingdao 266071, China and [4]Institute of Earth Sciences, Chinese University of Geosciences, Beijing 100083, China

*Corresponding author. E-mail: sgsong@pku.edu.cn

Received January 7, 2016; Accepted September 8, 2016

ABSTRACT

As the major component, Archean granitoids provide us with an insight into the formation of the early continental crust. We report the study of a series of Neoarchean granitoids, including tonalite–trondhjemite–granodiorite (TTG) and potassic granitoids, in the Xingcheng region of the eastern North China Craton. Zircon U–Pb dating shows that the TTG granitoids were emplaced in the Neoarchean within a 75 Myr period (2595–2520 Ma), with coeval mafic magmatic enclaves, followed by intrusion of potassic granitoids. The geochemistry of the TTG granitoids is consistent with partial melting of Mesoarchean enriched mafic crustal sources at different depths (up to 10–12 kbar equivalent pressure) during a continental collision event. The potassic granitoids are derived from either low-degree melting of Mesoarchean enriched mafic crustal sources or remelting of Mesoarchean TTGs in response to post-collisional extension, and were hybridized with Neoarchean mantle-derived mafic melts to various degrees. The TTG and potassic granitoids in the Xingcheng region record the evolution from collision of micro-continental blocks to post-collisional extension, consistent with other studies, suggesting that the amalgamation of micro-continental blocks is what gave rise to the cratonization of the North China Craton at the end of the Archean. The rock assemblage of these granitoids resembles those of syn- and post-collisional magmatism in Phanerozoic orogenic belts, and the estimated average composition is similar to that of the present-day upper continental crust, suggesting that a prototype upper continental crust might have been developed at the end of the Archean from a mixture of TTG and potassic granitoids. Together with concurrent high-grade metamorphism in the North China Craton, we conclude that collisional orogenesis is responsible for continental cratonization at the end of the Archean in the North China Craton.

Key words: TTG; potassic granitoids; cratonization; micro-continental collision; prototype upper continental crust; North China Craton

INTRODUCTION

Our knowledge of when and how the mature continental crust may have developed remains incomplete. As the main components of Archean terranes or primary architecture of the continental crust, sodic granitoids of varying composition, collectively called tonalite–trondhjemite–granodiorite (TTG) suites, have been extensively studied with the aim of understanding the

evolution of the Earth and constraining the differentiation processes of the continental crust (Barker 1979; Jahn *et al.*, 1981; Martin, 1999; Smithies, 2000; Condie, 2005*b*, 2014; Martin *et al.*, 2005; Moyen, 2011; Moyen & Martin, 2012). Many studies suggest that TTGs are generated by partial melting of mafic rocks under either amphibolite-facies conditions (less than 15 kbar; e.g. Foley *et al.*, 2002) or eclogite-facies conditions (more than 15–20 kbar; e.g. Rapp *et al.*, 2003). The compositional similarity between the Archean TTGs and Phanerozoic subduction-related adakites (e.g. Defant & Drummond, 1990; Castillo, 2012) has led to the popular acceptance that TTGs may have formed in Archean-type subduction settings (e.g. Condie, 2005*b*; Martin *et al.*, 2005; Niu *et al.*, 2013). Potassic granitoids are also an important crustal component, closely associated with the TTGs, especially in Neoarchean terranes. They have been previously interpreted as products of remelting of pre-existing TTGs (Sylvester, 1994; Moyen *et al.*, 2001, 2003; Bleeker, 2003; Whalen *et al.*, 2004; Watkins *et al.*, 2007), and as a marker for the final consolidation of the cratonic continental crust (Frost *et al.*, 1998; Whalen *et al.*, 2004; Martin *et al.*, 2005). However, the role of potassic granitoids in the growth of the continental crust has been less studied than that of TTGs.

The present-day upper continental crust is relatively rich in K_2O and heavy rare earth elements (HREE) [$K_2O/Na_2O = 0{\cdot}86$, $(La/Yb)_N = 11$; Rudnick & Gao, 2003], significantly different from Archean TTGs [$K_2O/Na_2O = 0{\cdot}35$, $(La/Yb)_N = 32$; Moyen & Martin, 2012]. It is therefore important to explore how the present-day upper continental crust may have evolved from the Archean TTG-dominated upper continental crust over the Earth's history. Condie (1993, 2014) proposed that after the Archean the TTG-dominated upper continental crust was gradually replaced by other calc-alkaline granitoids with geochemical features distinct from those of Archean TTGs, to form the mature, present-day, upper continental crust. As there are coeval calc-alkaline granitoids and TTGs reported from some Archean terranes (e.g. Samsonov *et al.*, 2005) and potassic granitoids are widely distributed in Archean cratons worldwide (Bleeker , 2003; Moyen *et al.*, 2003), there exists the possibility that in some cases the Archean upper continental crust might have already achieved the present-day upper continental crust composition.

The formation and evolution of the North China Craton (NCC) has been the focus of research for decades, with extensive investigations carried out to decipher its Precambrian history (e.g. Zhao *et al.*, 1998, 1999, 2001, 2005; Zhai *et al.*, 2010; Nutman *et al.*, 2011; Zhai & Santosh, 2011; Zhao & Cawood, 2012). The widely distributed Neoarchean to Paleoproterozoic igneous rocks of the NCC offer insights into its Archean to Paleoproterozoic crustal growth and its geodynamic evolution (e.g. Compston *et al.*, 1983; Jahn & Ernst, 1990; Kröner *et al.*, 1998; Yang *et al.*, 2008). However, the geodynamic regime of the NCC during the Neoarchean remains controversial; some researchers have suggested a mantle plume-related setting (e.g. Zhao *et al.*, 2001, 2005; Yang *et al.*, 2008), whereas others have argued for a subduction-related environment (e.g. Liu *et al.*, 2010, 2011; Wan *et al.*, 2010, 2011; Nutman *et al.*, 2011; Wang *et al.*, 2011, 2012, 2013).

We present results of *in situ* zircon U–Pb dating, bulk-rock geochemistry, including Nd isotopes, and *in situ* zircon Hf isotopes for the TTG granitoids and their mafic magmatic enclaves (MMEs) as well as the associated potassic granites in the eastern NCC. We show that these granitoids are products of partial melting of proto-crust during micro-continental collision and post-collisional extension at the end of the Archean. Therefore, a prototype upper continental crust might have been already developed by the end of the Archean in the NCC.

REGIONAL GEOLOGY

The NCC is the largest and oldest craton in China and preserves records of $\geq$3·8 Ga crustal remnants (Liu *et al.*, 1992; Song *et al.*, 1996; Wan *et al.*, 2005). It is suggested to have formed by collision between the Eastern Block and the Western Block along the Trans-North China Orogen (TNCO) at ~1·85 Ga (Fig. 1a; Zhao *et al.*, 2001, 2005; Guo *et al.*, 2002) or at ~1·95 Ga as argued by Qian *et al.* (2013), Zhang *et al.* (2013) and Wei *et al.* (2014). The Eastern Block underwent Paleoproterozoic intra-continental rifting along its eastern continental margin in the period 2·2–1·9 Ga and the rift system was finally terminated by subduction and continental collision at ~1·9 Ga, leading to the formation of the Jiao–Liao–Ji Belt (Fig. 1a; Li & Zhao, 2007; Tam *et al.*, 2011). The Western Block comprises two Archean micro-blocks, the Yinshan Block in the north and the Ordos Block in the south, which were amalgamated along the east–west-trending Khondalite Belt at ~1·95 Ga (Fig. 1a; Santosh *et al.*, 2007*a*, 2007*b*; Zhao *et al.*, 2010).

The exposures of Precambrian basement rocks of the Eastern Block are shown in Fig. 1a, except for a few outcrops in the central part (Western Shandong and Eastern Shandong). These are mainly distributed in the northern part in three major regions: Jidong (Eastern Hebei), Northern Liaoning–Southern Jilin and Western Liaoning. These Archean terranes contains ~3·8 Ga tonalites (Song *et al.*, 1996; Wan *et al.*, 2005) and experienced a complex evolutionary history from 3·8 to 2·5 Ga (Nutman *et al.*, 2011; Zhai & Santosh, 2011).

Our study area is in the northwestern part of the Eastern Block, one of the key regions with well-exposed Precambrian basement rocks of the NCC (Fig. 1a). It mainly consists of the Jidong–Jianping high-grade gneiss terrane, which has varying protoliths and metamorphic ages (2·6–2·5 Ga; Kröner *et al.*, 1998; Zhao *et al.*, 2001, 2005; Nutman *et al.*, 2011), and the Suizhong granitic terrane (e.g. Yang *et al.*, 2008), which includes some low- to medium-grade greenstones in

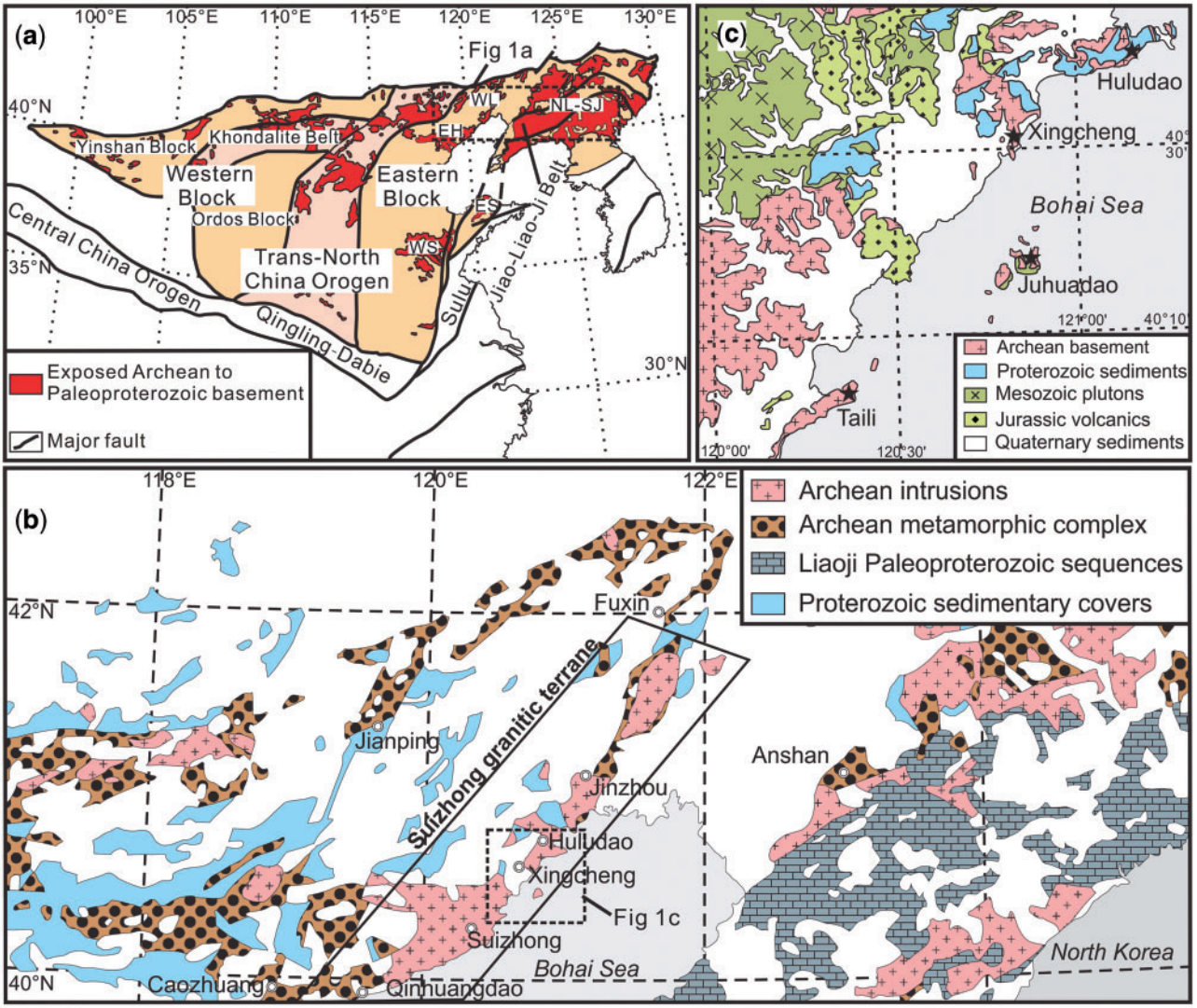

Fig. 1. (a) Schematic map showing major Precambrian tectonic units of the NCC [modified after Zhao *et al.* (2005)]. EH, Eastern Hebei; WL, Western Liaoning; NL-SJ, Northern Liaoning–Southern Jilin; WS, Western Shandong; ES: Eastern Shandong. (b) Simplified geological map of the northern part of the Eastern Block of the NCC. (c) Simplified geological map of the Xingcheng region; black stars indicate sampling locations.

the Fuxin region (Fig. 1b; Liu *et al.*, 2010; Wang *et al.*, 2011, 2012, 2015*b*). These units are partially obscured by Paleoproterozoic to Paleozoic platform strata and Mesozoic volcano-sedimentary sequences, and are intruded by Late Paleozoic to Mesozoic igneous rocks.

The Suizhong granitic terrane, previously termed 'Suizhong granitoids', is dominated by granitoids with the TTG assemblage plus minor monzogranite and potassic granite (Fig. 1b and c). Their precise ages and geochemical characteristics have not been well studied. The Qinhuangdao granitoid in the southern part of the Suizhong granitic terrane has long been treated as part of the Eastern Hebei Archean terrane, which has a rock assemblage of diorite, granodiorite and monzogranite emplaced at 2526–2515 Ma and metamorphosed at 2500–2490 Ma, subsequently intruded by K-feldspar granite (2440 Ma) (Fig. 1b; Yang *et al.*, 2008; Nutman *et al.*, 2011).

FIELD OCCURRENCE AND SAMPLES

The Xingcheng region lies in the central part of the Suizhong granitic terrane. Several outcrops of Neoarchean granitoid are exposed along the west coast of the Bohai Sea (Fig. 1b). Samples were collected from four representative locations: Taili, Xingcheng, Juhuadao and Huludao (Fig. 1c). The lithologies present in these four representative locations include gneissic granite, tonalite, trondhjemite, granodiorite with MMEs, red-colored potassic granite and locally red pegmatite dykes, which encompass almost all the rock types observed within the Suizhong granitic terrane. Owing to the extensive sedimentary cover, the field relationships between most of these lithologies are difficult to determine and map on outcrop scales. Nevertheless, study of samples from these representative outcrops can provide insightful information about the petrogenetic history of the Suizhong granitic terrane.

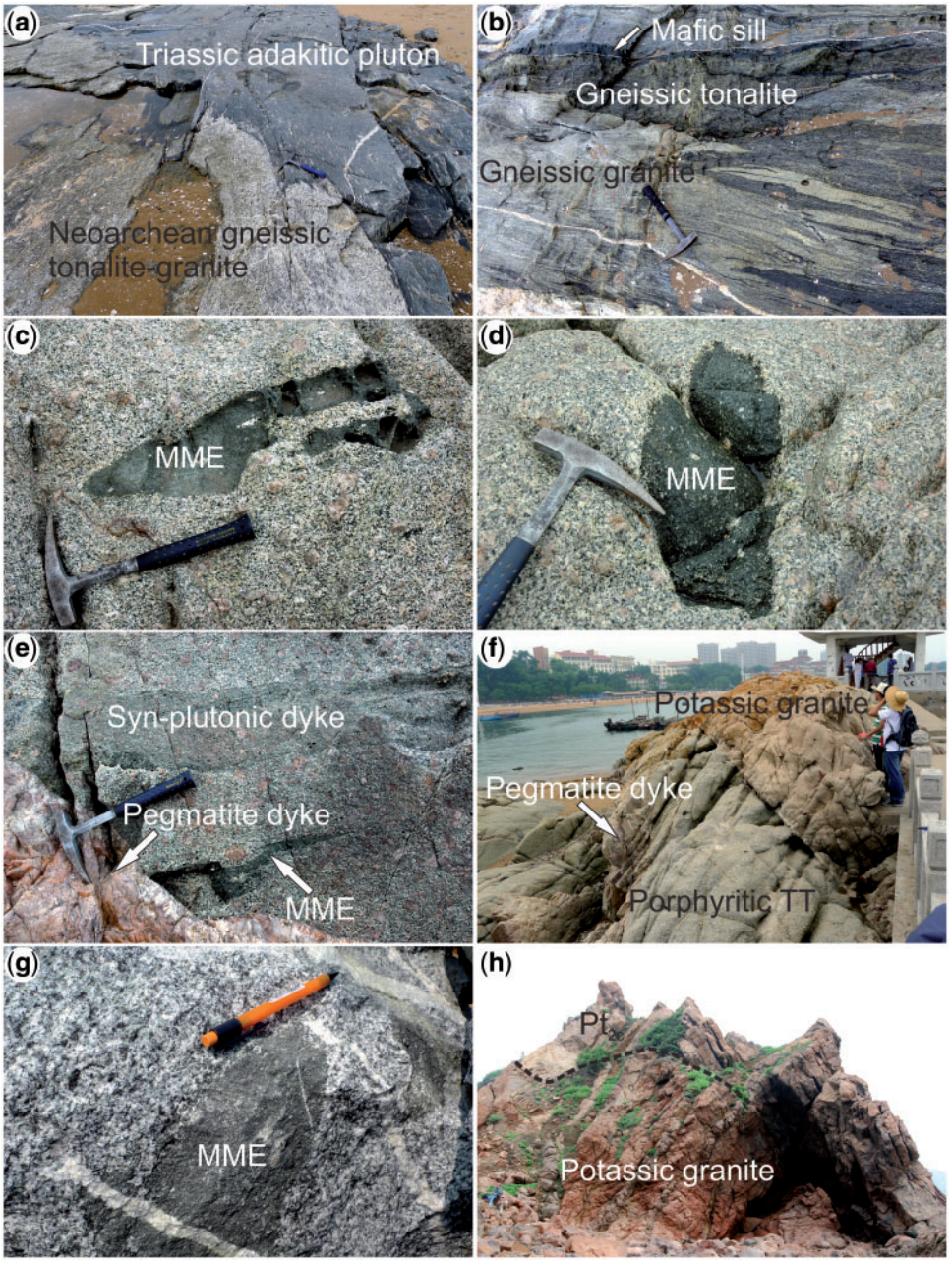

Fig. 2. Field photographs of the Neoarchean TTG and potassic granitoids in the Xingcheng region. (a) Neoarchean gneissic tonalite–granite at Taili intruded by Triassic adakitic pluton; (b) gneissic tonalite and gneissic granite at Taili; mafic sills are also shown; (c, d) tonalite–trondhjemite with MMEs at Xingcheng; (e) tonalite–trondhjemite, MMEs and syn-plutonic dyke at Xingcheng, intruded by pegmatite dyke; (f) tonalite–trondhjemites at Xingcheng intruded by potassic granite; both are intruded by a pegmatite dyke; (g) granodiorite and MMEs at Juhuadao; (h) potassic granite at Huludao, unconformably overlain by the Paleoproterozoic sedimentary rocks of the Changcheng formation (Pt_{2c}).

Taili gneissic tonalite–granites

All the Archean granitoids from Taili are strongly deformed with an east–west foliation. They are intruded by 230–220 Ma adakitic plutons (Wang *et al.*, 2015*a*), 155 Ma undeformed granites (our unpublished data) and as yet undated mafic dykes (Fig. 2a). The adakitic plutons show the same deformation character as the gneisses that they intrude (Fig. 2a), indicating that the Taili Archean granitoids experienced their latest deformation between 220 and 155 Ma.

Two Archean rock types have been identified in Taili, gneissic tonalite and porphyritic gneissic granite, which are interleaved with each other (Fig. 2b). The gneissic tonalites are dark grey, homogeneous and medium- to fine-grained without porphyroblasts. They have a mineral assemblage of plagioclase (50–60%), K-feldspar (10–20%), quartz (10–20%), amphibole (~5%), minor biotite and accessory zircon, magnetite and titanite. The porphyritic gneissic granites are pale grey, medium- to coarse-grained with feldspar phenocrysts in a matrix of

K-feldspar (40–50%), plagioclase (20–30%), quartz (20–30%), amphibole (~5%), minor biotite and accessory zircon, magnetite and titanite. Strongly deformed mafic dyke (sills) are present (Fig. 2b), but difficult to sample.

Xingcheng porphyritic tonalite–trondhjemites and potassic granites

The tonalite–trondhjemites from Xingcheng are grey, medium- to coarse-grained with plagioclase phenocrysts and contain some MMEs and syn-plutonic dykes. They have a porphyritic texture and consist of quartz, plagioclase, K-feldspar, minor hornblende and accessory zircon, magnetite and titanite (Fig. 2c–f). The MMEs are dark grey to black and irregular in shape, ranging in size from several to tens of centimeters, with relatively clear boundaries but no chilled margins (Fig. 2c–e). They have a fine- to medium-grained texture with plagioclase phenocrysts; their matrix consists of hornblende, plagioclase, minor biotite and accessory zircon, magnetite and titanite. The syn-plutonic dykes are darker in color than, and display clear boundaries with, their host; together with irregularly layered MMEs, this may suggest a cumulate origin (Fig. 2e). The tonalite–trondhjemites were intruded by later potassic granites with sharp intrusive contacts (Fig. 2f). The potassic granites are pinkish red, medium- to coarse-grained and are composed of quartz, K-feldspar, minor biotite and accessory zircon, magnetite and titanite. Both the tonalite–trondhjemites and the potassic granites are intruded by parallel, red-colored pegmatite dykes (Fig. 2e and f).

Juhuadao granodiorites

The granodiorites from Juhuadao are pale grey in color with a medium to coarse grain size and also contain MMEs. They are intruded by Mesozoic plutons (Fig. 1c). The granodiorites have the mineral assemblage quartz, plagioclase, hornblende, minor K-feldspar and accessory zircon, magnetite and titanite. The MMEs are fine- to medium-grained with the mineral assemblage hornblende, plagioclase, minor biotite and accessory zircon, magnetite and titanite, showing clear contacts with the host granodiorites (Fig. 2g).

Huludao potassic granites

The potassic granites from Huludao have a pinkish red color, fine- to medium-grained texture and are dominated by quartz, K-feldspar, minor biotite and accessory zircon, magnetite and titanite. They are unconformably overlain by Paleoproterozoic sedimentary rocks of the Changcheng formation (Pt_{2c}) (Figs 1c and 2h).

ANALYTICAL TECHNIQUES

In situ zircon U–Pb dating

Zircon grains were extracted from crushed samples by standard heavy liquid and magnetic techniques, and subsequently purified by hand-picking under a binocular microscope. The selected grains were embedded in epoxy resin discs and polished down to about half-sections to expose the grain interiors. Cathodoluminescence (CL) images were acquired using a Garton Mono CL3+ spectrometer installed on a Quanta 200F ESEM at Peking University; scanning conditions were 15 kV and 120 nA.

Measurements of U, Th and Pb in zircons were carried out by laser ablation inductively coupled plasma mass spectrometry (LA-ICP-MS) on an Agilent-7500a quadrupole ICP-MS system coupled with a New Wave UP-193 solid-state LA system in the Geological Lab Center, China University of Geosciences, Beijing (CUGB) following the analytical procedures of Song *et al.* (2010*a*). A laser spot size of 36 μm, laser energy density of 8·5 J cm^{-2} and a repetition rate of 10 Hz were used for analysis. The ablated sample material was carried into the ICP-MS system by high-purity helium gas. NIST 610 glass and Harvard standard zircon 91500 (Wiedenbeck *et al.*, 1995) were used as external standards, Si as the internal standard and the standard zircon TEMORA (417 Ma) from Australia (Black *et al.*, 2003) as a secondary standard. The software GLITTER (version 4.4, Macquarie University) was used for data reduction. The common lead correction was made following Andersen (2002). Age calculations and concordia diagrams were made using Isoplot (version 3.0) (Ludwig, 2003).

Bulk-rock major and trace element analyses

All the samples are fresh cuttings sampled away from late veinlets, with any surface contaminants trimmed off before being thoroughly cleaned. Fresh portions of the trimmed samples were crushed to 1–2 cm size chips using a percussion mill. These rock fragments were then ultrasonically cleaned in Milli-Q water, dried and powdered in a thoroughly cleaned agate mill to 200 mesh in the clean laboratory at the Langfang Regional Geological Survey, China.

Bulk-rock major and trace element analysis was carried out at CUGB, following Song *et al.* (2010*b*). Major elements were analyzed on a Leeman Prodigy inductively coupled plasma-optical emission spectroscopy (ICP-OES) system with high-dispersion Echelle optics. Based on USGS (US Geological Survey) rock standards AGV-2 and W-2, and CNGR (Chinese National Geological Reference) materials GSR-1 and GSR-3, the analytical precision (1σ) for most major element oxides is better than 1%, with the exception of TiO_2 (~1·5%) and P_2O_5 (~2·0%). Loss on ignition (LOI) was determined by placing 1 g of sample in a furnace at 1000°C for a few hours and then reweighing the cooled samples.

Bulk-rock trace elements were analyzed by ICP-MS using an Agilent-7500a quadrupole ICP-MS system. About 35 mg powder of each sample was dissolved in a distilled acid mixture (1:1 HF + HNO_3) in Teflon digesting vessels and heated on a hot plate at 195°C for 48 h

using high-pressure bombs for digestion. The sample was then evaporated to incipient dryness, refluxed with 1 ml of 6N HNO_3 and heated again to incipient dryness. The sample was again dissolved in 2 ml of 3N HNO_3 and heated at 165°C for further 24 h to guarantee complete digestion–dissolution. The sample was finally diluted with Milli-Q water to a dilution factor of 2000 in 2% HNO_3 solution for analysis. Rock standards USGS AGV-2, W-2 and BHVO-2 were used to monitor the analytical accuracy and precision. Analytical accuracy is indicated by a relative difference between measured and recommended values better than 5% for most elements, and 10–15% for Cu, Zn, Gd, and Ta.

Bulk-rock Nd isotope analyses

Separation and purification of Nd were carried out using conventional two-column ion exchange procedures in the ultraclean laboratory of the MOE Key Laboratory at Peking University. Approximately 250 mg powder of each sample was dissolved with a distilled acid mixture ($HF + HClO_4$) in a sealed Savillex beaker on a hot plate for 168 h. The ion exchange procedures include: (1) group separation of light rare earth elements (LREE) through a cation-exchange column ($1 \times 7{\cdot}5$ cm^2, packed with 200 mesh AG50W resin); (2) purification of Nd through a second cation-exchange column ($0{\cdot}5 \times 5{\cdot}5$ cm^2, packed with 200 mesh P507 resin), conditioned and cleaned with dilute HCl. Nd isotopic ratios were measured by thermal ionization mass spectrometry (TIMS) using a Thermo-Finnigan Triton system at the Isotope Laboratory of the Tianjin Institute of Geology and Mineral Resources. The $^{147}Sm/^{144}Nd$ ratios were calculated using ICP-MS analyzed Sm and Nd concentrations. Mass fractionation was corrected for by normalizing the measured $^{143}Nd/^{144}Nd$ against a $^{146}Nd/^{144}Nd$ ratio of 0·7219. Rock standard USGS BCR-2 was used to evaluate the separation and purification process of Nd, which yielded a weighted mean $^{143}Nd/^{144}Nd$ ratio of $0{\cdot}512632 \pm 4$ (2σ, $n = 100$). To monitor the data quality during the period of data acquisition, the LRIG Nd standard was analyzed and gave a weighted mean $^{143}Nd/^{144}Nd$ ratio of $0{\cdot}512206 \pm 6$ (2σ, $n = 100$).

In situ zircon Hf isotope analyses

In situ zircon Lu–Hf isotope analysis of dated samples from the Xingcheng region was carried out using a Neptune multi-collector ICP-MS system with an attached New Wave UP-213 LA system (LA-MC-ICP-MS) at the MLR Key Laboratory of Metallogeny and Mineral Assessment, Institute of Mineral Resources, Chinese Academy of Geological Sciences, Beijing. Analytical details have been given by Wu *et al.* (2006) and Hou *et al.* (2007). A laser spot size of 40 μm was used for analysis and helium gas was used as the carrier gas to transport the laser ablated sample from the LA cell to the ICP-MS torch via a mixing chamber where it was mixed with argon gas. Correction for the isobaric interferences of ^{176}Lu and ^{176}Yb on ^{176}Hf was after Wu *et al.* (2006) and Hou *et al.* (2007). Before the analysis, standard zircons (TEMORA, GJ1 and FM02) were analyzed and the efficacy of the correction method of isobaric interferences of Wu *et al.* (2006) and Hou *et al.* (2007) was shown to be efficient. Zircon GJ1 was used as the reference standard to monitor data quality during analysis, giving a weighted mean $^{176}Hf/^{177}Hf$ ratio of $0{\cdot}282007 \pm 7$ (2σ, $n = 36$), which is in accordance with the weighted mean $^{176}Hf/^{177}Hf$ ratio of $0{\cdot}282000 \pm 5$ (2σ) measured by the solution analysis method (Morel *et al.*, 2008).

RESULTS

Geochronology

Eight samples were selected for zircon U–Pb analysis, including gneissic granite (10TL13), tonalite–trondhjemite (10XC02), granodiorite (12XC22 and 12XC28), MMEs (11XC03 and 12XC15) and potassic granite (10XC05 and 10XC08) from the four outcrops in the Xingcheng region: Taili, Xingcheng, Juhuadao and Huludao (see Fig. 1c for sampling locations). CL images of representative zircons are shown in Fig. 3 and the *in situ* LA-ICP-MS U–Pb data are given in Table 1 and plotted in Fig. 4.

Zircon grains from all the eight dated samples are euhedral–prismatic, and have varying sizes (50–250 μm) with a length:width of 2:1–5:1. They show typical oscillatory growth zoning of magmatic origin in CL images (Fig. 3), suggesting that these zircons from the granitoids and their MMEs were crystallized from magmas parental to the host-rocks. Most of the zircon grains have Th/U ratios varying from 0·3 to 1·8; some are less than 0·3 possibly as a result of late-stage alteration.

Taili gneissic tonalite–granite

Sample 10TL13 is a gneissic granite from Taili (Figs 1 and 2a, b). U–Pb analysis for 25 zircon grains yielded $^{207}Pb/^{206}Pb$ ages ranging from 2581 ± 21 to 2525 ± 21 Ma (1σ), apart from two strongly discordant ages, which may be due to lead loss (2285 ± 47 and 2463 ± 47 Ma) (Table 1). The data form a discordant line with an upper intercept age of 2558 ± 16 Ma (MSWD = 0·50) (Fig. 4a). Nineteen analyses on or close to the concordia give a weighted mean $^{207}Pb/^{206}Pb$ age of 2551 ± 9 Ma (MSWD = 0·53), which is in accordance with the upper intercept age. Therefore, the Taili gneissic granites were emplaced at ~2558 Ma.

Xingcheng tonalite–trondhjemites and MMEs

Sample 10XC02 is a tonalite from Xingcheng (Figs 1 and 2c–f). Twenty-five zircon grains were analyzed and give a wide $^{207}Pb/^{206}Pb$ age range of 2578 ± 22 to 2388 ± 23 Ma (1σ) (Table 1). They fall on a discordant line with an upper intercept with the concordia at 2559 ± 23 Ma (MSWD = 0·88) (Fig. 4b). Seven near-concordant analyses of zircon grains give a weighted mean

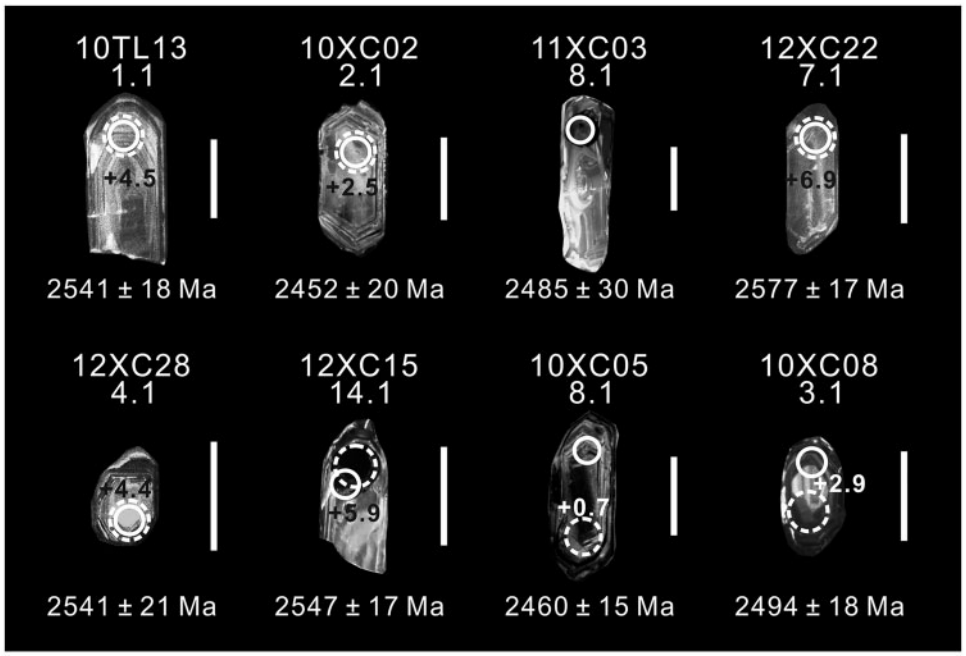

Fig. 3. Cathodoluminescence (CL) images of representative zircons from the Neoarchean TTG and potassic granitoids in the Xingcheng region. The continuous-line and dashed-line circles on the CL images are the spots of *in situ* zircon U–Pb dating and Hf isotope analyses, respectively. Also shown are the $^{207}Pb/^{206}Pb$ ages and $\varepsilon_{Hf}(t)$ values of the zircons. The scale bar represents 100 μm.

$^{207}Pb/^{206}Pb$ age of 2548 ± 17 Ma (MSWD = 1·05), agreeing well with the upper intercept age. Thus, the Xingcheng tonalite–trondhjemites crystallized at ~2559 Ma.

Sample 11XC03 is an MME hosted in the Xingcheng tonalite–trondhjemites (Fig. 2c–e). Ten zircon grains were analyzed and give a $^{207}Pb/^{206}Pb$ age range of 2487 ± 27 to 2236 ± 26 Ma (1σ) (Table 1). They are extremely discordant owing to lead loss and lie along a discordant line under the concordia with a projected upper intercept age of 2546 ± 55 Ma (MSWD = 0·61) (Fig. 4c). Thus, the crystallization age of the MMEs in Xingcheng is ~2546 Ma and coeval with the host tonalite–trondhjemites within error.

Juhuadao granodiorites and MMEs

Sample 12XC22 is a granodiorite from Juhuadao (Figs 1 and 2g). Thirty zircon grains were analyzed and give a wide $^{207}Pb/^{206}Pb$ age range of 2660 ± 17 to 2145 ± 18 Ma (1σ) owing to lead loss (Table 1). They define a discordant line and intercept the concordia at 2595 ± 14 Ma (MSWD = 1·20), which is in accordance with the weighted mean $^{207}Pb/^{206}Pb$ age of nine analyses indistinguishable from concordia (2587 ± 11 Ma; MSWD = 0·86) (Fig. 4d). Another granodiorite sample 12XC28 was also selected for dating. Thirty zircon grains were analyzed, which give a wide $^{207}Pb/^{206}Pb$ age range of 2582 ± 24 to 1822 ± 58 Ma (1σ) resulting from lead loss (Table 1). They are strongly discordant and form a discordant line intercepting the concordia at 2573 ± 28 Ma (MSWD = 2·90) (Fig. 4e). Therefore, the timing of emplacement of the Juhuadao granodiorites is between 2595 and 2574 Ma.

Sample 12XC15 is an MME hosted in the Juhuadao granodiorites (Fig. 2g). Twenty-four zircon grains were analyzed and gave a wide $^{207}Pb/^{206}Pb$ age range of 2583 ± 26 to 1626 ± 95 Ma (1σ), showing the effects of lead loss (Table 1). They fall on a discordant line with an upper intercept age of 2568 ± 13 Ma (MSWD = 2·80) (Fig. 4f). Thus, the MMEs crystallized at ~2568 Ma, coeval with the host granodiorite within error.

Xingcheng and Huludao potassic granites

Sample 10XC05 is a potassic granite intruding the Xingcheng tonalite–trondhjemites (Figs 1 and 2f). Fifteen zircon grains were analyzed, giving a $^{207}Pb/^{206}Pb$ age range of 2573 ± 16 to 2327 ± 15 Ma (1σ), in addition to two strongly discordant ages owing to lead loss (1985 ± 51 and 2021 ± 15 Ma) (Table 1). They define a discordant line intercepting the concordia at 2545 ± 20 Ma (MSWD = 0·98) (Fig. 4g), in accordance with the weighted mean $^{207}Pb/^{206}Pb$ age of eight analyses (2531 ± 23 Ma; MSWD = 2·7) near or close to the concordia. Therefore, the crystallization age of the Xingcheng potassic granites is ~2545 Ma, slightly younger than that of the intruded tonalite–trondhjemites; this is consistent with field observations of their relative ages (Fig. 2f).

Sample 10XC08 is a potassic granite from Huludao (Figs 1 and 2h). Nineteen zircon grains were analyzed giving a $^{207}Pb/^{206}Pb$ age range of 2544 ± 41 to 2334 ± 19 Ma (1σ) (Table 1). They are also strongly discordant

Table 1: In situ *LA-ICP-MS zircon U–Pb data for the Neoarchean TTG and potassic granitoids in the Xingcheng region*

Spot	Concentrations (ppm)			Th/U	Isotopic ratios						Isotopic ages (Ma)					
	Pb	U	Th		$^{207}Pb/^{206}Pb$*	±1σ	$^{207}Pb/^{235}U$	±1σ	$^{206}Pb/^{238}U$	±1σ	$^{207}Pb/^{206}Pb$	±1σ	$^{207}Pb/^{235}U$	±1σ	$^{206}Pb/^{238}U$	±1σ
10TL13																
1.1	99	177	107	0·61	0·16836	0·00343	10·52913	0·21126	0·45337	0·00541	2541	18	2482	19	2410	24
2.1	114	179	194	1·08	0·16833	0·00344	10·89588	0·21918	0·46925	0·00560	2541	18	2514	19	2480	25
3.1	96	207	113	0·55	0·16066	0·00437	8·29389	0·20021	0·37441	0·00469	2463	47	2264	22	2050	22
4.1	89	146	114	0·78	0·16696	0·00349	11·04128	0·22674	0·47943	0·00578	2527	19	2527	19	2525	25
5.1	130	226	190	0·84	0·16832	0·00344	10·31485	0·20728	0·44427	0·00527	2541	18	2463	19	2370	24
6.1	132	224	152	0·68	0·16840	0·00348	10·83504	0·21987	0·46645	0·00555	2542	19	2509	19	2468	24
7.1	214	411	250	0·61	0·16693	0·00342	9·65213	0·19466	0·41919	0·00496	2527	19	2402	19	2257	23
8.1	97	160	124	0·77	0·16988	0·00357	11·03919	0·22775	0·47111	0·00565	2556	19	2526	19	2488	25
9.1	68	110	92	0·83	0·16851	0·00361	11·10818	0·23368	0·47793	0·00580	2543	20	2532	20	2518	25
10.1	80	133	87	0·65	0·16884	0·00360	11·08213	0·23205	0·47588	0·00575	2546	19	2530	20	2509	25
11.1	74	120	111	0·92	0·16989	0·00370	10·79382	0·23040	0·46064	0·00561	2557	20	2506	20	2442	25
12.1	89	138	135	0·98	0·17010	0·00368	11·27141	0·23877	0·48044	0·00581	2559	20	2546	20	2529	25
13.1	78	129	101	0·78	0·17160	0·00373	11·05388	0·23550	0·46705	0·00566	2573	20	2528	20	2471	25
14.1	93	164	121	0·74	0·17020	0·00369	10·37456	0·22019	0·44196	0·00533	2560	20	2469	20	2359	24
15.1	225	1148	445	0·39	0·14477	0·00390	3·23391	0·07766	0·16201	0·00197	2285	47	1465	19	968	11
16.1	59	95	79	0·83	0·16799	0·00378	11·08530	0·24351	0·47846	0·00589	2538	21	2530	20	2521	26
17.1	131	224	164	0·73	0·17127	0·00373	10·88441	0·23169	0·46080	0·00553	2570	20	2513	20	2443	24
18.1	97	163	142	0·87	0·16905	0·00374	10·61618	0·22949	0·45536	0·00552	2548	20	2490	20	2419	24
19.1	68	117	92	0·78	0·17235	0·00390	10·66542	0·23563	0·44871	0·00552	2581	21	2494	21	2390	25
20.1	73	120	89	0·74	0·16772	0·00379	11·00906	0·24262	0·47595	0·00583	2535	21	2524	21	2510	25
21.1	97	163	110	0·68	0·17129	0·00384	11·13181	0·24374	0·47125	0·00571	2570	21	2534	20	2489	25
22.1	181	476	189	0·40	0·16901	0·00377	7·41609	0·16140	0·31819	0·00383	2548	21	2163	19	1781	19
23.1	170	339	227	0·67	0·16856	0·00381	9·29889	0·20505	0·40006	0·00485	2543	21	2368	20	2169	22
24.1	191	333	194	0·58	0·16937	0·00380	10·96702	0·24015	0·46957	0·00566	2551	21	2520	20	2482	25
25.1	107	257	237	0·93	0·16670	0·00382	7·38636	0·16455	0·32131	0·00391	2525	21	2159	20	1796	19
10XC02																
1.1	216	513	349	0·68	0·16152	0·00343	7·66776	0·16588	0·34424	0·00439	2472	20	2193	19	1907	21
2.1	232	621	547	0·88	0·15966	0·00340	6·60013	0·14342	0·29976	0·00382	2452	20	2059	19	1690	19
3.1	187	409	270	0·66	0·16568	0·00354	8·58031	0·18705	0·37552	0·00479	2514	20	2294	20	2055	22
4.1	188	418	280	0·67	0·16672	0·00358	8·40999	0·18412	0·36579	0·00467	2525	20	2276	20	2010	22
5.1	135	376	276	0·74	0·15971	0·00347	6·51651	0·14394	0·29587	0·00379	2453	21	2048	19	1671	19
6.1	215	558	367	0·66	0·15649	0·00473	6·72745	0·18198	0·31179	0·00421	2418	53	2076	24	1750	21
7.1	191	462	339	0·74	0·16239	0·00356	7·61619	0·16948	0·34008	0·00436	2481	21	2187	20	1887	21
8.1	88	147	171	1·16	0·16580	0·00372	10·47853	0·23825	0·45828	0·00595	2516	21	2478	21	2432	26
9.1	109	222	202	0·91	0·16783	0·00374	8·70800	0·19705	0·37623	0·00486	2536	21	2308	21	2059	23
10.1	195	477	390	0·82	0·16619	0·00368	7·52882	0·16913	0·32850	0·00422	2520	21	2176	20	1831	20
11.1	102	169	151	0·89	0·17213	0·00393	11·35416	0·26233	0·47830	0·00625	2578	22	2553	22	2520	27
12.1	92	152	229	1·50	0·16893	0·00386	10·48996	0·24256	0·45028	0·00587	2547	22	2479	21	2396	26
13.1	157	379	249	0·66	0·16705	0·00377	7·83094	0·17913	0·33993	0·00439	2528	22	2212	21	1886	21
14.1	170	529	432	0·82	0·15875	0·00360	5·80663	0·13317	0·26522	0·00342	2442	22	1947	20	1516	17
15.1	162	356	453	1·27	0·17124	0·00389	8·03153	0·18475	0·34010	0·00440	2570	22	2235	21	1887	21
16.1	46	78	55	0·70	0·16661	0·00394	10·98751	0·26222	0·47820	0·00632	2524	23	2522	22	2519	28
17.1	223	449	554	1·23	0·17132	0·00395	9·18680	0·21420	0·38884	0·00505	2571	22	2357	21	2117	23
18.1	183	373	248	0·66	0·16754	0·00386	9·25327	0·21551	0·40048	0·00518	2533	22	2363	21	2171	24
19.1	251	668	612	0·92	0·15520	0·00359	6·28863	0·14687	0·29382	0·00380	2404	23	2017	20	1661	19
20.1	202	484	360	0·74	0·16186	0·00375	7·53594	0·17654	0·33761	0·00437	2475	23	2177	21	1875	21
21.1	108	209	124	0·59	0·16208	0·00502	9·35390	0·26030	0·41855	0·00572	2478	54	2373	26	2254	26
22.1	49	82	58	0·70	0·17140	0·00415	11·42870	0·27872	0·48349	0·00642	2571	23	2559	23	2542	28
23.1	74	123	99	0·80	0·16915	0·00406	11·09244	0·26829	0·47552	0·00626	2549	23	2531	23	2508	27
24.1	207	718	1067	1·49	0·15375	0·00365	4·75209	0·11375	0·22412	0·00292	2388	23	1776	20	1304	15
25.1	90	171	80	0·47	0·16934	0·00408	10·49423	0·25435	0·44935	0·00591	2551	23	2479	22	2392	26
11XC03																
1.1	159	467	319	0·68	0·15943	0·00387	6·53596	0·16490	0·29730	0·00401	2450	25	2051	22	1678	20
2.1	179	624	638	1·02	0·14072	0·00344	4·44205	0·11277	0·22891	0·00309	2236	26	1720	21	1329	16
3.1	269	656	538	0·82	0·15778	0·00390	7·28731	0·18710	0·33494	0·00453	2432	26	2147	23	1862	22
4.1	220	501	545	1·09	0·16152	0·00404	7·87504	0·20438	0·35358	0·00479	2472	26	2217	23	1952	23
5.1	204	641	571	0·89	0·14793	0·00374	5·28056	0·13827	0·25887	0·00352	2322	27	1866	22	1484	18
6.1	200	440	292	0·66	0·16300	0·00421	8·34632	0·22332	0·37132	0·00507	2487	27	2269	24	2036	24
7.1	239	558	236	0·42	0·15907	0·00425	8·10277	0·22405	0·36940	0·00507	2446	28	2243	25	2027	24
8.1	226	439	281	0·64	0·16278	0·00450	9·62657	0·27455	0·42886	0·00595	2485	30	2400	26	2301	27
9.1	235	635	841	1·32	0·15695	0·00433	6·32256	0·18013	0·29214	0·00404	2423	30	2022	25	1652	20
10.1	232	580	523	0·90	0·15582	0·00432	6·95868	0·19924	0·32387	0·00448	2411	30	2106	25	1809	22
12XC22																
1.1	134	479	175	0·37	0·16121	0·00436	5·44924	0·12452	0·24516	0·00355	2468	47	1893	20	1413	18
2.1	129	216	141	0·65	0·17516	0·00334	12·01575	0·24544	0·49750	0·00716	2608	17	2606	19	2603	31
3.1	126	283	166	0·59	0·15599	0·00605	6·71794	0·23728	0·31236	0·00502	2413	67	2075	31	1752	25
4.1	104	228	86	0·38	0·16640	0·00461	8·96332	0·21062	0·39067	0·00575	2522	48	2334	21	2126	27
5.1	106	249	116	0·47	0·16698	0·00482	8·19624	0·20223	0·35600	0·00531	2528	50	2253	22	1963	25
6.1	147	240	195	0·81	0·17383	0·00334	11·86304	0·24359	0·49493	0·00714	2595	17	2594	19	2592	31
7.1	72	126	59	0·47	0·17199	0·00338	11·66775	0·24360	0·49197	0·00719	2577	17	2578	20	2579	31
8.1	176	383	169	0·44	0·17227	0·00323	9·45201	0·19081	0·39790	0·00566	2580	16	2383	19	2159	26
9.1	155	383	211	0·55	0·17360	0·00328	8·19718	0·16635	0·34244	0·00489	2593	17	2253	18	1898	23
10.1	162	485	460	0·95	0·17407	0·00330	6·70082	0·13612	0·27916	0·00398	2597	17	2073	18	1587	20
11.1	175	425	228	0·54	0·16626	0·00321	8·05266	0·16577	0·35126	0·00506	2520	17	2237	19	1941	24
12.1	172	730	408	0·56	0·15666	0·00297	4·33220	0·08813	0·20054	0·00285	2420	17	1700	17	1178	15
13.1	138	251	146	0·58	0·17382	0·00335	11·12443	0·22895	0·46413	0·00669	2595	17	2534	19	2458	29
14.1	150	361	184	0·51	0·16889	0·00321	8·26141	0·16827	0·35473	0·00506	2547	17	2260	18	1957	24
15.1	161	518	246	0·47	0·15947	0·00304	5·89199	0·12031	0·26795	0·00382	2450	17	1960	18	1530	19
16.1	176	541	297	0·55	0·16291	0·00311	6·25067	0·12759	0·27825	0·00396	2486	17	2012	18	1583	20
17.1	131	296	168	0·57	0·17420	0·00337	8·99370	0·18537	0·37441	0·00538	2598	17	2337	19	2050	25
18.1	138	382	228	0·60	0·16983	0·00328	7·13564	0·14716	0·30470	0·00437	2556	17	2129	18	1715	22

(continued)

Table 1: Continued

Spot	Concentrations (ppm)			Th/U	Isotopic ratios						Isotopic ages (Ma)					
	Pb	U	Th		$^{207}Pb/^{206}Pb^*$	±1σ	$^{207}Pb/^{235}U$	±1σ	$^{206}Pb/^{238}U$	±1σ	$^{207}Pb/^{206}Pb$	±1σ	$^{207}Pb/^{235}U$	±1σ	$^{206}Pb/^{238}U$	±1σ
19.1	128	200	86	0·43	0·17159	0·00345	11·56417	0·24587	0·48874	0·00720	2573	18	2570	20	2565	31
20.1	113	195	101	0·52	0·17290	0·00343	11·73715	0·24693	0·49230	0·00719	2586	17	2584	20	2581	31
21.1	144	274	79	0·29	0·18079	0·00359	11·66874	0·24544	0·46806	0·00682	2660	17	2578	20	2475	30
22.1	134	280	196	0·70	0·16735	0·00328	9·48389	0·19790	0·41098	0·00592	2531	17	2386	19	2219	27
23.1	217	1604	1379	0·86	0·13350	0·00260	2·07408	0·04300	0·11267	0·00161	2145	18	1140	14	688	9
24.1	177	410	263	0·64	0·17172	0·00336	8·49988	0·17671	0·35895	0·00515	2574	17	2286	19	1977	24
25.1	97	167	87	0·52	0·17254	0·00360	11·74836	0·25692	0·49377	0·00740	2582	18	2585	20	2587	32
26.1	156	238	288	1·21	0·17530	0·00352	12·06470	0·25644	0·49911	0·00730	2609	18	2609	20	2610	31
27.1	169	506	325	0·64	0·16234	0·00320	6·29619	0·13164	0·28125	0·00404	2480	18	2018	18	1598	20
28.1	133	237	239	1·01	0·17232	0·00343	10·45083	0·22031	0·43982	0·00636	2580	17	2476	20	2350	28
29.1	115	203	108	0·53	0·17009	0·00350	11·41264	0·24684	0·48658	0·00718	2559	18	2557	20	2556	31
30.1	97	164	97	0·59	0·17389	0·00355	11·89487	0·25567	0·49605	0·00728	2595	18	2596	20	2597	31
12XC28																
1.1	152	702	177	0·25	0·15749	0·00354	4·25413	0·09912	0·19587	0·00289	2429	21	1685	19	1153	16
2.1	139	664	77	0·12	0·15763	0·00436	4·19575	0·09872	0·19304	0·00282	2430	48	1673	19	1138	15
3.1	165	980	164	0·17	0·14414	0·00412	3·06494	0·07522	0·15422	0·00226	2277	50	1424	19	925	13
4.1	109	209	140	0·67	0·16829	0·00388	10·04039	0·23893	0·43263	0·00648	2541	21	2439	22	2318	29
5.1	148	850	95	0·11	0·14002	0·00428	2·98320	0·07960	0·15453	0·00230	2227	54	1403	20	926	13
6.1	141	786	108	0·14	0·14569	0·00418	3·30925	0·08147	0·16474	0·00243	2296	50	1483	19	983	13
7.1	201	691	424	0·61	0·15780	0·00537	5·18964	0·15676	0·23852	0·00374	2432	59	1851	26	1379	19
8.1	154	655	174	0·27	0·14801	0·00449	4·26626	0·11223	0·20906	0·00316	2323	53	1687	22	1224	17
9.1	175	726	407	0·56	0·14500	0·00526	3·88751	0·12692	0·19444	0·00307	2288	64	1611	26	1145	17
10.1	160	729	94	0·13	0·15079	0·00445	4·09197	0·10423	0·19682	0·00293	2355	52	1653	21	1158	16
11.1	163	506	377	0·74	0·15900	0·00377	5·72963	0·13937	0·26129	0·00392	2445	22	1936	21	1496	20
12.1	187	383	531	1·39	0·16842	0·00398	8·31480	0·20211	0·35799	0·00536	2542	22	2266	22	1973	25
13.1	186	767	218	0·28	0·14456	0·00455	4·22683	0·11665	0·21206	0·00320	2283	55	1679	23	1240	17
14.1	126	755	129	0·17	0·14210	0·00436	2·91957	0·07816	0·14902	0·00224	2253	54	1387	20	895	13
15.1	199	1526	171	0·11	0·11135	0·00350	1·83570	0·05079	0·11957	0·00177	1822	58	1058	18	728	10
16.1	201	1143	261	0·23	0·12939	0·00427	2·74263	0·08033	0·15373	0·00234	2090	59	1340	22	922	13
17.1	232	811	207	0·25	0·16375	0·00394	5·82444	0·14367	0·25791	0·00386	2495	22	1950	21	1479	20
18.1	163	685	184	0·27	0·15379	0·00481	4·41219	0·12072	0·20808	0·00316	2389	55	1715	23	1219	17
19.1	186	710	371	0·52	0·14720	0·00529	4·34966	0·14051	0·21430	0·00338	2314	63	1703	27	1252	18
20.1	135	938	135	0·14	0·13386	0·00426	2·37363	0·06652	0·12861	0·00195	2149	57	1235	20	780	11
21.1	157	707	162	0·23	0·14381	0·00461	3·88840	0·10962	0·19610	0·00298	2274	56	1611	23	1154	16
22.1	95	157	119	0·76	0·17235	0·00455	11·61222	0·31000	0·48852	0·00787	2581	24	2574	25	2564	34
23.1	203	558	315	0·56	0·15949	0·00397	7·05721	0·17930	0·32084	0·00486	2450	23	2119	23	1794	24
24.1	266	761	430	0·57	0·14892	0·00553	5·79619	0·19417	0·28228	0·00450	2334	65	1946	29	1603	23
25.1	135	814	256	0·31	0·13665	0·00466	2·71613	0·08233	0·14416	0·00224	2185	61	1333	22	868	13
26.1	80	143	101	0·70	0·17250	0·00447	10·81478	0·28425	0·45457	0·00710	2582	24	2507	24	2416	31
27.1	119	308	82	0·27	0·16206	0·00515	7·62506	0·21176	0·34125	0·00526	2477	55	2188	25	1893	25
28.1	171	654	218	0·33	0·14271	0·00503	4·32520	0·13669	0·21981	0·00345	2260	62	1698	26	1281	18
29.1	159	964	120	0·12	0·13135	0·00436	2·64876	0·07807	0·14625	0·00224	2116	60	1314	22	880	13
30.1	168	752	272	0·36	0·15105	0·00388	4·11604	0·10747	0·19757	0·00302	2358	25	1657	21	1162	16
12XC15																
1.1	101	233	58	0·25	0·16849	0·00452	9·07919	0·24599	0·39069	0·00607	2543	25	2346	25	2126	28
2.1	145	877	552	0·63	0·13624	0·00369	2·64930	0·07242	0·14099	0·00219	2180	27	1314	20	850	12
3.1	151	250	239	0·96	0·17028	0·00467	11·10899	0·30718	0·47300	0·00748	2560	26	2532	26	2497	33
4.1	120	200	139	0·69	0·17261	0·00474	11·72069	0·32434	0·49231	0·00778	2583	26	2582	26	2581	34
5.1	100	1385	981	0·71	0·10011	0·00498	0·82149	0·03835	0·05952	0·00102	1626	95	609	21	373	6
6.1	111	313	144	0·46	0·16634	0·00456	7·11234	0·19669	0·31001	0·00485	2521	26	2126	25	1741	24
7.1	167	533	293	0·55	0·16029	0·00635	5·46886	0·19698	0·24745	0·00409	2459	69	1896	31	1425	21
8.1	121	670	432	0·64	0·14498	0·00402	3·08874	0·08621	0·15446	0·00242	2288	27	1430	21	926	14
9.1	147	709	345	0·49	0·14603	0·00409	3·66606	0·10328	0·18202	0·00286	2300	27	1564	22	1078	16
10.1	149	1266	1132	0·89	0·11452	0·00324	1·52724	0·04338	0·09669	0·00152	1872	29	941	17	595	9
11.1	138	1351	1173	0·87	0·12223	0·00348	1·40299	0·04005	0·08322	0·00131	1989	29	890	17	515	8
12.1	166	496	246	0·50	0·16362	0·00463	6·42534	0·18276	0·28470	0·00449	2493	27	2036	25	1615	23
13.1	153	305	163	0·53	0·16766	0·00477	9·78540	0·27948	0·42315	0·00670	2534	27	2415	26	2275	30
14.1	171	402	231	0·57	0·16757	0·00479	8·19642	0·23509	0·35462	0·00561	2534	27	2253	26	1957	27
15.1	147	384	190	0·50	0·16568	0·00478	7·46622	0·21596	0·32672	0·00519	2514	28	2169	26	1822	25
16.1	146	496	685	1·38	0·16001	0·00464	5·58246	0·16212	0·25294	0·00403	2456	28	1913	25	1454	21
17.1	123	670	392	0·58	0·15262	0·00446	3·49685	0·10227	0·16611	0·00266	2375	29	1527	23	991	15
18.1	141	829	434	0·52	0·14563	0·00430	2·99452	0·08846	0·14908	0·00239	2295	29	1406	22	896	13
19.1	172	376	222	0·59	0·16639	0·00492	8·83543	0·26155	0·38496	0·00618	2522	29	2321	27	2099	29
20.1	190	1043	698	0·67	0·15276	0·00286	3·27716	0·06602	0·15558	0·00221	2377	17	1476	16	932	12
21.1	168	1111	960	0·86	0·13723	0·00260	2·35245	0·04784	0·12432	0·00177	2193	17	1228	14	755	10
22.1	146	1252	1194	0·95	0·12114	0·00232	1·59781	0·03275	0·09566	0·00136	1973	18	969	13	589	8
23.1	145	780	426	0·55	0·15022	0·00285	3·31450	0·06745	0·16001	0·00228	2348	17	1484	16	957	13
24.1	118	858	637	0·74	0·14900	0·00285	2·37305	0·04854	0·11550	0·00165	2334	17	1235	15	705	10
10XC05																
1.1	141	842	338	0·40	0·12195	0·00344	2·29081	0·05725	0·13624	0·00177	1985	51	1209	18	823	10
2.1	96	178	151	0·85	0·16770	0·00281	9·87753	0·17427	0·42709	0·00532	2535	14	2423	16	2293	24
3.1	29	46	55	1·21	0·16654	0·00316	10·90193	0·21369	0·47467	0·00620	2523	17	2515	18	2504	27
4.1	42	64	85	1·32	0·17154	0·00307	11·14555	0·20811	0·47115	0·00602	2573	16	2535	17	2489	26
5.1	119	197	217	1·10	0·16952	0·00284	10·79594	0·19075	0·46180	0·00573	2553	14	2506	16	2448	25
6.1	44	89	111	1·25	0·16296	0·00294	8·33760	0·15663	0·37100	0·00470	2487	16	2268	17	2034	22
7.1	161	1103	435	0·39	0·12443	0·00210	2·24319	0·03983	0·13072	0·00162	2021	15	1195	12	792	9
8.1	224	603	613	1·02	0·16041	0·00268	6·51598	0·11480	0·29455	0·00364	2460	15	2048	16	1664	18
9.1	39	65	69	1·06	0·16668	0·00308	10·55981	0·20220	0·45939	0·00588	2525	16	2485	18	2437	26
10.1	147	207	219	1·06	0·16345	0·00661	9·78188	0·36635	0·43405	0·00661	2492	70	2414	35	2324	30
11.1	39	67	80	1·19	0·16324	0·00641	8·86819	0·31933	0·39401	0·00617	2490	68	2325	33	2141	29
12.1	224	618	996	1·61	0·15538	0·00271	5·42702	0·09896	0·25327	0·00315	2406	15	1889	16	1455	16
13.1	203	833	615	0·74	0·14837	0·00256	4·06905	0·07352	0·19887	0·00246	2327	15	1648	15	1169	13

(continued)

Table 1: Continued

Spot	Concentrations (ppm)			Th/U	Isotopic ratios						Isotopic ages (Ma)					
	Pb	U	Th		$^{207}Pb/^{206}Pb$*	±1σ	$^{207}Pb/^{235}U$	±1σ	$^{206}Pb/^{238}U$	±1σ	$^{207}Pb/^{206}Pb$	±1σ	$^{207}Pb/^{235}U$	±1σ	$^{206}Pb/^{238}U$	±1σ
14.1	36	58	76	1·32	0·16384	0·00326	10·56115	0·21597	0·46742	0·00611	2496	18	2485	19	2472	27
15.1	31	49	73	1·50	0·16306	0·00346	10·05910	0·21772	0·44733	0·00600	2488	19	2440	20	2383	27
10XC08																
1.1	208	574	534	0·93	0·15301	0·00536	5·52864	0·17666	0·26205	0·00377	2380	61	1905	27	1500	19
2.1	207	489	215	0·44	0·16173	0·00309	8·12081	0·16040	0·36410	0·00458	2474	17	2245	18	2002	22
3.1	101	213	145	0·68	0·16370	0·00326	8·68478	0·17764	0·38469	0·00492	2494	18	2305	19	2098	23
4.1	152	297	65	0·22	0·16862	0·00405	10·49582	0·21520	0·45146	0·00566	2544	41	2480	19	2402	25
5.1	185	491	415	0·85	0·15945	0·00308	6·87381	0·13699	0·31260	0·00393	2450	18	2095	18	1753	19
6.1	86	230	159	0·69	0·15997	0·00318	6·78309	0·13850	0·30747	0·00390	2455	18	2084	18	1728	19
7.1	102	288	456	1·58	0·16692	0·00332	6·71287	0·13709	0·29161	0·00370	2527	18	2074	18	1650	18
8.1	141	246	261	1·06	0·16492	0·00549	9·57308	0·28803	0·42100	0·00599	2507	57	2395	28	2265	27
9.1	146	307	240	0·78	0·15665	0·00503	7·75313	0·22443	0·35897	0·00496	2420	56	2203	26	1977	24
10.1	191	843	767	0·91	0·14897	0·00300	3·82223	0·07887	0·18605	0·00235	2334	19	1597	17	1100	13
11.1	74	115	139	1·21	0·16320	0·00340	10·88160	0·23183	0·48347	0·00622	2489	19	2513	20	2542	27
12.1	80	206	45	0·22	0·16451	0·00425	7·72400	0·17328	0·34052	0·00436	2503	44	2199	20	1889	21
13.1	162	637	302	0·47	0·15189	0·00432	4·41524	0·11113	0·21082	0·00278	2367	50	1715	21	1233	15
14.1	123	275	181	0·66	0·15633	0·00477	7·63884	0·20851	0·35440	0·00482	2416	53	2189	25	1956	23
15.1	121	266	131	0·49	0·16685	0·00462	8·73500	0·21284	0·37970	0·00502	2526	48	2311	22	2075	23
16.1	146	356	250	0·70	0·16426	0·00346	7·58397	0·16286	0·33480	0·00428	2500	20	2183	19	1862	21
17.1	128	288	259	0·90	0·15999	0·00529	7·42654	0·22209	0·33666	0·00473	2456	57	2164	27	1871	23
18.1	265	617	361	0·58	0·15951	0·00643	6·18658	0·23235	0·28129	0·00409	2451	70	2003	33	1598	21
19.1	59	138	92	0·67	0·16004	0·00512	7·37588	0·21230	0·33426	0·00466	2456	55	2158	26	1859	23

*Corrected ratios.

and define a discordant line intercepting the concordia at 2520 ± 25 Ma (MSWD = 1·04) (Fig. 4h). Therefore, the crystallization ages of the potassic granites in the Xingcheng region range from 2545 to 2520 Ma.

Summary

The emplacement age of Neoarchean granitoids in the studied region is between 2595 and 2520 Ma. The TTG granitoids were emplaced during the period 2595–2558 Ma, which is coeval with the hosted MMEs of 2568–2546 Ma, followed by intrusion of potassic granites at 2545–2520 Ma.

Geochemistry

Bulk-rock major and trace elements

Forty-eight fresh or least altered samples from four representative outcrops of Neoarchean granitoids in the Xingcheng region, including gneissic granite, tonalite–trondhjemite, granodiorite, MMEs and potassic granite, were selected for bulk-rock major and trace element analyses; the data are reported in Table 2. The samples vary in composition from diorite to granodiorite to quartz monzonite and granite. Most of these samples are sub-alkaline, although some plot in the alkaline field (Fig. 5a).

Taili gneissictonalite–granite. The gneissic granite samples from Taili are characterized by enrichment in K_2O over Na_2O ($K_2O/Na_2O = 0·96–2·41$) and relatively high total alkali contents (Figs 5a, d and 6a), and show a relatively large compositional range in terms of other major elements (Table 2; Figs 5 and 6). They are all metaluminous, plotting in the granite field in the An–Ab–Or diagram (Table 2; Fig. 5b and c). The Taili gneissic granite samples with lower SiO_2 contents have elevated P_2O_5 and TiO_2 contents (Fig. 6b and c). They also have low concentrations of Cr and Ni but relatively high Y and variable Sr abundances (Table 2; Fig. 6e and f). They are all enriched in LREE with varying $(La/Yb)_N$ ratios of 8–51 (Table 2; Fig. 7a). They have obvious negative Eu anomalies ($Eu/Eu^* = 0·50–0·93$) and superchondritic heavy rare earth element (HREE) abundances (Fig. 7a). Primitive mantle (PM)-normalized trace element patterns (Fig. 8a) are relatively enriched in large ion lithophile elements (LILE; e.g. Cs, Rb, Ba and Th), with limited variation, and depleted in high field strength elements (HFSE; negative Nb anomalies, but no Zr and Hf depletion). They also show a large range of Sr/Y ratios of 7–62.

The Taili gneissic tonalite samples have relatively high SiO_2 and K_2O/Na_2O (0·71–0·82) (Table 2; Fig. 5d). They are all metaluminous and fall near the TTG field in the An–Ab–Or diagram (Table 2; Fig. 5b and c). They also have low concentrations of Cr, Ni and Y but relatively high Sr (Table 2; Fig. 6e and f). They show the typical fractionated REE patterns of TTGs (or adakites), with high $(La/Yb)_N$ ratios of 72–74 without negative Eu anomalies ($Eu/Eu^* = 1·11–1·19$) (Table 2; Fig. 7a). In the PM-normalized trace element diagram (Fig. 8a), they are enriched in LILE, with significant negative anomalies of some HFSE (e.g. Nb and Ti) without Zr and Hf depletion. They have positive Sr anomalies with high Sr/Y ratios of 161–172.

Xingchengtonalite–trondhjemites and MMEs. The tonalite–trondhjemite samples from Xingcheng are intermediate to felsic in composition (Table 2). They are relatively enriched in Na_2O relative to K_2O ($K_2O/Na_2O = 0·20–0·67$) (Fig. 5d), and all plot in or near the trondhjemite field in the An–Ab–Or diagram (Fig. 5b). They also have low Cr, Ni and Y, but relatively high Sr (Table 2; Fig. 6e and f). They have uniform REE patterns with moderate depletion in HREE [$(La/Yb)_N$ = 25–47] and weakly negative to positive Eu anomalies ($Eu/Eu^* =$

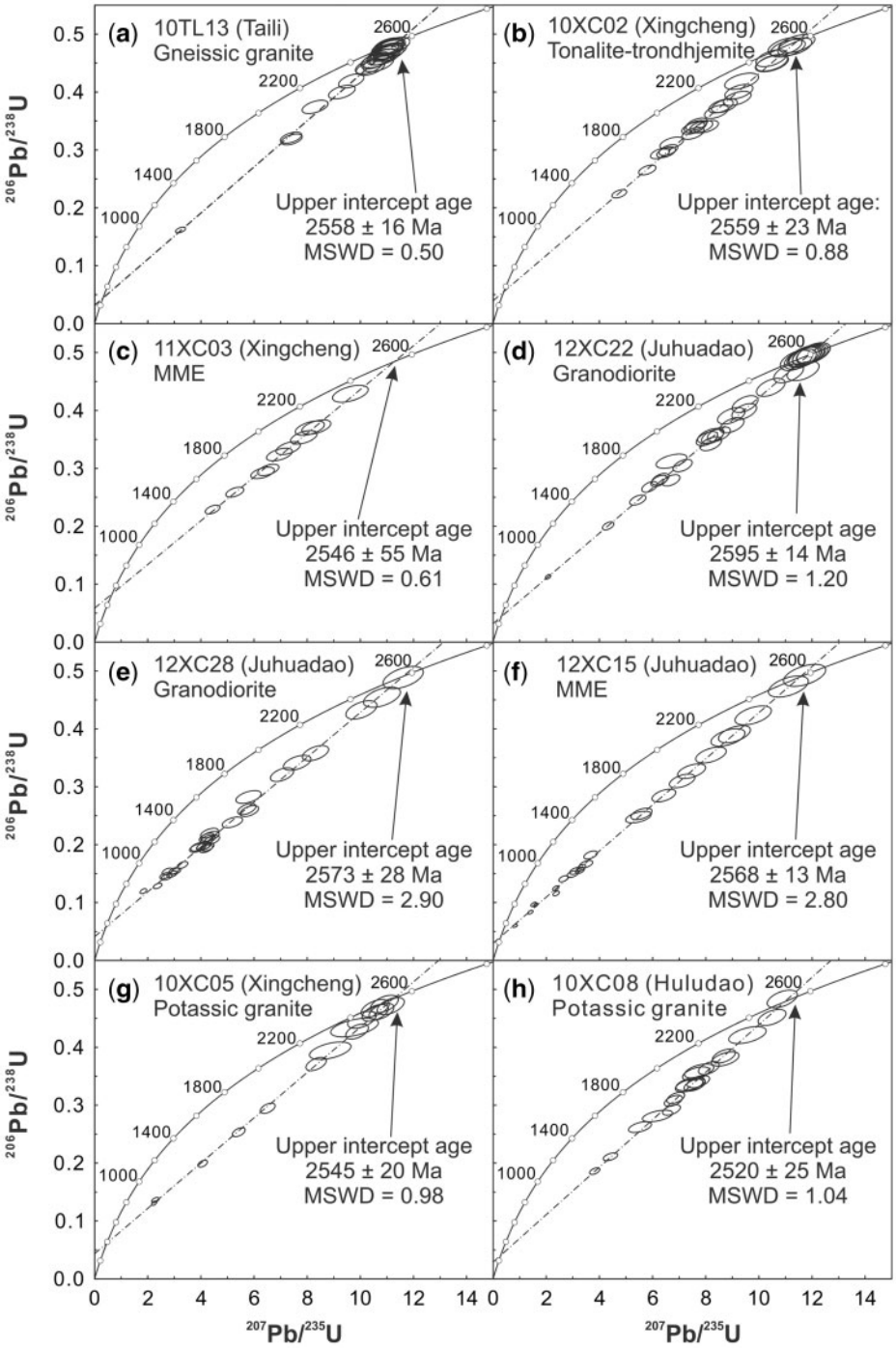

Fig. 4. U–Pb concordia diagrams for the Neoarchean TTG and potassic granitoids.

0·76–1·16) (Fig. 7b). In PM-normalized trace element patterns (Fig. 8b), they are enriched in LILE and depleted in Nb, Ta and Ti, and show positive Sr anomalies with high Sr/Y ratios of 83–145.

The MMEs hosted within the Xingcheng tonalite–trondhjemites are mafic to intermediate in composition (Table 2). In contrast to their host, the MMEs have higher TiO_2, Al_2O_3, total Fe_2O_3, MgO and CaO, similar Cr, Ni, Sr and K_2O/Na_2O (0·42–0·87) (Fig. 5d), but lower Ba, Th and U (Table 2; Fig. 6). They have higher HREE with lower $(La/Yb)_N$ ratios of 11–13 than their host and show weakly negative Eu anomalies ($Eu/Eu^* = 0·68$–0·94) (Fig. 7b). In PM-normalized trace element patterns (Fig. 8b), the MMEs are relatively depleted in some LILE (e.g. Ba and Th) and show depletion of HFSE with negative anomalies of Nb, Zr, Hf and Ti and

Table 2: Major and trace element data for the Neoarchean TTG and potassic granitoids in the Xingcheng region

No.:	10TL08	10TL09	10TL10	10TL13	12XC09	12XC10	12XC11	12XC12	13TL07	13TL08	15TL01	15TL02	15TL03	15TL05	10TL11	10TL12
Lithology:	GG	GG	GG	GG	GG	GG	GG	GG	GG	GG	GG	GG	GG	GG	GT	GT
Location:	TL	TL	TL	TL	TL	TL	TL	TL	TL	TL	TL	TL	TL	TL	TL	TL
Major elements (wt%)																
SiO_2	73·22	66·66	68·01	69·23	68·09	69·92	67·96	67·20	63·57	61·37	62·32	60·66	69·43	60·16	70·51	70·18
TiO_2	0·31	0·63	0·63	0·21	0·50	0·43	0·46	0·60	0·85	1·10	0·90	1·08	0·33	1·08	0·30	0·31
Al_2O_3	13·02	14·78	14·75	16·25	14·50	14·48	15·32	14·84	15·15	15·30	13·94	14·58	14·21	14·99	14·81	14·78
Fe_2O_{3T}	1·57	4·05	3·35	1·38	3·32	2·54	2·92	3·79	5·88	6·78	6·38	8·12	3·16	7·96	2·25	2·23
MnO	0·02	0·06	0·04	0·03	0·04	0·03	0·04	0·05	0·06	0·08	0·08	0·10	0·05	0·09	0·03	0·03
MgO	0·45	1·12	0·66	0·33	0·97	0·61	0·73	1·04	1·53	1·97	1·82	2·12	1·22	2·25	1·13	1·12
CaO	1·12	2·06	1·75	1·66	1·96	1·78	1·98	2·16	2·47	3·21	3·59	4·18	2·57	4·10	2·09	1·95
Na_2O	3·19	3·69	3·09	4·54	3·34	3·81	4·07	3·68	3·83	4·11	3·49	3·81	3·61	3·89	5·26	4·91
K_2O	5·86	5·94	7·46	6·17	5·88	5·11	5·24	5·20	5·07	4·40	4·27	3·67	3·86	3·92	3·72	4·01
P_2O_5	0·13	0·34	0·21	0·09	0·24	0·17	0·20	0·28	0·55	0·72	0·71	0·87	0·12	0·87	0·15	0·11
LOI	0·24	0·40	0·28	0·42	0·62	0·52	0·54	0·62	0·71	0·70	2·21	0·73	0·61	0·67	0·33	0·29
Total	99·14	99·73	100·23	100·32	99·47	99·40	99·46	99·47	99·68	99·74	99·70	99·92	99·20	99·97	100·58	99·93
K_2O/Na_2O	1·83	1·61	2·41	1·36	1·76	1·34	1·29	1·41	1·33	1·07	1·22	0·96	1·07	1·01	0·71	0·82
A/CNK	0·96	0·91	0·90	0·95	0·94	0·96	0·96	0·95	0·93	0·88	0·83	0·82	0·96	0·83	0·90	0·93
Mg#	40·0	39·1	31·3	35·9	40·4	35·7	36·9	39·1	37·8	40·4	39·9	37·9	47·3	39·8	53·9	54·0
Trace elements (ppm)																
Li	18·05	36·24	26·64	8·77	33·45	23·88	34·00	37·08	64·88	62·64	—	—	—	—	23·10	23·02
P	721	1994	1845	876	986	722	802	1117	2416	3224	4377	5067	831	5429	1103	1142
K	43100	42220	53340	44500	47880	43360	42760	42180	49880	44520	49477	40718	40759	48851	27140	30300
Sc	1·77	8·96	7·41	1·09	4·79	4·05	2·56	7·01	10·51	12·12	10·35	12·41	8·82	15·54	3·39	3·33
Ti	2054	3910	3980	1209	3243	2902	2970	3874	5456	7028	8285	9563	2765	10307	1810	1875
V	18·48	43·70	42·38	15·61	38·67	33·46	35·96	45·30	84·32	102·00	94·40	120·29	40·04	126·75	27·64	28·44
Cr	5·98	19·60	14·75	5·28	33·93	11·40	11·53	18·72	17·62	22·16	18·58	22·98	31·58	25·26	33·58	26·86
Co	1·59	5·08	3·21	1·16	5·37	4·17	4·19	6·07	10·67	12·80	16·96	18·18	8·84	19·34	3·87	3·95
Ni	3·49	9·70	7·09	2·83	16·55	6·58	6·00	9·40	10·87	14·08	16·26	17·38	16·94	20·13	13·98	12·15
Cu	10·01	16·14	26·92	7·85	11·59	12·98	9·41	21·76	30·02	14·86	34·43	32·34	11·06	43·50	12·34	1·10
Zn	32·42	65·16	53·52	35·30	77·62	54·10	57·88	74·80	88·70	110·54	95·36	104·62	52·69	96·70	38·78	33·10
Ga	13·36	17·38	17·14	16·01	18·37	17·98	18·76	18·93	22·34	24·28	26·91	29·20	20·85	30·70	15·82	16·08
Rb	176	227	271	140	189	187	168	191	210	228	162	192	164	196	100	126
Sr	313	316	255	516	450	353	370	349	390	687	555	695	423	853	720	761
Y	19·37	32·94	34·08	8·28	27·07	23·50	26·52	36·08	24·90	30·20	24·98	32·46	12·08	33·49	4·47	4·43
Zr	194	272	322	138	253	265	283	353	280	382	281	315	163	386	132	144
Nb	16·07	29·80	31·12	8·55	23·78	19·36	23·48	27·57	33·50	39·54	27·07	43·59	12·58	43·23	8·48	8·78
Cs	1·78	2·25	2·02	0·99	2·24	1·74	1·65	2·42	3·10	4·58	1·28	3·83	2·56	3·59	1·32	1·75
Ba	760	884	779	1415	1117	1175	1080	1095	1417	1127	1254	870	950	1048	1321	1609
La	75·46	66·48	51·66	46·66	78·41	52·12	31·26	76·92	65·34	65·96	71·72	76·42	34·00	77·97	29·58	29·00
Ce	122·82	156·30	123·66	69·38	171·22	130·54	87·18	193·16	155·02	176·74	151·14	177·81	57·08	173·90	51·58	49·24
Pr	11·54	17·19	15·44	6·20	18·97	15·20	11·76	23·02	17·48	20·70	19·06	22·41	6·48	22·81	5·06	4·98
Nd	38·06	62·42	58·02	19·74	64·93	53·44	44·90	80·60	61·08	74·52	63·21	74·53	20·42	76·44	17·39	17·06
Sm	5·84	10·00	9·83	2·74	10·25	8·67	8·31	12·94	9·60	11·92	9·79	11·81	3·33	12·08	2·46	2·38
Eu	0·98	1·55	1·44	0·76	1·64	1·52	1·39	2·08	2·03	2·57	2·11	2·47	0·89	2·60	0·79	0·82
Gd	4·57	7·47	7·38	2·08	7·52	6·41	6·33	9·52	7·18	8·85	7·18	8·67	2·72	8·97	1·73	1·66
Tb	0·60	0·96	0·98	0·25	0·95	0·82	0·86	1·24	0·86	1·06	0·94	1·14	0·38	1·16	0·18	0·17
Dy	3·17	5·14	5·25	1·28	5·12	4·44	4·82	6·74	4·67	5·65	4·63	5·81	2·05	5·84	0·79	0·78
Ho	0·58	0·94	0·97	0·23	0·97	0·85	0·94	1·29	0·89	1·07	0·90	1·14	0·42	1·13	0·13	0·13
Er	1·63	2·70	2·81	0·69	2·82	2·44	2·71	3·71	2·48	2·98	2·35	3·06	1·15	2·98	0·35	0·34
Tm	0·24	0·39	0·41	0·10	0·41	0·35	0·40	0·53	0·35	0·42	0·33	0·44	0·17	0·42	0·05	0·05
Yb	1·39	2·43	2·48	0·65	2·73	2·34	2·68	3·48	2·39	2·82	2·15	2·89	1·12	2·75	0·29	0·28
Lu	0·19	0·33	0·34	0·10	0·39	0·34	0·39	0·48	0·35	0·42	0·31	0·42	0·17	0·40	0·04	0·04
Hf	3·96	4·99	5·83	2·69	6·15	6·13	6·74	8·21	6·39	8·26	6·46	7·38	3·97	8·31	2·52	2·71
Ta	1·09	2·11	2·12	0·69	1·42	1·18	1·65	1·86	2·04	2·44	1·62	2·43	0·83	3·06	0·48	0·50
Pb	17	18	25	24	30	21	21	21	19	21	17	16	15	13	18	17
Th	11·77	10·61	7·06	6·41	16·36	9·46	7·39	10·55	14·83	11·13	7·58	9·45	18·93	8·07	4·76	4·51
U	0·97	1·48	1·16	0·73	2·06	1·48	2·13	1·73	2·36	2·07	1·54	1·47	1·86	1·43	1·27	1·30
ΣREE	267	334	281	151	366	279	204	416	330	376	336	389	130	389	110	107
Eu/Eu*	0·56	0·53	0·50	0·93	0·55	0·60	0·56	0·55	0·72	0·73	0·73	0·71	0·87	0·73	1·11	1·19
$(La/Yb)_N$	39	20	15	51	21	16	8	16	20	17	24	19	22	20	72	74
Sr/Y	16	10	7	62	17	15	14	10	16	23	22	21	35	25	161	172
ΔRb	30·4	114·1	151·0	14·2	68·3	57·9	48·6	75·2	112·4	141·0	70·0	108·6	37·0	115·0	–32·5	–5·3
ΔTh	–4·8	–2·7	–6·9	–8·2	2·3	–5·5	–6·6	–3·1	3·1	0·4	–3·6	–0·9	4·2	–2·0	–10·5	–10·6
ΔSr	77·7	–51·0	–84·4	200·8	112·2	51·6	28·8	–6·9	–39·1	214·5	101·2	208·4	111·2	356·7	430·1	464·4
ΔY	10·9	16·3	19·1	–5·2	12·2	10·9	11·5	20·1	4·4	6·9	2·9	8·3	–1·1	8·7	–7·4	–7·9
ΔNb	8·7	20·1	21·9	–0·2	14·6	10·8	14·3	18·1	22·7	28·0	15·9	31·8	3·9	31·3	0·2	0·3

(continued)

Table 2: Continued

No.:	10XC02	10XC03	11XC02	12XC04	11XC01-1	11XC01-2	11XC03	11XC06	10XC05	11XC07	12XC01	12XC02	12XC14	12XC17	12XC18	12XC19
Lithology:	TT	TT	TT	TT	MME	MME	MME	MME	PG	PG	PG	PG	GD	GD	GD	GD
Location:	XC	XC	XC	XC	XC	XC	XC	XC	XC	XC	XC	XC	JHD	JHD	JHD	JHD
Major elements (wt%)																
SiO_2	70·84	64·70	71·48	65·00	57·47	58·34	53·66	56·13	73·57	76·11	73·80	73·61	64·40	66·21	65·33	64·95
TiO_2	0·47	0·39	0·42	0·43	0·78	0·76	0·87	0·77	0·27	0·09	0·21	0·21	0·44	0·41	0·46	0·40
Al_2O_3	14·44	15·63	13·86	16·36	16·42	15·83	15·15	16·83	12·97	11·54	13·40	13·03	18·20	15·43	15·27	16·17
Fe_2O_{3T}	3·09	3·44	3·51	3·96	8·62	8·20	11·86	8·42	1·70	0·86	1·53	1·47	3·35	4·44	4·89	4·38
MnO	0·03	0·05	0·04	0·05	0·09	0·10	0·18	0·12	0·03	0·01	0·03	0·03	0·05	0·07	0·08	0·07
MgO	1·49	1·31	2·15	1·45	3·77	3·62	4·47	3·07	0·33	0·14	0·37	0·35	1·21	1·58	1·76	1·51
CaO	0·76	2·49	0·67	3·22	2·87	3·36	5·96	5·38	0·88	0·90	0·90	1·17	2·22	3·75	4·21	3·85
Na_2O	6·49	5·91	3·85	4·92	4·62	4·57	3·07	4·53	3·19	3·56	3·20	3·40	5·00	4·13	4·20	4·45
K_2O	1·30	3·93	1·72	3·16	2·12	1·94	2·66	2·42	5·66	5·35	5·28	5·45	3·03	2·35	1·94	2·71
P_2O_5	0·23	0·22	0·20	0·25	0·43	0·42	0·25	0·48	0·11	0·01	0·06	0·06	0·14	0·15	0·18	0·15
LOI	1·32	1·24	1·26	0·66	2·06	2·10	1·15	1·11	0·53	0·58	0·52	0·54	1·43	0·85	1·06	0·77
Total	100·47	99·31	99·16	99·47	99·25	99·25	99·29	99·25	99·23	99·16	99·31	99·32	99·47	99·38	99·39	99·43
K_2O/Na_2O	0·20	0·67	0·45	0·64	0·46	0·42	0·87	0·53	1·78	1·50	1·65	1·60	0·61	0·57	0·46	0·61
A/CNK	1·07	0·84	1·47	0·94	1·09	1·01	0·81	0·85	1·00	0·87	1·06	0·96	1·17	0·96	0·92	0·94
Mg#	52·9	47·0	58·8	46·1	50·5	50·7	46·8	46·0	31·4	28·0	35·8	36·0	45·7	45·4	45·6	44·6
Trace elements (ppm)																
Li	13·55	12·11	19·34	29·82	37·22	35·28	36·31	22·70	9·66	3·79	8·29	8·95	18·30	40·90	45·36	39·90
P	1542	1343	888	1007	1855	1937	1061	2084	1007	94	236	252	527	615	730	591
K	10338	27220	16250	26080	19886	19450	24276	22580	39160	46560	41940	44480	24880	19466	16101	21700
Sc	5·14	4·91	5·05	5·64	16·82	18·79	22·03	14·43	2·63	1·38	2·35	2·05	4·84	8·93	10·26	7·83
Ti	2984	2422	2976	2782	5614	5924	6017	5510	1575	575	1311	1298	2830	2650	2882	2530
V	41·24	44·94	33·52	57·02	134·20	130·44	186·75	113·48	15·82	6·36	15·05	131·44	23·62	63·78	68·35	61·58
Cr	12·77	11·95	21·26	13·99	21·44	13·66	30·22	4·85	3·96	11·14	14·19	5·14	8·49	19·72	22·97	21·54
Co	6·15	6·17	7·04	8·71	16·95	16·73	23·43	16·05	1·28	0·82	1·84	1·74	4·89	9·94	10·51	9·53
Ni	9·50	8·87	14·73	11·34	24·24	18·13	33·16	13·14	2·16	5·42	11·11	2·82	4·56	10·21	11·08	10·65
Cu	36·96	34·56	5·16	33·84	595·80	644·60	532·27	437·60	7·05	14·74	29·94	5·53	10·12	19·63	7·64	29·98
Zn	72·90	46·28	76·40	90·12	160·60	126·60	134·06	121·96	32·24	33·32	79·32	47·54	55·62	66·40	71·93	63·58
Ga	13·46	16·73	12·94	20·46	23·54	24·12	22·23	23·96	15·22	13·68	16·22	16·68	20·56	18·15	18·74	17·99
Rb	46	86	41	150	143	130	107	122	271	151	228	246	135	167	166	138
Sr	732	931	1117	1064	650	750	958	1251	230	259	213	241	384	457	472	452
Y	8·87	7·29	7·70	10·00	15·80	19·01	17·15	14·58	9·40	5·41	15·80	15·75	6·70	17·08	21·79	15·11
Zr	133	124	140	127	121	115	136	133	190	85	215	164	214	169	181	131
Nb	8·80	6·69	10·74	6·77	13·37	16·27	15·15	12·38	22·96	9·30	16·11	15·78	9·25	9·97	12·42	9·27
Cs	0·26	0·77	0·28	3·53	1·49	1·36	3·59	3·08	1·30	1·35	1·31	1·48	1·74	5·01	5·49	4·35
Ba	447	1768	435	1431	283	280	362	449	537	424	570	575	755	704	504	937
La	28·86	21·34	35·12	28·52	22·02	24·14	20·26	15·97	29·12	19·70	60·72	53·50	38·26	35·40	32·85	28·74
Ce	58·38	42·24	69·32	61·26	59·30	70·62	61·61	47·06	68·48	36·62	120·24	103·00	68·36	67·50	65·72	56·34
Pr	7·03	5·06	8·11	7·68	8·94	10·91	9·05	7·37	5·97	3·62	11·16	10·64	7·00	7·35	7·54	6·27
Nd	27·58	19·55	30·00	29·28	39·00	47·76	36·62	33·36	20·14	11·45	34·58	34·14	23·18	26·20	28·19	22·64

(continued)

Table 2: Continued

No.:	10XC02	10XC03	11XC02	12XC04	11XC01-1	11XC01-2	11XC03	11XC06	10XC05	11XC07	12XC01	12XC02	12XC14	12XC17	12XC18	12XC19
Lithology:	TT	TT	TT	TT	MME	MME	MME	MME	PG	PG	PG	PG	GD	GD	GD	GD
Location:	XC	XC	XC	XC	XC	XC	XC	XC	XC	XC	XC	XC	JHD	JHD	JHD	JHD
Sm	4·53	3·18	4·79	4·94	7·34	8·91	6·37	6·68	3·24	1·68	5·29	5·44	3·40	4·67	5·30	4·01
Eu	0·98	1·06	1·10	1·39	1·57	1·94	1·78	1·34	0·55	0·37	0·82	0·84	1·13	1·20	1·19	1·13
Gd	3·00	2·24	3·20	3·51	5·17	6·30	4·92	4·90	2·22	1·27	3·93	4·03	2·64	3·97	4·63	3·38
Tb	0·33	0·25	0·35	0·41	0·61	0·75	0·62	0·58	0·30	0·16	0·52	0·53	0·29	0·54	0·66	0·46
Dy	1·57	1·21	1·66	2·00	3·11	3·77	3·27	2·93	1·68	0·86	2·89	2·92	1·40	3·12	3·85	2·69
Ho	0·26	0·21	0·28	0·36	0·55	0·66	0·60	0·51	0·31	0·17	0·56	0·56	0·25	0·62	0·78	0·54
Er	0·72	0·57	0·76	0·98	1·48	1·77	1·63	1·37	0·99	0·53	1·68	1·66	0·67	1·82	2·30	1·60
Tm	0·09	0·08	0·10	0·13	0·20	0·24	0·21	0·17	0·16	0·08	0·26	0·25	0·09	0·27	0·34	0·24
Yb	0·56	0·50	0·61	0·83	1·22	1·46	1·38	1·08	1·18	0·63	1·80	1·73	0·55	1·82	2·32	1·62
Lu	0·08	0·07	0·08	0·11	0·16	0·19	0·19	0·14	0·17	0·11	0·27	0·25	0·09	0·28	0·35	0·24
Hf	2·48	2·29	3·10	3·01	2·91	2·64	3·23	3·15	4·10	2·75	5·58	4·56	5·17	4·31	4·55	3·28
Ta	0·60	0·44	0·74	0·40	0·85	1·23	0·99	0·85	2·02	0·76	1·02	1·09	0·57	0·67	0·81	0·64
Pb	9	11	8	18	18	18	11	18	25	26	48	43	16	20	19	19
Th	4·83	3·36	7·42	6·38	1·74	1·84	1·58	1·72	23·80	52·94	45·46	40·36	9·73	10·03	9·84	9·26
U	1·06	0·77	0·99	1·38	0·52	0·56	0·62	0·56	3·35	3·93	4·92	4·72	0·90	2·00	11·97	1·86
ΣREE	134	98	155	141	151	179	149	123	135	77	245	219	147	155	156	130
Eu/Eu*	0·76	1·16	0·81	0·97	0·74	0·75	0·94	0·68	0·59	0·74	0·52	0·52	1·11	0·83	0·72	0·91
$(La/Yb)_N$	37	31	41	25	13	12	11	11	18	22	24	22	50	14	10	13
Sr/Y	83	128	145	106	41	39	56	86	25	48	13	15	57	27	22	30
ΔRb	–87·7	–17·7	–95·9	45·4	75·7	57·9	59·1	61·0	123·4	–9·1	79·2	97·9	33·3	55·8	59·8	33·6
ΔTh	–10·6	–9·0	–8·3	–6·1	–7·0	–7·3	–5·3	–6·3	7·0	34·9	28·6	23·6	–2·5	–3·1	–2·8	–3·2
ΔSr	449·2	524·7	846·5	664·2	99·7	216·4	331·3	673·1	1·8	81·1	–10·8	12·9	–27·8	81·1	79·0	51·0
ΔY	–2·6	–11·8	–2·9	–8·7	–12·4	–8·1	–15·8	–15·3	1·4	0·6	8·0	7·8	–12·8	–0·2	3·5	–3·7
ΔNb	0·6	–3·7	2·8	–3·5	0·5	3·7	0·9	–1·0	15·7	2·9	8·9	8·5	–1·2	0·1	2·3	–1·0

(continued)

Table 2: Continued

No.:	12XC20	12XC21	12XC22	12XC23	12XC24	12XC25	12XC27	12XC28	12XC15	12XC16	10XC08	12XC29	12XC30	12XC31	12XC32	12XC33
Lithology:	GD	GD	GD	GD	GD	GD	GD	GD	MME	MME	PG	PG	PG	PG	PG	PG
Location:	JHD	JHD	JHD	JHD	JHD	JHD	JHD	JHD	JHD	JHD	HLD	HLD	HLD	HLD	HLD	HLD
Major elements (wt%)																
SiO_2	63·15	62·99	64·45	64·73	66·00	66·89	68·72	67·69	52·06	53·83	71·78	69·69	70·03	71·45	72·32	71·50
TiO_2	0·46	0·50	0·42	0·47	0·57	0·73	0·44	0·61	0·64	0·58	0·22	0·35	0·33	0·20	0·41	0·23
Al_2O_3	16·72	16·39	16·25	15·39	17·21	15·40	14·81	15·52	18·13	17·69	14·74	14·98	15·05	14·99	13·37	13·75
Fe_2O_{3T}	5·18	4·60	4·61	5·08	3·81	4·59	3·85	3·98	10·25	9·47	1·92	1·65	1·82	1·06	2·36	1·99
MnO	0·09	0·13	0·09	0·08	0·06	0·08	0·06	0·07	0·19	0·19	0·02	0·01	0·01	0·01	0·03	0·01
MgO	1·63	1·74	1·13	1·86	1·09	1·14	0·94	0·97	3·45	3·12	0·70	0·63	0·42	0·47	0·43	0·48
CaO	4·40	5·13	3·82	4·11	1·99	3·08	1·89	3·11	6·04	6·95	0·47	0·45	0·32	0·30	0·36	0·25
Na_2O	4·16	5·03	4·22	4·28	4·47	3·60	4·44	3·69	4·41	4·59	4·15	0·88	2·38	2·20	1·72	0·42
K_2O	2·32	1·62	3·14	2·10	2·78	2·74	2·95	2·53	2·73	1·87	4·84	9·67	7·68	7·77	7·13	9·77
P_2O_5	0·17	0·21	0·16	0·18	0·12	0·22	0·11	0·19	0·25	0·23	0·07	0·15	0·16	0·09	0·17	0·08
LOI	0·97	1·10	1·15	1·13	1·32	0·91	1·17	0·97	1·55	1·00	0·94	1·03	1·26	0·88	1·08	0·98
Total	99·25	99·43	99·44	99·41	99·42	99·36	99·38	99·33	99·69	99·54	99·85	99·48	99·45	99·41	99·37	99·44
K_2O/Na_2O	0·56	0·32	0·74	0·49	0·62	0·76	0·66	0·69	0·62	0·41	1·17	11·04	3·23	3·54	4·16	23·04
A/CNK	0·96	0·85	0·94	0·92	1·23	1·06	1·06	1·07	0·86	0·80	1·14	1·18	1·18	1·19	1·20	1·17
Mg#	42·3	46·8	36·4	46·0	40·1	36·7	36·3	36·2	43·9	43·4	45·7	47·0	34·9	50·6	29·9	36·0
Trace elements (ppm)																
Li	47·60	36·52	37·74	48·40	21·76	24·96	25·64	22·84	55·64	35·88	10·29	11·53	11·29	11·95	6·58	7·09
P	734	811	648	705	463	825	456	742	1061	962	730	577	641	386	685	328
K	21280	13186	26260	17426	22280	21660	25140	20740	24100	16164	33880	73895	64620	68000	58760	79220
Sc	11·09	10·44	9·59	11·18	8·20	10·74	7·27	9·66	27·70	24·60	2·81	3·33	3·33	3·06	3·87	2·87
Ti	3558	3164	2706	3090	3550	4554	2980	3842	4674	4118	1308	2057	2184	1371	2644	1423
V	80·52	64·20	76·54	72·42	29·86	17·74	15·02	17·95	223·20	208·60	23·14	29·58	25·22	25·44	28·38	23·24
Cr	29·60	26·40	22·74	65·88	8·93	10·27	7·95	9·66	10·34	11·89	12·96	21·96	17·56	19·81	4·57	12·04
Co	11·95	8·59	8·01	11·28	5·10	5·33	3·96	4·62	26·14	23·46	2·33	2·87	3·53	1·42	6·54	2·14
Ni	14·19	14·40	10·78	30·64	5·69	4·90	5·12	4·79	10·46	10·46	5·44	10·17	7·70	6·09	12·01	7·92
Cu	9·27	9·33	7·25	9·08	5·11	13·82	8·97	9·04	84·96	77·68	22·50	2·83	19·61	4·14	21·30	2·64
Zn	70·44	85·80	84·28	74·30	65·58	87·68	57·20	75·44	156·66	116·36	43·42	80·30	75·92	99·72	129·56	64·16
Ga	21·42	23·74	22·62	18·99	20·08	19·63	18·35	19·46	24·62	22·16	17·61	18·47	19·12	20·32	15·97	17·28
Rb	164	155	239	191	147	133	130	121	312	159	165	251	246	258	207	258
Sr	564	566	404	486	331	294	248	304	485	495	307	61	157	157	71	50
Y	21·02	22·32	21·74	20·98	7·91	13·43	10·07	13·17	40·34	32·60	5·20	9·02	7·47	5·17	9·97	11·17
Zr	181	182	163	159	148	121	283	145	118	123	135	222	214	131	249	134
Nb	11·32	18·38	13·74	12·24	12·35	20·01	11·10	17·27	13·77	11·04	6·20	9·97	12·60	8·81	18·60	9·84
Cs	4·31	4·02	5·14	6·17	2·59	3·88	2·95	3·06	10·46	5·79	4·72	4·32	3·57	3·10	4·57	3·81
Ba	799	254	876	532	832	743	875	672	228	171	1089	1322	1798	1470	789	1084
La	34·60	29·44	42·40	33·96	25·44	30·92	56·08	34·34	23·28	18·50	26·86	44·23	28·80	24	34	45
Ce	69·10	60·36	79·48	67·06	36·52	60·68	103·36	70·18	60·70	49·94	46·42	85·48	56·36	45	65	88
Pr	7·80	6·98	8·60	7·61	4·73	6·83	10·64	7·42	8·64	7·14	4·75	8·96	6·03	4·63	6·81	9·38
Nd	28·72	26·36	30·66	28·22	16·35	24·72	35·16	26·34	37·02	30·24	16·18	29·89	20·80	15	22	31
Sm	5·29	4·98	5·40	5·25	2·78	4·53	5·02	4·62	8·33	6·58	2·32	4·53	3·27	2·32	3·41	4·77
Eu	1·40	1·19	1·13	1·26	1·15	1·11	1·29	1·08	2·14	2·07	0·64	1·06	0·86	0·64	0·76	1·06

(continued)

Table 2: Continued

No.:	12XC20	12XC21	12XC22	12XC23	12XC24	12XC25	12XC27	12XC28	12XC15	12XC16	10XC08	12XC29	12XC30	12XC31	12XC32	12XC33
Lithology:	GD	GD	GD	GD	GD	GD	GD	GD	MME	MME	PG	PG	PG	PG	PG	PG
Location:	JHD	JHD	JHD	JHD	JHD	JHD	JHD	JHD	JHD	JHD	HLD	HLD	HLD	HLD	HLD	HLD
Gd	4·50	4·31	4·68	4·55	2·59	4·11	4·00	4·04	7·28	5·79	1·64	3·24	2·46	1·79	2·68	3·58
Tb	0·62	0·61	0·64	0·64	0·32	0·52	0·45	0·51	1·09	0·88	0·18	0·38	0·28	0·21	0·35	0·44
Dy	3·58	3·58	3·71	3·71	1·70	2·78	2·21	2·70	6·58	5·31	0·84	1·90	1·39	1·05	1·92	2·27
Ho	0·73	0·75	0·75	0·75	0·31	0·52	0·39	0·51	1·37	1·11	0·15	0·35	0·27	0·19	0·37	0·41
Er	2·14	2·28	2·17	2·22	0·77	1·35	1·01	1·33	4·14	3·35	0·42	0·94	0·78	0·56	1·09	1·11
Tm	0·32	0·36	0·33	0·33	0·09	0·17	0·13	0·17	0·64	0·52	0·06	0·14	0·12	0·09	0·17	0·15
Yb	2·22	2·54	2·27	2·27	0·57	0·97	0·84	1·01	4·54	3·63	0·42	0·90	0·83	0·64	1·16	0·97
Lu	0·34	0·40	0·35	0·34	0·09	0·14	0·14	0·15	0·70	0·56	0·06	0·14	0·14	0·11	0·19	0·14
Hf	4·06	4·52	4·16	3·99	3·48	3·04	6·67	3·59	2·60	2·74	2·68	5·09	4·89	3·38	6·20	3·33
Ta	0·67	1·17	0·83	0·83	0·73	1·23	0·62	1·01	0·86	0·71	0·45	0·61	0·79	0·53	1·20	0·61
Pb	21	42	48	21	39	16	13	15	57	39	9	13	12	14	20	14
Th	9·36	8·65	11·70	9·71	5·24	7·50	11·90	8·42	3·70	2·28	7·73	20·89	9·22	22·42	16·46	26·72
U	2·36	3·03	4·00	1·99	0·71	0·66	1·02	0·77	9·43	9·46	1·19	2·21	1·82	1·56	2·26	1·51
ΣREE	161	144	183	158	93	139	221	154	166	136	101	182	122	97	140	189
Eu/Eu*	0·85	0·77	0·67	0·77	1·29	0·77	0·85	0·75	0·82	1·00	0·95	0·81	0·88	0·92	0·74	0·75
$(La/Yb)_N$	11	8	13	11	32	23	48	24	4	4	46	35	25	27	21	33
Sr/Y	27	25	19	23	42	22	25	23	12	15	59	7	21	30	7	4
ΔRb	67·8	60·0	136·5	87·6	36·9	18·2	6·8	2·6	271·9	109·9	25·7	123·0	116·0	120·9	65·2	120·1
ΔTh	−2·2	−2·8	−0·5	−2·7	−7·8	−5·9	−2·5	−5·4	−2·3	−4·6	−8·2	6·0	−5·8	6·7	0·3	11·0
ΔSr	127·4	126·3	−7·3	80·1	−49·5	−68·3	−77·6	−42·0	−173·9	−128·2	42·6	−245·0	−142·6	−114·4	−182·7	−220·5
ΔY	0·0	1·1	2·3	1·9	−9·6	−2·9	−4·0	−2·2	5·4	−0·1	−5·1	−3·9	−5·0	−5·5	0·4	0·5
ΔNb	0·4	7·4	3·3	1·9	2·4	10·4	2·1	8·0	−1·0	−3·1	−1·7	1·4	4·1	0·8	10·9	1·9

GG, gneissic granite; GT, gneissic tonalite; TT, tonalite–trondhjemite; MME, mafic magmatic enclave; PG, potassic granite; GD, granodiorite; TL, Taili; XC, Xingcheng; JHD, Juhuadao; HLD, Huludao. For X as any given element, $\Delta X = X - (a SiO_2 + b)$; for Rb, $a = 5$, $b = -220$; for Th, $a = 0{\cdot}5$, $b = -20$; for Sr, $a = -20$, $b = 1700$; for Y, $a = -1{\cdot}25$, $b = 100$; for Nb, $a = -0{\cdot}35$, $b = 33$ (Moyen et al., 2010).

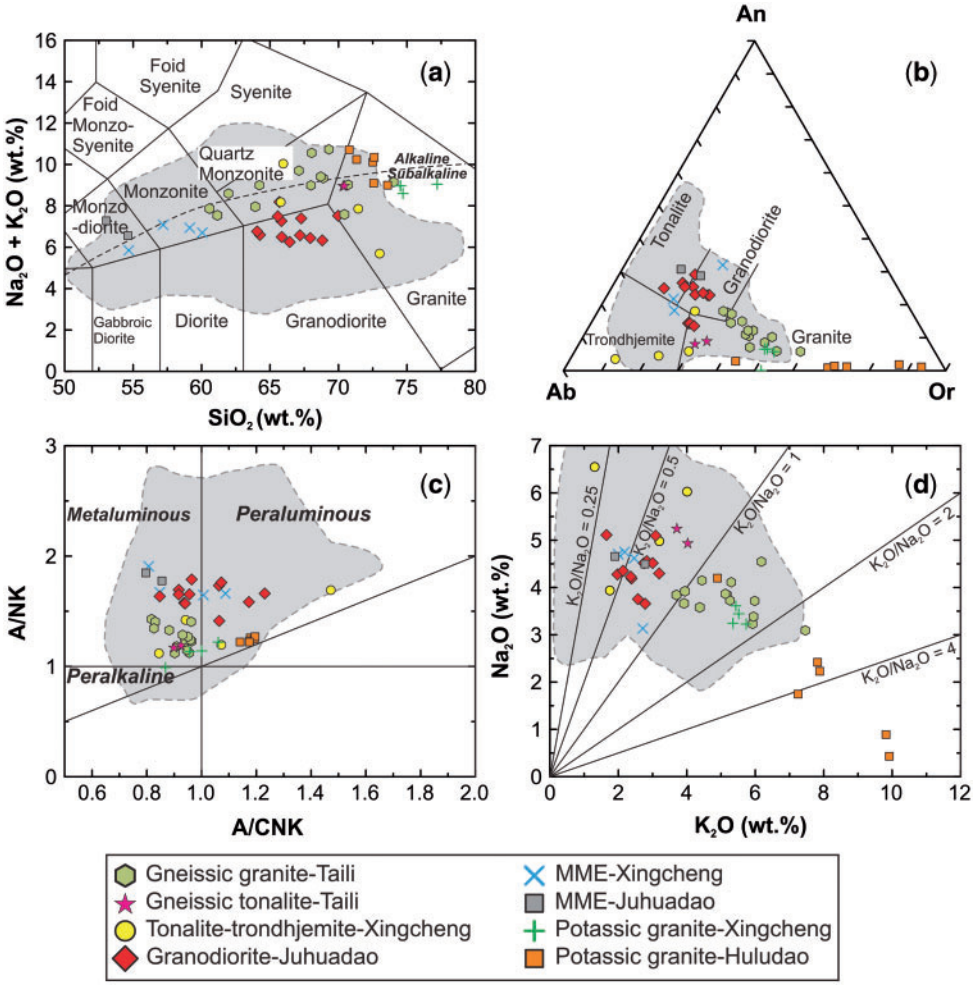

Fig. 5. (a) ($Na_2O + K_2O$)–SiO_2 diagram, (b) normative An–Ab–Or triangle (Barker, 1979), (c) A/NK–A/CNK diagram and (d) Na_2O vs K_2O for the Neoarchean TTG and potassic granitoids in the Xingcheng region. Grey fields are the fields of experimental metabasalt melts at 1–4 GPa, which are constructed using data from Sen & Dunn (1994), Rapp & Watson (1995), Rapp *et al.* (1999, 2002, 2003), Skjerlie & Patiño Douce (2002) and references therein.

moderate positive Sr anomalies with relatively high Sr/Y ratios of 39–86.

Juhuadao granodiorites and MMEs. The granodiorite samples from Juhuadao are compositionally intermediate to felsic (Table 2), with high Na_2O and thus lower K_2O/Na_2O (0·32–0·76), similar to the Xingcheng tonalite–trondhjemites (Table 2; Fig. 5d). They fall in the tonalite–trondhjemite–granodiorite field in the An–Ab–Or diagram (Fig. 5b), and have intermediate Y and Sr abundances. They are all enriched in LREE with significantly varying HREE depletion, thus giving varying $(La/Yb)_N$ (8–50) (Fig. 7c). They have varying Eu/Eu* (0·67–1·29) and an inverse Yb–SiO_2 correlation (Table 2; figure not shown). In PM-normalized trace element patterns (Fig. 8c), they are enriched in LILE and depleted in Nb, Ta and Ti, with varying Sr/Y ratios (19–57).

The MMEs in the Juhuadao granodiorites are mafic with relatively low SiO_2 and high K_2O/Na_2O (0·41–0·62), consistent with the host granodiorite (Table 2; Fig. 5d). They have low TiO_2, MgO, Cr, Ni, and Sr (Table 2; Fig. 6). In contrast to their host, they have flat LREE patterns with high HREE and thus weak REE fractionation [$(La/Yb)_N \sim 4$], lower Sr/Y ratios (12–15), and no obvious Eu anomaly (Fig. 7c). In PM-normalized trace element patterns (Fig. 8c), they are depleted in some LILE (e.g. Th and U) and have negative anomalies of HFSE (Nb, Ta, Zr, Hf and Ti).

Xingcheng and Huludao potassic granites. The potassic granites intruding the Xingcheng tonalite–trondhjemites have high SiO_2, and are metaluminous to slightly peraluminous (Table 2; Fig. 5c), enriched in K_2O ($K_2O/Na_2O = 1·50–1·78$; Fig. 5d), and fall in the granite field in the An–Ab–Or diagram (Fig. 5b). They have relatively low Cr, Ni, Y and Sr concentrations (Table 2; Fig. 6e and f). They have fractionated REE patterns [$(La/Yb)_N = 18–24$] with negative Eu anomalies ($Eu/Eu^* = 0·52–0·74$) and concave HREE patterns (Fig. 7d). In PM-normalized trace element patterns (Fig. 8d), they are enriched in LILE and depleted in some HFSE such as Nb and Ti, but with no depletion of Zr and Hf. They are also depleted in Sr, with moderate Sr/Y ratios of 13–48 (Fig. 12b).

The potassic granite samples from Huludao are peraluminous (Fig. 5c) and are strongly enriched in K_2O, with

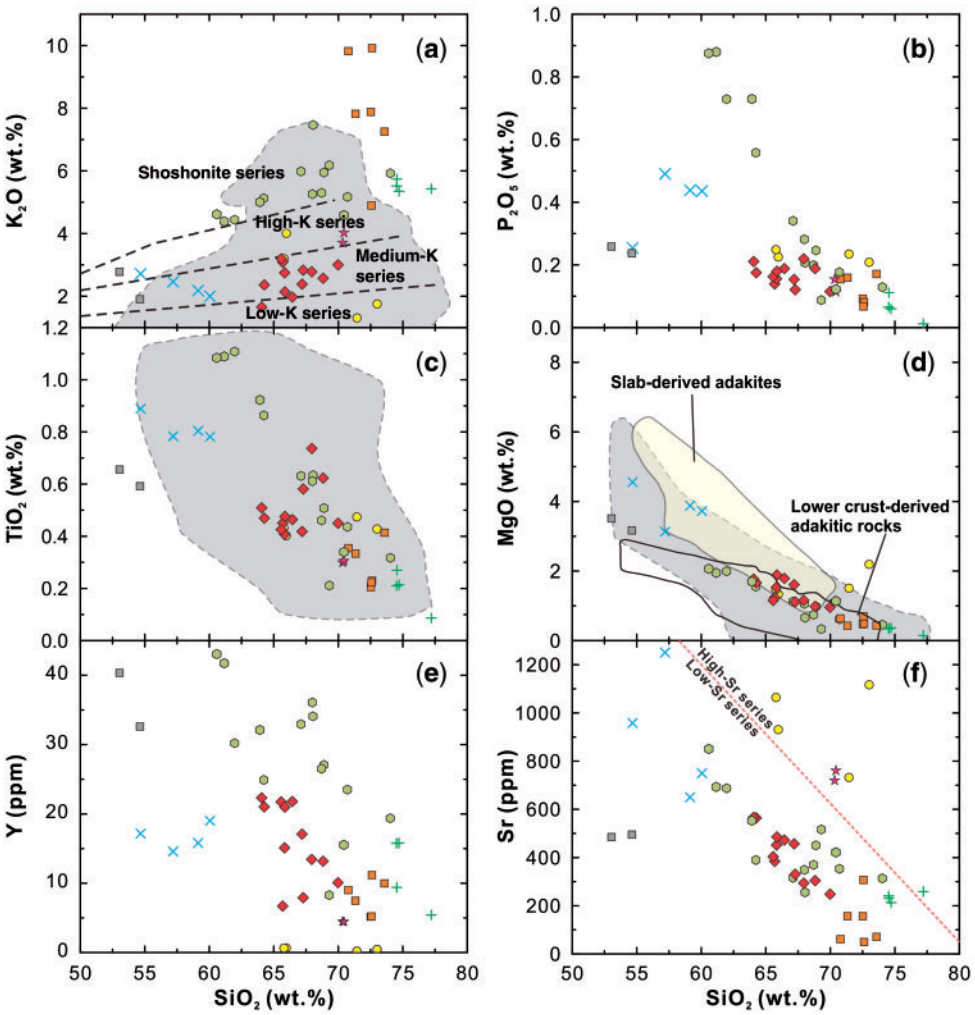

Fig. 6. Harker diagrams for the Neoarchean TTG and potassic granitoids in the Xingcheng region. (a) K_2O–SiO_2; (b) P_2O_5–SiO_2; (c) TiO_2–SiO_2; (d) MgO–SiO_2; (e) Y–SiO_2; (f) Sr–SiO_2. Grey fields are for experimental metabasalt melts at 1–4 GPa. Data sources are the same as for Fig. 5. The fields of slab-derived adakites and lower crust-derived adakitic rocks in (d) are after Wang *et al.* (2006). The dividing line between high-Sr and low-Sr series in (f) is from Moyen *et al.* (2007). Legends are the same as in Fig. 5.

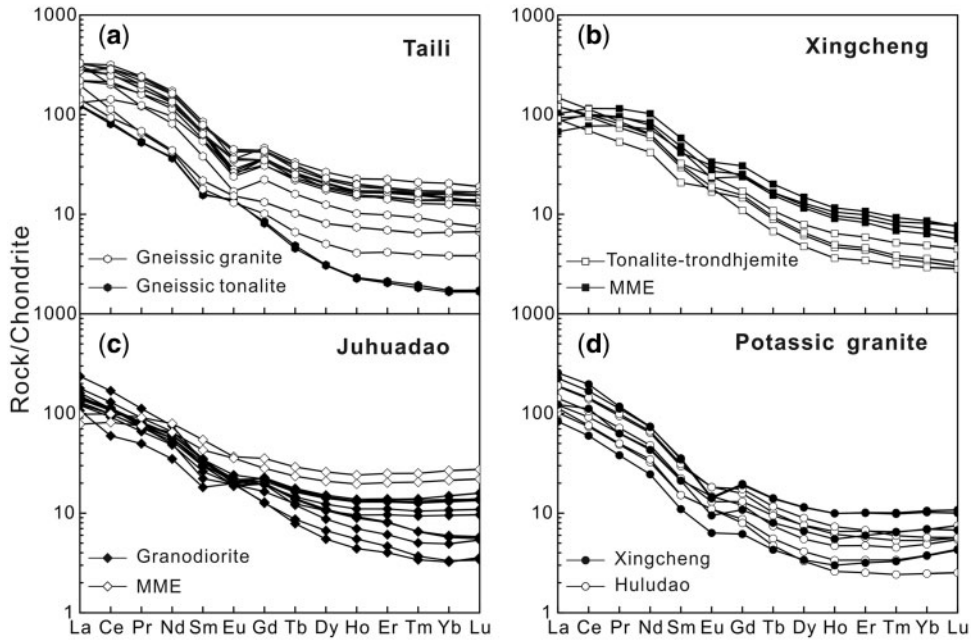

Fig. 7. Chondrite-normalized REE patterns for the Neoarchean TTG and potassic granitoids in the Xingcheng region. The chondrite values are from Sun & McDonough (1989).

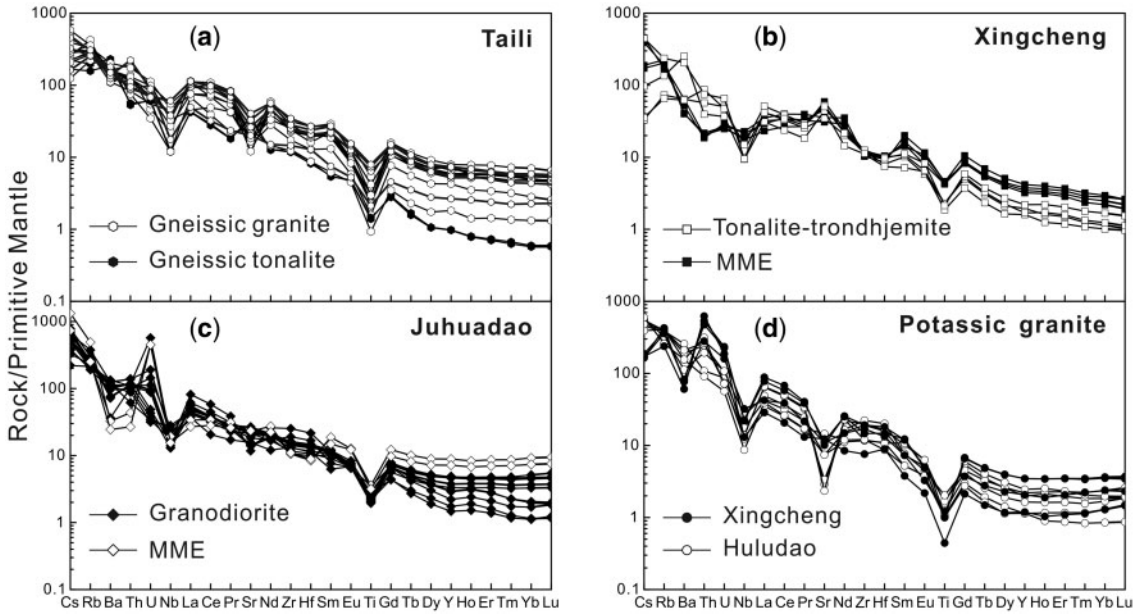

Fig. 8. Primitive mantle (PM)-normalized trace element patterns for the Neoarchean TTG and potassic granitoids in the Xingcheng region. The values of PM are from Sun & McDonough (1989).

Table 3: Bulk-rock Nd isotopic compositions of the Neoarchean TTG and potassic granitoids in the Xingcheng region

Sample	Lithology	Location	Sm (ppm)	Nd (ppm)	$^{147}Sm/^{144}Nd$	$^{143}Nd/^{144}Nd$	2σ	$\varepsilon_{Nd}(0)$	$(^{143}Nd/^{144}Nd)_i$*	$\varepsilon_{Nd}(t)$*	T_{DM1} (Ma)	T_{DM2} (Ma)	$f_{Sm/Nd}$
13TL07	GG	TL	9·60	61·08	0·0997	0·511007	7	–31·8	0·509325	–0·2	2848	2903	–0·49
13TL08	GG	TL	11·92	74·52	0·1015	0·511032	4	–31·3	0·509320	–0·2	2859	2911	–0·48
11XC02	TT	XC	4·79	30·00	0·1013	0·511020	5	–31·6	0·509310	–0·4	2871	2926	–0·48
11XC04	TT	XC	3·06	26·08	0·0744	0·510621	4	–39·4	0·509364	0·6	2752	2841	–0·62
11XC05	TT	XC	3·53	27·33	0·0819	0·510733	5	–37·2	0·509351	0·3	2778	2861	–0·58
12XC04	TT	XC	4·94	29·28	0·1070	0·511055	4	–30·9	0·509248	–1·6	2975	3023	–0·46
11XC01-1	MME	XC	7·34	39·00	0·1194	0·511312	5	–25·9	0·509307	–0·7	2951	2945	–0·39
11XC01-2	MME	XC	8·91	47·76	0·1184	0·511303	8	–26·1	0·509314	–0·6	2936	2935	–0·40
11XC03	MME	XC	6·37	36·62	0·1104	0·511114	15	–29·7	0·509261	–1·7	2983	3018	–0·44
11XC06	MME	XC	6·68	33·36	0·1270	0·511434	5	–23·5	0·509302	–0·8	2996	2954	–0·35
11XC07	PG	XC	1·68	11·45	0·0930	0·510963	6	–32·7	0·509403	1·0	2745	2798	–0·53
12XC01	PG	XC	5·29	34·58	0·0971	0·510923	4	–33·5	0·509294	–1·1	2892	2968	–0·51
12XC19	GD	JHI	4·01	22·64	0·1124	0·511258	10	–26·9	0·509335	1·0	2829	2843	–0·43
12XC20	GD	JHI	5·29	28·72	0·1168	0·511166	9	–28·7	0·509167	–2·3	3099	3106	–0·41
12XC24	GD	JHI	2·78	16·35	0·1081	0·511136	10	–29·3	0·509302	–0·2	2887	2920	–0·45
12XC27	GD	JHI	5·02	35·16	0·0907	0·510859	5	–34·7	0·509321	0·1	2821	2892	–0·54
12XC15	MME	JHI	8·33	37·02	0·1428	0·511714	5	–18·0	0·509295	–0·4	3067	2937	–0·27
12XC16	MME	JHI	6·58	30·24	0·1380	0·511552	4	–21·2	0·509215	–1·9	3194	3063	–0·30
12XC29	PG	HLD	4·53	29·89	0·0962	0·510926	16	–33·4	0·509328	–1·1	2866	2945	–0·51
12XC30	PG	HLD	3·27	20·80	0·0998	0·510971	5	–32·5	0·509313	–1·4	2897	2969	–0·49

*Calculated at zircon U–Pb ages

GG, gneissic granite; TT, tonalite–trondhjemite; MME, mafic magmatic enclave; PG, potassic granite; GD, granodiorite; TL, Taili; XC, Xingcheng; JHD, Juhuadao; HLD, Huludao. Parameters used in the calculation are as follows: ^{147}Sm decay $\lambda = 6{\cdot}54 \times 10^{-12}$ a^{-1}; $(^{147}Sm/^{144}Nd)_{CHUR} = 0{\cdot}1967$; $(^{143}Nd/^{144}Nd)_{CHUR} = 0{\cdot}512638$; $(^{147}Sm/^{144}Nd)_{DM} = 0{\cdot}2137$; $(^{143}Nd/^{144}Nd)_{DM} = 0{\cdot}51315$.

elevated K_2O/Na_2O (1·17–23·04; Fig. 5d). They have low Cr, Ni, Y and Sr abundances (Table 2; Fig. 6e and f). They have fractionated REE patterns [$(La/Yb)_N$ = 21–46] and negative Eu anomalies (Eu/Eu* = 0·74–0·95), with HREE patterns being flat to concave (Fig. 7d). In PM-normalized trace element patterns (Fig. 8d), they are enriched in LILE and depleted in Nb, Ta and Ti. They are strongly depleted in Sr with moderate Sr/Y ratios of 4–59.

Bulk-rock Nd isotopic compositions

Bulk-rock Sm–Nd isotopic data for the Neoarchean TTG and potassic granitoids in the Xingcheng region are given in Table 3 and plotted in Fig. 9. Two Taili gneissic granite samples have uniform initial $^{143}Nd/^{144}Nd$ ratios (0·509320–0·509325) with $\varepsilon_{Nd}(t)$ values of –0·2 and two-stage depleted mantle Nd model ages (T_{DM2}) of 2·91–2·90 Ga. Four Xingcheng tonalite–trondhjemite samples

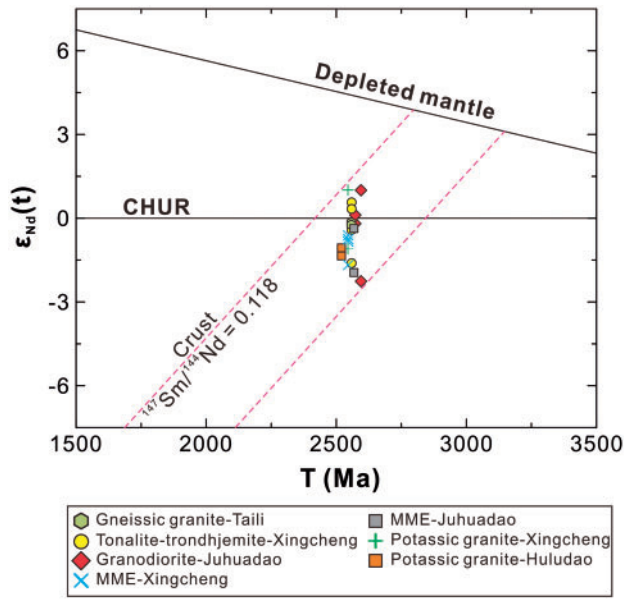

Fig. 9. $\varepsilon_{Nd}(t)$–t diagram for the Neoarchean TTG and potassic granitoids in the Xingcheng region. It should be noted that the MMEs and their host TTG have overlapping $\varepsilon_{Nd}(t)$ values. The $\varepsilon_{Nd}(t)$ values of the potassic granitoids are also indistinguishable from those of the TTG granitoids. Legends are the same as in Fig. 5.

have a narrow range of initial $^{143}Nd/^{144}Nd$ ratios (0·509248–0·509364), with $\varepsilon_{Nd}(t)$ values from –1·6 to –0·6 and two-stage depleted mantle Nd model ages (T_{DM2}) of 3·02–2·84 Ga. The MMEs within the Xingcheng tonalite–trondhjemites exhibit homogeneous initial $^{143}Nd/^{144}Nd$ ratios (0·509261–0·509314), with $\varepsilon_{Nd}(t)$ values of –1·7 to –0·6 and T_{DM2} model ages of 3·02–2·94 Ga, essentially the same as their host. Four Juhuadao granodiorite samples have initial $^{143}Nd/^{144}Nd$ ratios of 0·509167–0·509335, with $\varepsilon_{Nd}(t)$ values from –2·3 to + 1·0 and T_{DM2} model ages of 3·10–2·84 Ga. The MMEs contained within the Juhuadao granodiorites have uniform $^{143}Nd/^{144}Nd$ ratios (0·509295–0·509313), with $\varepsilon_{Nd}(t)$ values of –1·9 to –0·4 and T_{DM2} model ages of 3·06–2·94 Ga. The Xingcheng potassic granite samples have initial $^{143}Nd/^{144}Nd$ ratios of 0·509313–0·509403, with $\varepsilon_{Nd}(t)$ values of –1·4 to + 1·0 and T_{DM2} ages of 2·97–2·80 Ga. The Huludao potassic granite samples show narrow ranges of initial $^{143}Nd/^{144}Nd$ ratios (0·509313–0·509328), with $\varepsilon_{Nd}(t)$ values of –1·4 to –1·1 and T_{DM2} ages of 2·97–2·95 Ga.

Zircon Hf isotopic compositions

Zircon Hf isotopic data for these Neoarchean granitoids are given in Table 4 and plotted in Figs 10 and 11. Zircons of the Taili gneissic granite (sample 10TL13) have a narrow range of initial $^{176}Hf/^{177}Hf$ ratios (0·281207–0·281277), with $\varepsilon_{Hf}(t)$ values of + 2·0 to + 7·3 and two-stage depleted mantle Hf model ages (T_{DM2}) of 2·85–2·59 Ga, slightly younger than the Nd model ages. Zircons of the Xingcheng tonalite–trondhjemite (sample 10XC02) have uniform initial $^{176}Hf/^{177}Hf$ ratios of 0·281179–0·281242, $\varepsilon_{Hf}(t)$ values of 1·1–3·3 and T_{DM2} model ages of 2·89–2·79 Ga. Zircons from the Juhuadao granodiorite (samples 12XC22 and 12XC28) have initial $^{176}Hf/^{177}Hf$ ratios of 0·281192–0·281356, with $\varepsilon_{Hf}(t)$ values of 1·9–7·7 and T_{DM2} ages of 2·87–2·58 Ga. Zircons from the MMEs hosted within the Juhuadao granodiorite (sample 12XC15) have uniform initial $^{176}Hf/^{177}Hf$ ratios of 0·281276–0·281320, $\varepsilon_{Hf}(t)$ values of 4·8–6·3 and T_{DM2} model ages of 2·72–2·65 Ga. Zircons from the Xingcheng potassic granite (sample 10XC05) have homogeneous Hf isotopic compositions with initial $^{176}Hf/^{177}Hf$ ratios of 0·281165–0·281261, $\varepsilon_{Hf}(t)$ values of 0·2–3·7 and T_{DM2} model ages of 2·92–2·76 Ga. Zircons from the Huludao potassic granite (sample 10XC08) have relatively large range of initial $^{176}Hf/^{177}Hf$ ratios from 0·281175 to 0·281301, $\varepsilon_{Hf}(t)$ values from 0·0 to + 6·7 and T_{DM2} model ages of 2·91–2·57 Ga.

DISCUSSION

Petrogenesis of Neoarchean TTG granitoids and MMEs

TTG granitoids: partial melting of Mesoarchean enriched mafic crust at varying depths

Even though exposed in different locations and showing large compositional variation from sodic tonalite–trondhjemite-granodiorites (the Xingcheng tonalite–trondhjemites and the Juhuadao granodiorites) to potassic gneissic tonalites (the Taili gneissic tonalites), the age and isotopic data (Tables 3 and 4; Figs 9–11) suggest that the TTG granitoids in the Xingcheng region were emplaced contemporaneously and thus should share similar magma sources.

The Neoarchean TTG granitoids in the Xingcheng region have relatively high SiO_2 and low MgO, Cr and Ni contents, indicating a crustal source rather than being directly derived from the mantle (Table 2; Fig. 6d). They have bulk-rock $\varepsilon_{Nd}(t)$ values of –2·3 to 1·0 and Nd T_{DM2} model ages of 3·10–2·84 Ga (Table 3 and Fig. 9), and their zircons have positive $\varepsilon_{Hf}(t)$ values of 1·1–7·7 and Hf T_{DM2} ages of 2·89–2·62 Ga (Table 4 and Figs 10 and 11), pointing to a Mesoarchean (3·1–2·9 Ga) crustal source without the involvement of Paleo- to Eoarchean crustal materials (Fig. 11). Additionally, their major element compositions are similar to those of experimental metabasalt melts (Figs 5, 6 and 12c). However, Mesoarchean rocks in the eastern NCC are mainly TTG and to date no mafic magmatism has been reported. Some of the Mesoarchean TTG are characterized by negative zircon $\varepsilon_{Hf}(t)$ values (e.g. Tiejiashan granites in the Anshan area; Wan *et al.*, 2007; Fig. 11), which is consistent with an origin by reworking of Paleo- to Eoarchean crustal materials, and cannot act as the sources of the Neoarchean TTG granitoids in the Xingcheng region. Some Mesoarchean TTG exhibit depleted zircon Hf isotopic compositions (e.g. Mesoarchean TTG in Eastern Shandong; Liu *et al.*, 2013*a*; Wang *et al.*, 2014*b*; Wu *et al.*, 2014; Xie *et al.*, 2014; Fig. 11), which are best

Table 4: Zircon Hf isotopic compositions of the Neoarchean TTG and potassic granitoids in the Xingcheng region

Spot	t (Ma)	$^{176}Yb/^{177}Hf$	2σ	$^{176}Lu/^{177}Hf$	2σ	$^{176}Hf/^{177}Hf$	2σ	$(^{176}Hf/^{177}Hf)_i$	$\varepsilon_{Hf}(0)$	$\varepsilon_{Hf}(t)$	T_{DM1} (Ma)	T_{DM2} (Ma)	$f_{Lu/Hf}$
10TL13													
1.1	2558	0·021396	0·000256	0·000813	0·000010	0·281317	0·000019	0·281277	–51·5	4·5	2687	2724	–0·98
2.1	2558	0·010755	0·000088	0·000417	0·000003	0·281261	0·000017	0·281240	–53·4	3·2	2734	2788	–0·99
3.1	2558	0·017761	0·000150	0·000629	0·000005	0·281269	0·000021	0·281238	–53·2	3·1	2738	2792	–0·98
4.1	2558	0·034066	0·000382	0·001098	0·000009	0·281321	0·000021	0·281267	–51·3	4·2	2701	2742	–0·97
5.1	2558	0·021570	0·000583	0·000717	0·000016	0·281301	0·000021	0·281266	–52·0	4·1	2701	2743	–0·98
6.1	2558	0·025856	0·000203	0·000896	0·000005	0·281314	0·000018	0·281271	–51·5	4·3	2695	2735	–0·97
7.1	2558	0·021523	0·000138	0·000738	0·000007	0·281391	0·000019	0·281355	–48·8	7·3	2581	2588	–0·98
8.1	2558	0·038337	0·001641	0·001248	0·000055	0·281307	0·000016	0·281246	–51·8	3·4	2730	2778	–0·96
9.1	2558	0·022314	0·000333	0·000807	0·000005	0·281311	0·000017	0·281272	–51·7	4·3	2694	2733	–0·98
10.1	2558	0·034304	0·000401	0·001183	0·000014	0·281308	0·000018	0·281250	–51·8	3·6	2724	2771	–0·96
11.1	2558	0·025556	0·000157	0·000815	0·000007	0·281316	0·000021	0·281276	–51·5	4·5	2687	2725	–0·98
12.1	2558	0·024173	0·000354	0·000810	0·000008	0·281286	0·000019	0·281247	–52·5	3·4	2728	2777	–0·98
13.1	2558	0·026668	0·000325	0·000913	0·000005	0·281301	0·000018	0·281256	–52·0	3·8	2715	2760	–0·97
14.1	2558	0·024650	0·000132	0·000850	0·000008	0·281313	0·000019	0·281272	–51·6	4·3	2693	2733	–0·97
15.1	2558	0·030324	0·000237	0·001115	0·000014	0·281262	0·000020	0·281207	–53·4	2·0	2783	2846	–0·97
10XC02													
1.1	2559	0·028273	0·001198	0·001057	0·000040	0·281269	0·000016	0·281217	–53·2	2·5	2769	2828	–0·97
2.1	2559	0·035514	0·000231	0·001230	0·000006	0·281280	0·000018	0·281220	–52·8	2·5	2766	2823	–0·96
3.1	2559	0·030472	0·000438	0·001098	0·000014	0·281233	0·000014	0·281179	–54·4	1·1	2821	2894	–0·97
4.1	2559	0·049514	0·000909	0·001464	0·000021	0·281263	0·000016	0·281191	–53·4	1·5	2807	2873	–0·96
5.1	2559	0·025117	0·000266	0·000940	0·000007	0·281277	0·000015	0·281231	–52·9	2·9	2749	2803	–0·97
6.1	2559	0·023294	0·000466	0·000857	0·000013	0·281269	0·000016	0·281227	–53·2	2·8	2755	2811	–0·97
7.1	2559	0·012761	0·000269	0·000489	0·000014	0·281238	0·000016	0·281214	–54·3	2·3	2770	2834	–0·99
8.1	2559	0·021480	0·000293	0·000737	0·000008	0·281277	0·000018	0·281240	–52·9	3·3	2735	2787	–0·98
9.1	2559	0·032504	0·001190	0·001182	0·000039	0·281266	0·000015	0·281208	–53·3	2·1	2782	2844	–0·96
10.1	2559	0·015687	0·000427	0·000588	0·000014	0·281226	0·000018	0·281198	–54·7	1·7	2793	2862	–0·98
11.1	2559	0·040625	0·001890	0·001573	0·000067	0·281281	0·000019	0·281204	–52·7	2·0	2790	2851	–0·95
12.1	2559	0·025134	0·000254	0·000957	0·000016	0·281273	0·000016	0·281226	–53·0	2·7	2756	2812	–0·97
13.1	2559	0·028017	0·000446	0·001170	0·000018	0·281278	0·000014	0·281221	–52·8	2·5	2765	2822	–0·96
14.1	2559	0·027675	0·000357	0·001067	0·000012	0·281294	0·000014	0·281242	–52·3	3·3	2735	2785	–0·97
15.1	2559	0·014526	0·000375	0·000569	0·000014	0·281252	0·000017	0·281224	–53·8	2·7	2757	2816	–0·98
12XC22													
1.1	2595	0·045424	0·002526	0·001131	0·000071	0·281366	0·000027	0·281310	–49·7	6·6	2641	2654	–0·97
2.1	2595	0·057298	0·001655	0·001421	0·000040	0·281369	0·000018	0·281299	–49·6	6·2	2657	2674	–0·96
3.1	2595	0·072076	0·006100	0·001732	0·000155	0·281384	0·000026	0·281298	–49·1	6·2	2659	2675	–0·95
4.1	2595	0·041675	0·002943	0·001115	0·000082	0·281357	0·000026	0·281301	–50·1	6·3	2653	2670	–0·97
5.1	2595	0·043004	0·000431	0·001058	0·000013	0·281350	0·000021	0·281297	–50·3	6·2	2659	2677	–0·97
6.1	2595	0·043223	0·004240	0·001096	0·000102	0·281365	0·000024	0·281311	–49·8	6·6	2640	2653	–0·97
7.1	2595	0·079776	0·005050	0·001970	0·000129	0·281416	0·000025	0·281319	–47·9	6·9	2630	2639	–0·94
8.1	2595	0·053140	0·003457	0·001266	0·000078	0·281382	0·000026	0·281319	–49·2	6·9	2629	2638	–0·96
9.1	2595	0·016274	0·000590	0·000413	0·000017	0·281235	0·000024	0·281215	–54·3	3·2	2768	2821	–0·99
10.1	2595	0·026392	0·001510	0·000714	0·000038	0·281331	0·000025	0·281296	–51·0	6·1	2660	2679	–0·98
11.1	2595	0·038235	0·001065	0·000974	0·000027	0·281353	0·000024	0·281305	–50·2	6·4	2648	2663	–0·97
12.1	2595	0·058734	0·003600	0·001420	0·000079	0·281399	0·000024	0·281328	–48·6	7·3	2616	2622	–0·96
13.1	2595	0·064034	0·006086	0·001720	0·000139	0·281410	0·000028	0·281324	–48·2	7·1	2622	2629	–0·95
14.1	2595	0·054779	0·003951	0·001378	0·000099	0·281397	0·000024	0·281329	–48·6	7·3	2616	2621	–0·96
15.1	2595	0·033663	0·001252	0·000914	0·000067	0·281338	0·000021	0·281293	–50·7	6·0	2664	2684	–0·97
12XC28													
1.1	2573	0·037577	0·004067	0·001080	0·000162	0·281372	0·000022	0·281319	–49·5	6·4	2630	2646	–0·97
2.1	2573	0·044263	0·007510	0·001136	0·000198	0·281381	0·000028	0·281325	–49·2	6·7	2621	2635	–0·97
3.1	2573	0·044736	0·002953	0·001145	0·000109	0·281359	0·000023	0·281302	–50·0	5·8	2653	2675	–0·97
4.1	2573	0·045870	0·003312	0·001274	0·000064	0·281326	0·000062	0·281263	–51·2	4·4	2707	2744	–0·96
5.1	2573	0·041565	0·003475	0·001159	0·000117	0·281249	0·000105	0·281192	–53·9	1·9	2804	2868	–0·97
6.1	2573	0·035079	0·003813	0·001051	0·000094	0·281369	0·000029	0·281318	–49·6	6·4	2631	2648	–0·97
7.1	2573	0·028076	0·001309	0·000762	0·000064	0·281345	0·000021	0·281307	–50·5	6·0	2645	2666	–0·98
8.1	2573	0·043964	0·002386	0·001256	0·000044	0·281364	0·000099	0·281302	–49·8	5·8	2653	2676	–0·96
9.1	2573	0·053367	0·002264	0·001378	0·000112	0·281423	0·000034	0·281356	–47·7	7·7	2580	2581	–0·96
10.1	2573	0·045096	0·003187	0·001354	0·000141	0·281391	0·000029	0·281324	–48·8	6·6	2622	2636	–0·96
11.1	2573	0·047215	0·006264	0·001410	0·000228	0·281406	0·000044	0·281337	–48·3	7·1	2605	2614	–0·96
12.1	2573	0·052082	0·003416	0·001520	0·000067	0·281388	0·000048	0·281313	–48·9	6·2	2638	2655	–0·95
13.1	2573	0·029177	0·000996	0·000791	0·000058	0·281360	0·000029	0·281321	–49·9	6·5	2627	2642	–0·98
14.1	2573	0·028390	0·001213	0·000855	0·000067	0·281384	0·000048	0·281342	–49·1	7·3	2598	2605	–0·97
15.1	2573	0·026413	0·002856	0·000759	0·000122	0·281324	0·000025	0·281287	–51·2	5·3	2673	2702	–0·98
12XC15													
1.1	2568	0·037806	0·004644	0·001049	0·000133	0·281344	0·000021	0·281293	–50·5	5·4	2665	2693	–0·97
2.1	2568	0·038547	0·001917	0·000931	0·000039	0·281359	0·000021	0·281314	–50·0	6·1	2637	2657	–0·97
3.1	2568	0·062136	0·004203	0·001484	0·000089	0·281368	0·000022	0·281295	–49·7	5·5	2664	2689	–0·96
4.1	2568	0·070345	0·007137	0·001647	0·000162	0·281401	0·000030	0·281320	–48·5	6·3	2630	2646	–0·95
5.1	2568	0·076301	0·007758	0·002049	0·000218	0·281377	0·000020	0·281276	–49·3	4·8	2691	2722	–0·94

(continued)

Table 4: Continued

Spot	*t* (Ma)	$^{176}Yb/^{177}Hf$	2σ	$^{176}Lu/^{177}Hf$	2σ	$^{176}Hf/^{177}Hf$	2σ	$(^{176}Hf/^{177}Hf)_i$	$\varepsilon_{Hf}(0)$	$\varepsilon_{Hf}(t)$	T_{DM1} (Ma)	T_{DM2} (Ma)	$f_{Lu/Hf}$
6.1	2568	0·060050	0·001087	0·001464	0·000026	0·281364	0·000021	0·281292	−49·8	5·4	2668	2694	−0·96
7.1	2568	0·039128	0·000571	0·000972	0·000016	0·281328	0·000019	0·281280	−51·1	4·9	2682	2715	−0·97
8.1	2568	0·033227	0·000641	0·000862	0·000024	0·281330	0·000023	0·281287	−51·0	5·2	2672	2702	−0·97
9.1	2568	0·081032	0·007512	0·002283	0·000219	0·281395	0·000033	0·281283	−48·7	5·0	2683	2710	−0·93
10.1	2568	0·064137	0·004769	0·001570	0·000111	0·281374	0·000028	0·281297	−49·4	5·5	2661	2685	−0·95
11.1	2568	0·058328	0·008839	0·001662	0·000240	0·281359	0·000031	0·281278	−50·0	4·8	2688	2720	−0·95
12.1	2568	0·051725	0·003568	0·001352	0·000081	0·281357	0·000021	0·281291	−50·0	5·3	2669	2696	−0·96
13.1	2568	0·039231	0·000797	0·001054	0·000019	0·281340	0·000022	0·281289	−50·6	5·2	2671	2700	−0·97
14.1	2568	0·060534	0·003153	0·001451	0·000066	0·281379	0·000023	0·281308	−49·3	5·9	2645	2666	−0·96
10XC05													
1.1	2545	0·026440	0·000521	0·000659	0·000012	0·281204	0·000028	0·281172	−55·5	0·5	2828	2912	−0·98
2.1	2545	0·022417	0·000499	0·000568	0·000013	0·281213	0·000023	0·281185	−55·1	1·0	2809	2888	−0·98
3.1	2545	0·060909	0·001075	0·001205	0·000016	0·281294	0·000026	0·281236	−52·3	2·8	2745	2800	−0·96
4.1	2545	0·027440	0·000169	0·000599	0·000003	0·281260	0·000024	0·281231	−53·5	2·6	2748	2809	−0·98
5.1	2545	0·042667	0·001063	0·000995	0·000021	0·281227	0·000025	0·281179	−54·6	0·7	2821	2900	−0·97
6.1	2545	0·042172	0·000970	0·001071	0·000021	0·281313	0·000021	0·281261	−51·6	3·7	2709	2756	−0·97
7.1	2545	0·024619	0·001694	0·000582	0·000037	0·281216	0·000024	0·281188	−55·0	1·1	2805	2883	−0·98
8.1	2545	0·040373	0·000296	0·000916	0·000008	0·281223	0·000023	0·281178	−54·8	0·7	2821	2901	−0·97
9.1	2545	0·035771	0·000697	0·001051	0·000021	0·281275	0·000018	0·281224	−52·9	2·3	2760	2821	−0·97
10.1	2545	0·045724	0·000515	0·001042	0·000011	0·281233	0·000020	0·281182	−54·4	0·9	2816	2893	−0·97
11.1	2545	0·019801	0·000175	0·000451	0·000005	0·281251	0·000022	0·281229	−53·8	2·5	2749	2811	−0·99
12.1	2545	0·041392	0·000277	0·000834	0·000005	0·281258	0·000025	0·281218	−53·5	2·1	2767	2831	−0·97
13.1	2545	0·067286	0·001685	0·001300	0·000029	0·281228	0·000025	0·281165	−54·6	0·2	2842	2924	−0·96
14.1	2545	0·029115	0·000116	0·000570	0·000003	0·281270	0·000023	0·281242	−53·1	3·0	2733	2789	−0·98
15.1	2545	0·082453	0·001516	0·001588	0·000018	0·281313	0·000025	0·281235	−51·6	2·7	2747	2801	−0·95
10XC08													
1.1	2520	0·056771	0·000951	0·001237	0·000017	0·281360	0·000022	0·281301	−49·9	4·5	2657	2695	−0·96
2.1	2520	0·030677	0·000956	0·000675	0·000024	0·281239	0·000023	0·281206	−54·2	1·1	2782	2860	−0·98
3.1	2520	0·033572	0·000340	0·000786	0·000012	0·281294	0·000026	0·281256	−52·3	2·9	2716	2773	−0·98
4.1	2520	0·052554	0·001893	0·000990	0·000026	0·281340	0·000023	0·281293	−50·6	4·2	2667	2709	−0·97
5.1	2520	0·031436	0·001854	0·000638	0·000035	0·281270	0·000023	0·281239	−53·1	2·3	2738	2802	−0·98
6.1	2520	0·025497	0·000282	0·000561	0·000007	0·281279	0·000022	0·281252	−52·8	2·8	2720	2780	−0·98
7.1	2520	0·044377	0·000628	0·000849	0·000005	0·281309	0·000022	0·281268	−51·7	3·3	2699	2751	−0·97
8.1	2520	0·036333	0·001111	0·000799	0·000024	0·281240	0·000025	0·281201	−54·2	1·0	2789	2868	−0·98
9.1	2520	0·051620	0·001260	0·001077	0·000016	0·281227	0·000026	0·281175	−54·6	0·0	2827	2913	−0·97
10.1	2520	0·046460	0·000272	0·000993	0·000003	0·281291	0·000022	0·281243	−52·4	2·5	2734	2795	−0·97
11.1	2520	0·024366	0·001238	0·000539	0·000025	0·281248	0·000023	0·281222	−53·9	1·7	2760	2832	−0·98
12.1	2520	0·049782	0·000379	0·001058	0·000006	0·281300	0·000024	0·281249	−52·1	2·7	2726	2785	−0·97
13.1	2520	0·056384	0·000961	0·001097	0·000021	0·281243	0·000023	0·281190	−54·1	0·5	2807	2888	−0·97
14.1	2520	0·135431	0·002583	0·002276	0·000027	0·281473	0·000024	0·281364	−45·9	6·7	2572	2584	−0·93
15.1	2520	0·033383	0·000407	0·000673	0·000007	0·281301	0·000020	0·281269	−52·0	3·3	2698	2751	−0·98
16.1	2520	0·053345	0·000302	0·001074	0·000010	0·281352	0·000024	0·281300	−50·2	4·5	2656	2695	−0·97
17.1	2520	0·112112	0·001007	0·002057	0·000013	0·281354	0·000030	0·281255	−50·1	2·9	2724	2775	−0·94
18.1	2520	0·056625	0·001730	0·001038	0·000015	0·281289	0·000023	0·281239	−52·5	2·3	2740	2803	−0·97
19.1	2520	0·066692	0·001562	0·001128	0·000030	0·281238	0·000025	0·281183	−54·3	0·3	2817	2900	−0·97

[a]Calculated at zircon U–Pb ages.
Parameters used in the calculation are as follows: ^{176}Lu decay $\lambda = 1{\cdot}867 \times 10^{-11}$ a^{-1}; average continental crust $^{176}Lu/^{177}Hf = 0{\cdot}015$; $(^{176}Lu/^{177}Hf)_{CHUR} = 0{\cdot}0332$; $(^{176}Hf/^{177}Hf)_{CHUR} = 0{\cdot}282772$; $(^{176}Lu/^{177}Hf)_{DM} = 0{\cdot}0384$; $(^{176}Hf/^{177}Hf)_{DM} = 0{\cdot}28325$.

explained as resulting from melting of mantle-derived basaltic materials of Mesoarchean age. This would point to the existence of Mesoarchean juvenile mafic magmatism in the eastern NCC. Furthermore, the wide range of SiO_2 contents of the Neoarchean TTG granitoids and their MMEs required a mafic precursor instead of felsic sources like TTG. All these observations and inferences indeed suggest that the Neoarchean TTG granitoids in the Xingcheng region must have been derived from Mesoarchean juvenile mafic crustal sources.

The Neoarchean TTG granitoids in the Xingcheng region show large major and trace element compositional variation, with enrichment of LILE (e.g. Rb, Ba and Sr) and depletion of HFSE (e.g. Nb, Ta and Ti) (Figs 5–9). As suggested previously (e.g. Moyen *et al.*, 2007, 2010), the compositions of TTG are mainly controlled by the source compositions and the pressures or depths of melting. The enrichment of LILE (Figs 6a and 8) and relatively higher K_2O/Na_2O of the studied TTG granitoids suggest that their Mesoarchean juvenile mafic sources should be more enriched than those of the typical sodic TTG (typical Archean TTG $K_2O/Na_2O = 0{\cdot}35$; Moyen & Martin, 2012; Fig. 5d). Therefore, the Neoarchean TTG granitoids in the Xingcheng region are probably derived from Mesoarchean mafic crustal rocks that are more enriched than the present-day mid-ocean ridge basalt (MORB) [enriched (E)-MORB-like?] (Smithies, 2000; Qian & Hermann, 2013). An enriched mafic source has also been proposed to explain the compositions of TTG in other Archean cratons (e.g. Champion & Smithies, 2007; Moyen *et al.*, 2007; Smithies *et al.*, 2009). In addition, most Archean mafic magmatic rocks are characterized

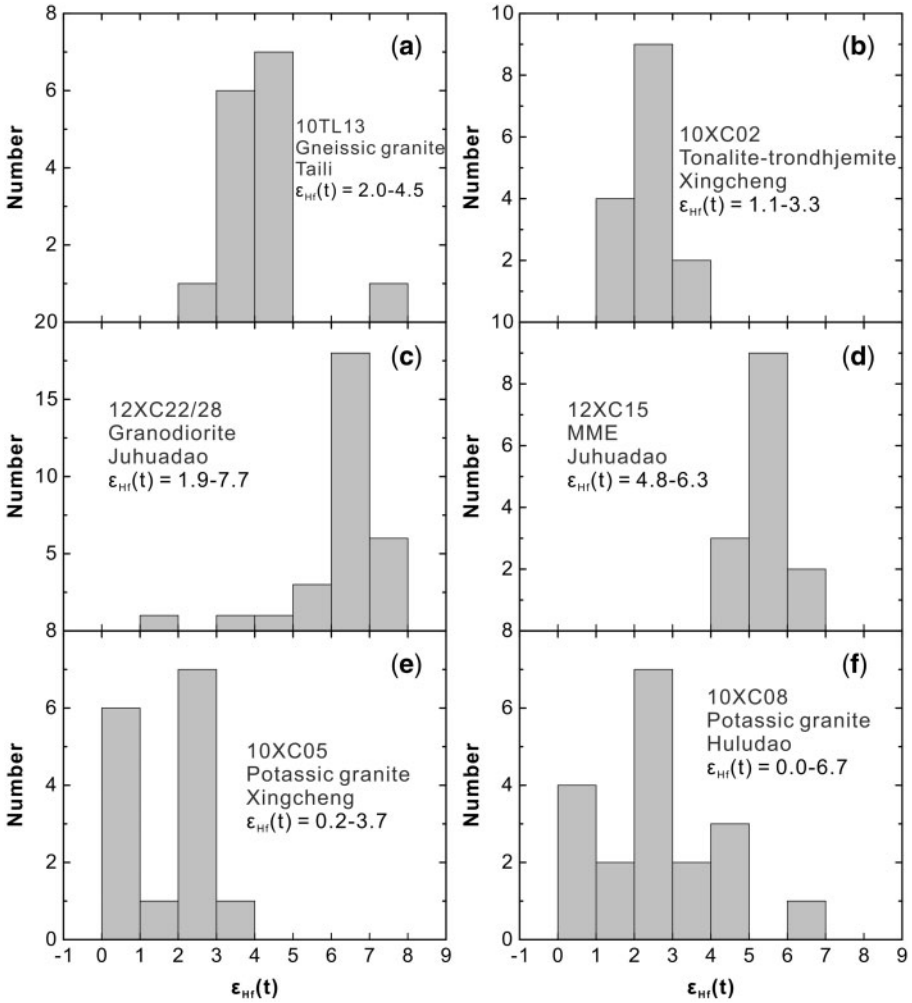

Fig. 10. Histograms of $\varepsilon_{Hf}(t)$ values for the zircons from the Neoarchean TTG and potassic granitoids in the Xingcheng region. It should be noted that the $\varepsilon_{Hf}(t)$ values of zircons from the Taili gneissic granite and the Xingcheng tonalite–trondhjemite are similar. The same goes for the Juhuadao granodiorite and the hosted MMEs; their $\varepsilon_{Hf}(t)$ values are slightly higher than those of the the Taili gneissic granite and the Xingcheng tonalite–trondhjemite. The $\varepsilon_{Hf}(t)$ values of zircons from the Xingcheng potassic granites are similar to those of the Huludao potassic granites.

by somewhat enriched trace element signatures (Jahn *et al.*, 1980; Condie, 2005*a*; Hollings & Kerrich, 2006; Moyen & Martin, 2012; van Hunen & Moyen, 2012). It should be noted that to accurately determine the nature and the enrichment mechanism of the Mesoarchean enriched mafic crustal rocks is not straightforward because no Mesoarchean mafic magmatism has been reported in the eastern NCC. It is possible that the enrichment reflects a prior mantle source metasomatism caused by recycled even earlier crustal components (Smithies *et al.*, 2009).

The Xingcheng tonalite-trondhjemites, the Taili gneissic tonalites and some of the Juhuadao granodiorites are characterized by high $(La/Yb)_N$ and Sr/Y ratios and thus plot in the TTG–adakite field in the $(La/Yb)_N$–$(Yb)_N$ and Sr/Y–Y diagrams (Fig. 12a and b), suggesting the presence of garnet as a residual phase in the magma source region. They all have positive or slightly negative Eu anomalies and belong to the high-Sr series defined by Moyen *et al.* (2007), implying that there was no or little plagioclase left in the magma sources (Fig. 7). In Fig. 13, the pressure-controlled ΔX parameters on the vertical axes for these samples suggest that they were formed at higher pressures than the other samples, reflecting the presence or absence of some pressure-sensitive minerals such as garnet, plagioclase and rutile in the magma sources (Moyen *et al.*, 2010). Thus these samples were most probably derived from mafic crustal sources at relatively high pressures (~10–12 kbar), with garnet and amphibole present as residual phases with little or no plagioclase (Rapp *et al.*, 1991; Sen & Dunn, 1994; Qian & Hermann, 2013). Geochemical modeling illustrated in Fig. 12a shows that they could be generated by 10–25% partial melting of a mafic crustal source (E-MORB-like) with varying proportions of garnet. Thus, the appropriate source lithology for samples with high Sr/Y and $(La/Yb)_N$ ratios is likely to be garnet amphibolite rather than eclogite. These samples should correspond to the medium-pressure group of TTGs defined by Moyen (2011).

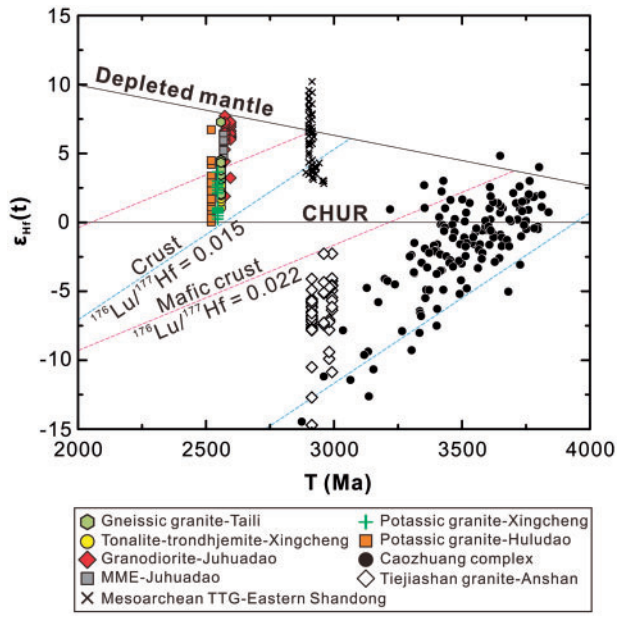

Fig. 11. Comparison of Hf isotopes of zircons from the Neoarchean TTG and potassic granitoids in the Xingcheng region with those of zircons from the Caozhuang complex and the Mesoarchean TTGs in Eastern Shandong and Anshan; the zircon Hf isotope data are from Wu *et al.* (2005*a*, 2014), Wan *et al.* (2007), Liu *et al.* (2013*a*, 2013*b*), Wang *et al.* (2014*b*) and Xie *et al.* (2014). It should be noted that almost all the data fall between the evolution lines of the depleted mantle and the chondritic uniform reservoir (CHUR). Paleo- to Eoarchean crustal materials were not involved in the generation of the Neoarchean TTG and potassic granitoids as the Paleo- to Eoarchean zircons and Mesoarchean granitoids derived from Paleo- to Eoarchean crustal materials exhibit a different evolutionary trend. The Mesoarchean TTGs in Eastern Shandong were derived from juvenile mafic sources, and the Neoarchean granitoids in the Xingcheng region may be derived from these Mesoarchean TTGs and their juvenile mafic sources.

In contrast, other samples of the Juhuadao granodiorites are distinct in having lower Sr, Sr/Y and $(La/Yb)_N$, higher Y, and negative Eu and Sr anomalies (Fig. 6e and f), plotting in the field of typical arc rocks in $(La/Yb)_N$–$(Yb)_N$ and Sr/Y–Y diagrams (Fig. 12a and b). However, they are similar to samples with high Sr/Y and $(La/Yb)_N$ ratios in terms of major elements and bulk-rock Nd and zircon Hf isotopic compositions. Thus, they may be derived from a similar Mesoarchean mafic crustal source, but at lower pressures (<10 kbar) (Qian & Hermann, 2013), which is further supported by the relative positions of these samples compared with their high-pressure counterparts in Fig. 13. The obvious negative Eu and Sr anomalies of these samples (Figs 7 and 8) are best explained by the presence of plagioclase as a residual phase during partial melting, although the effect of plagioclase crystallization cannot be ruled out. The relatively flat to concave HREE patterns also point to the presence of amphibole as a residual phase. Geochemical modeling, illustrated in Fig. 12a, shows that they could be generated by partial melting of a mafic crustal source (E-MORB-like) metamorphosed into garnet-free amphibolite. The appropriate source lithology for these samples with lower Sr/Y and $(La/Yb)_N$ ratios should be amphibolite (Foley *et al.*, 2002), corresponding to a shallower depth and the medium-pressure group of TTG defined by Moyen (2011). Therefore, it is reasonable to conclude that the Neoarchean TTG in the Xingcheng region resulted from partial melting of an enriched basaltic protolith at varying depths (Moyen, 2011).

The bulk-rock Nd isotopic compositions of the Neoarchean TTG granitoids in the Xingcheng region have a small range of variation around chondritic values (Table 3; Fig. 9), whereas their zircon Hf isotopic compositions show larger variation from chondritic to depleted mantle values (Table 4; Figs 10 and 11). Some would explain such differential variation as the result of the shorter half-life of ^{176}Lu (36 Ga) relative to that of ^{147}Sm (108 Ga) and the variation of Lu/Hf ratios being larger than that of Sm/Nd ratios during partial melting processes, resulting in the fact that, during a given timespan, the variation of $^{176}Hf/^{177}Hf$ is larger than that of $^{143}Nd/^{144}Nd$ (Wu *et al.*, 2007). On the other hand, zircons can record changes of the ambient melts during their growth and crystallization. It is common that zircons yield homogeneous U–Pb ages but with heterogeneous Hf isotopic compositions, which is interpreted by some as resulting from replenishment of magmas from distinctively different sources (e.g. Griffin *et al.*, 2002; Belousova *et al.*, 2006; Yang *et al.*, 2008; Zeh *et al.*, 2009). This interpretation advocates open-system magma evolution and most probably reflects the involvement of Neoarchean juvenile mantle-derived melts rather than the contribution of heterogeneous sources, as their bulk-rock Nd isotopic compositions are relatively homogeneous. In the magmatic process, the bulk-rock Nd isotopic compositions of the magmas did not significantly change if the addition of juvenile mantle-derived mafic melts was not obvious; thus, the contaminated magmas had bulk-rock Nd isotopic compositions similar to the original magmas and the bulk-rock Nd isotopic compositions may record more reliable information about the crustal residence time of the source materials (Wan *et al.*, 2015). Juvenile mantle-derived mafic magmatism has been reported to take place in the eastern NCC during the Neoarchean (e.g. Wan *et al.*, 2010; Bai *et al.*, 2016, and references therein), which may provide heat to trigger partial melting of the Mesoarchean mafic crustal source for the granitoid magmatism we discuss here, and also contribute to the compositional complexities of our samples (Figs 9–11).

In summary, the Neoarchean TTGs in the Xingcheng region were sourced from partial melting of a Mesoarchean lower crustal source, at varying depths and pressures, heated and contaminated by Neoarchean juvenile mantle-derived mafic magmas.

MMEs: cumulates resulting from fractional crystallization of the TTG granitoids

The TTG granitoids in the Xingcheng region show large compositional variation (Fig. 6), which is probably the combined effect of modal mineralogy variation and

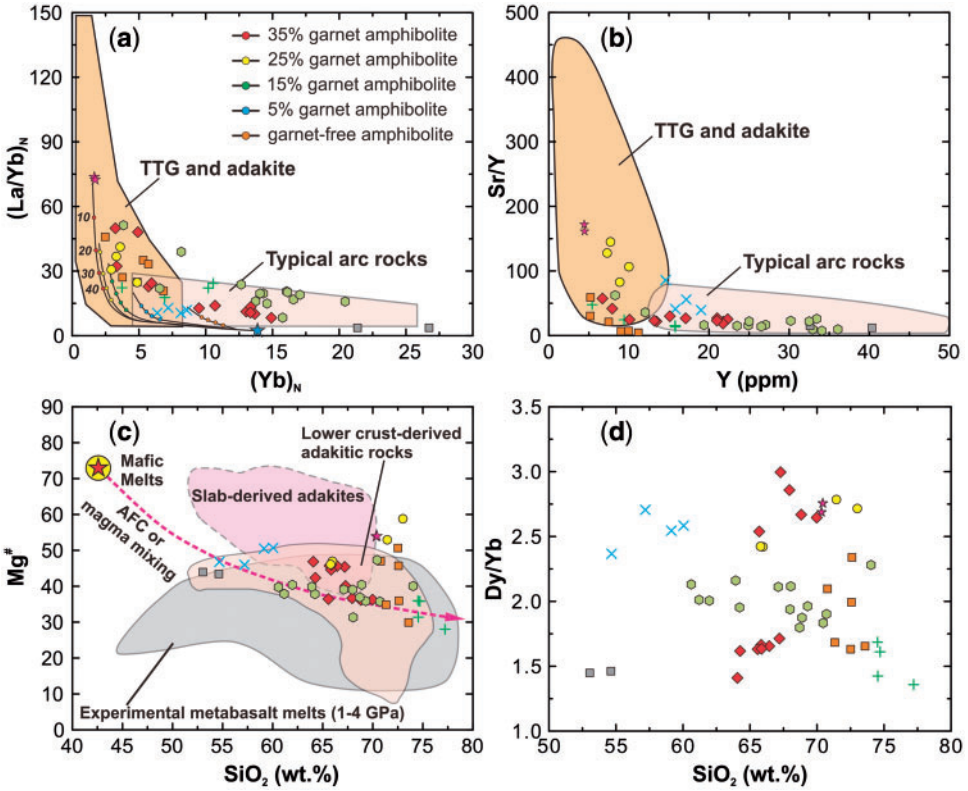

Fig. 12. Co-variation diagrams of (a) chondrite-normalized $(La/Yb)_N$ vs $(Yb)_N$, (b) Sr/Y vs Y, (c) Mg# vs SiO_2 and (d) Dy/Yb vs SiO_2 for the Neoarchean TTG and potassic granitoids in the Xingcheng region. In (a), batch melting curves of an E-MORB-like source (Sun & McDonough, 1989) were constructed using the partition coefficients of Bédard (2006). In (c), a crustal AFC process involving mantle-derived mafic melts is from Yang *et al.* (2008). Data sources in (c) are the same as for Figs 5 and 6d. Symbols are the same as in Fig. 5.

fractional crystallization. The slightly concave HREE patterns of some samples indicate that amphibole might be a fractionating phase, as well as being a residual phase in the source (Fig. 7). Furthermore, the Sr concentrations show negative correlation with SiO_2, implying the role of plagioclase as a crystallizing phase. The 'fan-like' HREE patterns of TTG–adakitic granitoids (Fig. 8) have commonly been explained as the result of fractional crystallization of garnet-bearing assemblages at high pressure (e.g. Macpherson *et al.*, 2006). However, this is not the case for the TTG granitoids in the Xingcheng region mainly for the following reasons: (1) there is no increase of Dy/Yb with differentiation (Fig. 12d), which should be expected if garnet ($D_{Yb}/D_{Dy} > 1$) was a liquidus phase; (2) crystallization of garnet from TTG magmas needs a high-pressure condition over 14 kbar (e.g. Adam *et al.*, 2012; Hoffmann *et al.*, 2014; Song *et al.*, 2014); (3) in partial melts (usually tonalitic) of mafic rocks, as calculated by Hoffmann *et al.* (2014), the potential of garnet as a fractionating phase is limited. Therefore, low-pressure (<10 kbar) fractional crystallization of amphibole and plagioclase should contribute to the evolution of the TTG granitoids in the Xingcheng region, as evident by the existence of MMEs within them. We performed trace element geochemical modelling of fractional crystallization of amphibole and plagioclase from the TTG granitoid sample with the lowest SiO_2 content, but, as pointed out by Moyen *et al.* (2007, 2010), fractional crystallization of this assemblage has limited effects on the compositions of the TTG granitoids (results not shown).

MMEs are common in intermediate to felsic granitoids within continental arcs and collisional belts. Various models have been proposed to explain the origin of MMEs, including recrystallized and refractory restite (Chappell *et al.*, 1987; Chappell, 1999; Chen *et al.*, 2014), inclusion of mafic magma derived from the mantle (Vernon, 1984; Holden *et al.*, 1987; Chen *et al.*, 2002; Yang *et al.*, 2007) or early crystallized cumulates (Wall *et al.*, 1987; Niu *et al.*, 2013; Huang *et al.*, 2014; Chen *et al.*, 2015). The MMEs hosted in the TTG granitoids in the Xingcheng region are coeval with their host and have almost overlapping bulk-rock Nd isotopic compositions (Fig. 9), implying a genetic connection. The relatively low contents of MgO, Cr and Ni imply that they were not mantle-derived melts. Several observations are supportive of a cumulate origin for the MMEs: (1) the MMEs have essentially the same mineral assemblages as their host, except for lacking K-feldspar, which is a later liquidus phase, and match the predicted low-pressure fractional crystallization assemblage of the TTG granitoids; (2) the MMEs have higher HREE

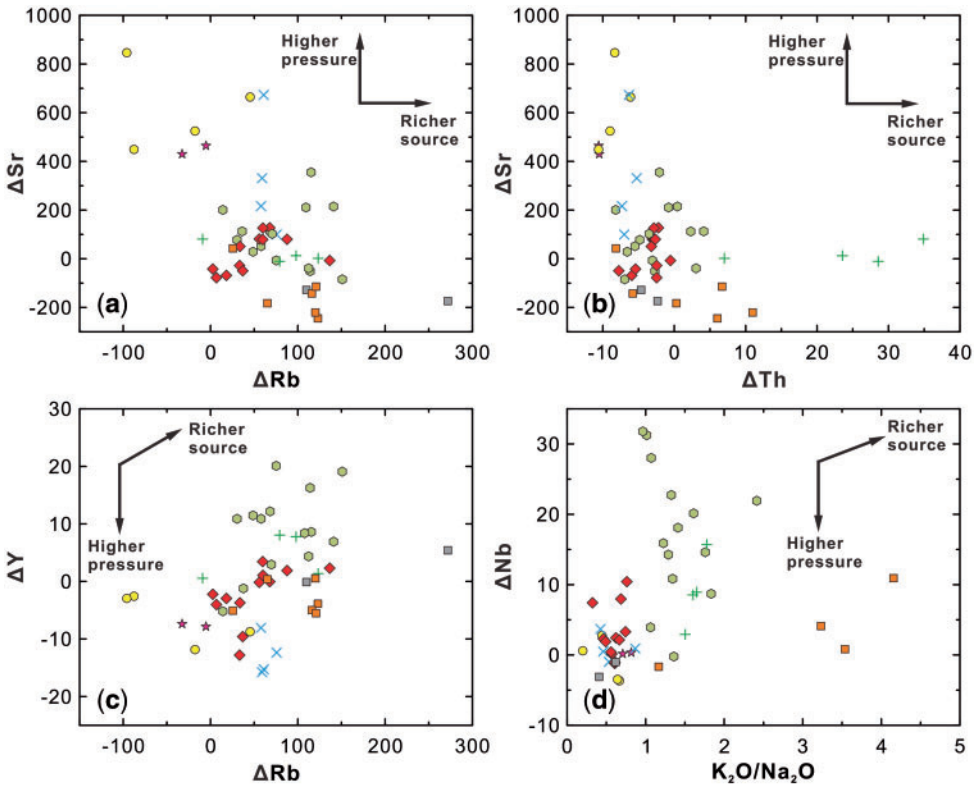

Fig. 13. (a) ΔSr vs ΔRb, (b) ΔSr vs ΔTh, (c) ΔY vs ΔRb and (d) ΔNb vs K_2O/Na_2O for the Neoarchean granitoids in the Xingcheng region. For *X* as any given element, the Δ*X* parameter is given by $\Delta X = X - (aSiO_2 + b)$; constants *a* and *b* were empirically estimated by Moyen *et al.* (2010) and express the distance between the analyzed value and a reference line in an *X*–SiO_2 (Harker) diagram, which removes the contribution of SiO_2-related evolution. The vertical axes of these diagrams are for pressure-controlled elements and the horizontal axes for source enrichment-controlled elements or ratios. These diagrams can simultaneously reveal information about both the source composition or enrichment and the depth or pressure of melting. Vectors showing the trends of these parameters towards higher pressures and more enriched sources are from Moyen *et al.* (2010). It should be noted that two Huludao potassic granites with extremely high K_2O/Na_2O ratios were omitted in (d). Legends are the same as in Fig. 5.

abundances than their hosts, and their hosts exhibit fan-shaped REE patterns with the negative Yb–SiO_2 correlation (figure not shown); (3) the MMEs and their hosts have overlapping and indistinguishable bulk-rock Nd and zircon Hf isotopic compositions (Figs 9–11). Therefore, these MMEs are most consistent with an origin as early crystallized cumulates that were mixed into the magma by periodic replenishment of magma and subsequent induced convection in the magma chamber (Chen *et al.*, 2015, 2016).

Petrogenesis of potassic granitoids

In most Archean cratons (e.g. Barberton, Dharwar, Zimbabwe and Slave cratons; Bleeker, 2003; Moyen *et al.*, 2003), potassic granitoids are widespread and voluminous and show a great compositional diversity such as CA1-type (Archean calc-alkaline granites formed by partial melting of the mid- to lower continental crust under granulite-facies conditions leaving plagioclase and othopyroxene as residual phases), CA2-type (Archean calc-alkaline granites formed by partial melting of the lower continental crust under granulite-facies conditions but leaving plagioclase and garnet as residual phases), sanukitoid suite, A-type and S-type (Sylvester, 1994; Jayananda *et al.*, 2006), which then played an important role in balancing the average compositions of the upper continental crust. Such a compositional diversity indicates a variety of processes, such as the involvement of various sources melted at different depths and fractional crystallization.

Three types of potassic granitoid have been recognized in the studied region: (1) the Taili gneissic granites; (2) Xingcheng potassic granites; (3) Huludao potassic granites. Their ages range from 2558 to 2520 Ma. These potassic granitoids could be generated through various scenarios, such as (1) (low-degree?) remelting of former TTG, (2) low-degree melting of enriched [E-MORB or ocean island basalt (OIB) affinity] mafic crustal sources, (3) low-degree partial melting of an enriched mantle, (4) final products of fractional crystallization of felsic magmas, or (5) high-degree fractionation of hydrous medium- to high-K basaltic magmas.

It should be noted that the potassic granitoids in the Xingcheng region form linear trends with the TTG in Harker variation diagrams (Fig. 6) and have almost indistinguishable bulk-rock Nd and zircon Hf isotopic compositions from the TTG granitoids, which points to

the possibility that these potassic granites might be the final products of fractionation of the TTG magmas. However, as the gap between formation ages of the TTG granitoids (2595–2558 Ma) and the potassic granites (2545–2520 Ma) is large, it is difficult to envisage that such a long-lived fractionation process of relatively cool and viscous felsic TTG magmas could generate these potassic granites. Potassium-rich felsic melts can also be produced through high degrees of fractionation of hydrous medium- to high-K basaltic magmas, especially under high-pressure conditions (e.g. Sisson *et al.*, 2005), but the absence of contemporaneous K-rich basaltic magmas in the Xingcheng region and the confined range of SiO_2 contents of these potassic granites preclude this scenario as the generation mechanism of the potassic granites.

Taili gneissic granites: melting of Mesoarchean enriched mafic crust at low-pressure hybridized with Neoarchean mantle-derived mafic melts

The Taili gneissic granites are characterized by relatively high K_2O contents and are distinct from the TTG granitoids (Fig. 6a). In Fig. 13, the source composition-controlled ΔX parameters on the horizontal axes of these diagrams indicate that they should be sourced from a more enriched source compared with that of the TTG granitoids, which is also reflected by their enriched LILE concentrations (Fig. 8a). Their bulk-rock Nd and zircon Hf T_{DM2} ages point to a source that was ultimately extracted from the mantle in the Mesoarchean (Tables 3 and 4). The Taili high-K gneissic granites have low Y and Sr abundances (Fig. 6e and f) and show negative Eu and Sr anomalies (Figs 7a and 8a). Their pressure-controlled ΔX parameters also imply that they should be formed under lower pressures (Fig. 13).

Some Taili high-K gneiss samples are characterized by low SiO_2 (five samples <65 wt %), elevated TiO_2, P_2O_5 and MgO contents (Fig. 6b, c and d), as well as higher compatible trace elements such as Cr and Ni (Table 2), which can exclude the possibility of remelting of former TTG and final products of fractionation crystallization of felsic magmas. The coupled enrichment in LILE and compatible trace elements strongly indicates the contribution of a component with a mantle signature (Miller *et al.*, 2008), which is also supported by the zircon Hf isotopic composition [$\varepsilon_{Hf}(t) > +2$] of the Taili gneissic granites (Figs 10 and 11). One zircon gives $\varepsilon_{Hf}(t)$ of 7·3 and T_{DM2} of 2588 Ma, implying hybridization of a Neoarchean, juvenile, mantle-derived magma. The negative but near-chondritic $\varepsilon_{Nd}(t)$ values (–0·2) suggest little crustal contamination, if any. In the Mg#–SiO_2 diagram (Fig. 12c), these rocks follow an assimilation–fractional crystallization (AFC) or magma mixing trend of mantle-derived mafic melts. Therefore, it is reasonable to conclude that the Taili high-K gneissic granites were produced from low-pressure melts of Mesoarchean E-MORB- or OIB-like enriched mafic crust with hybridization of Neoarchean juvenile mantle-derived mafic melts. It should be noted that fractional crystallization could also contribute to the compositional variation, but it should be a second-order effect.

Huludao potassic granites: remelting of Mesoarchean TTG at low pressure

The 2520 Ma Huludao potassic granites are characterized by subvertical trends in the K_2O–SiO_2 diagram (Fig. 6a), and they have relatively high K_2O/Na_2O ratios (Fig. 5d) and LILE concentrations (Fig. 8d). These potassic granites also define a trend towards a more enriched source compared with that of the TTG granitoids in Fig. 13. In addition, they are all peraluminous with A/CNK ratios of 1·14–1·20 (Fig. 5c). These geochemical features are usually attributed to partial melting of comparatively enriched and relatively potassic sources (Moyen *et al.*, 2007). Like the TTG granitoids, their bulk-rock Nd and zircon Hf isotopic compositions point to a source that was extracted from the mantle during the Mesoarchean (Table 4). Thus the likely source of these potassic granites might be the Mesoarchean TTG sourced from juvenile mantle-derived rocks (Fig. 11). Based on field and experimental investigations, some researchers proposed that Archean potassic granites result from partial melting of former TTG and represent the products of within-crust differentiation (Moyen *et al.*, 2001, 2003; Castro, 2003; Whalen *et al.*, 2004; Patiño Douce, 2005; Watkins *et al.*, 2007; Xiao & Clemens, 2007). Partial melting of TTG is usually related to the breakdown of amphibole and biotite, which releases potassium into the melt (Watkins *et al.*, 2007). However, partial melting of typical sodic TTG will generate relatively sodic melts and only if the source comprises potassic TTG will the partial melts be enriched in K_2O (Patiño Douce & Beard, 1995; Skjerlie & Johnston, 1996; Castro, 2003; Watkins *et al.*, 2007). As estimated above, the TTG granitoids in the Xingcheng region should be sourced from a Mesoarchean enriched mafic crustal source and it is highly likely that there exist some potassic TTG derived from these enriched sources. Remelting of these relatively potassic TTG would facilitate the generation of the Huludao potassic granites. However, it should be noted that these potassic granites are unlikely to be derived from the contemporaneous TTG granitoids as there are no signs of partial melting observed in these lithologies. The potassic granites have lower concentrations of Y and Sr (Fig. 6e and f), and are characterized by negative Sr and Eu anomalies (Figs 7d and 8d), implying the presence of plagioclase and the absence of garnet in the source. Also, in Fig. 13 they show a trend towards lower pressures of melting. Therefore these potassic granites are best explained as parental melts resulting from relatively low-pressure melting. It should be noted that some of the potassic granites have higher $(La/Yb)_N$ and Sr/Y ratios and accordingly plot in the TTG and adakite field in Fig. 12a and b. A possible explanation for this

feature could be inheritance from their TTG source rocks.

Xingcheng potassic granites: low-degree partial melting of enriched mafic crust

Experimental investigations have suggested that low degrees of partial melting (<20%) of alkali metabasalt could lead to potassic felsic melts (e.g. Sen & Dunn, 1994) as potassium is highly incompatible during partial melting (Qian & Hermann, 2013). The 2545 Ma Xingcheng potassic granites are metaluminous with A/CNK ratios of 0·87–1·06 (Fig. 5c) and have obvious negative Eu anomalies (Fig. 7d). They exhibit distinct geochemical features from the potassic granites in many Archean cratons; that is, relatively high Sr/Y and $(La/Yb)_N$ ratios, falling in or near the TTG–adakite fields in Fig. 12a and b, which are similar to the potassic C-type adakites of mafic crust origin (Rapp *et al.*, 2002). Their middle REE (MREE)-depleted patterns (Fig. 7d) are also similar to some post-collisional, potassic granites in the Paleozoic North Qaidam ultrahigh-pressure metamorphic belt (Wang *et al.*, 2014*a*). Additionally, they plot in the fields of experimental metabasalt melts, implying that they might be sourced by partial melting of mafic rocks. These potassic granites show concave HREE patterns, implying that amphibole should be left in the residue or be a fractionating phase. As illustrated in Fig. 12a, the Xingcheng potassic granites could be generated by low degrees (<20%) of partial melting of an enriched mafic source metamorphosed to garnet amphibolite, with varying proportions of garnet. Importantly, these potassic granites have similar bulk-rock Nd and zircon Hf isotopic compositions to those of the coexisting TTG granitoids (Figs 9–11). Therefore, the potassic granites and the TTG granitoids probably share the same Mesoarchean enriched mafic crustal sources. Considering the fact that these potassic granites have fairly high SiO_2 contents (up to 76·11 wt %), low-degree partial melting of an enriched mafic source might be able to facilitate the generation of the potassic granites in the Xingcheng region. Compared with the Taili gneissic granites, they have a narrow range of high SiO_2 contents, implying limited interaction with Neoarchean mantle-derived mafic melts.

Table 5: Average compositions of TTG granitoids and potassic granites and calculated composition of Archean upper continental crust in the Xingcheng–Qinhuangdao region

	Average TTG granitoids	Average potassic granites	Calculated TTG granitoids/potassic granites= 9:1	Upper continental crust
Major elements (wt %)				
SiO_2	65·72	73·79	66·52	66·6
TiO_2	0·52	0·16	0·48	0·64
Al_2O_3	15·43	13·55	15·24	15·4
Fe_2O_{3T}	4·43	1·25	4·11	5·04
MnO	0·06	0·02	0·06	0·1
MgO	1·73	0·32	1·59	2·48
CaO	3·08	0·78	2·85	3·59
Na_2O	4·37	2·95	4·23	3·27
K_2O	3·18	5·98	3·46	2·8
P_2O_5	0·23	0·06	0·22	0·15
K_2O/Na_2O	0·73	2·03	0·82	0·86
Trace elements (ppm)				
V	58	19	54	97
Cr	31	7	29	92
Co	9·1	1·7	8·4	17·3
Ni	15	4	14	47
Cu	19	8	18	28
Zn	67	42	65	67
Ga	18·0	15·5	17·8	17·5
Rb	129	216	138	82
Sr	630	209	588	320
Y	16	11	16	21
Zr	184	133	179	193
Nb	13	9	13	12
Cs	2·6	2·6	2·6	4·9
Ba	904	943	908	628
La	37	31	36	31
Ce	78	58	76	63
Pr	9·0	5·6	8·6	7·1
Nd	33·3	18·3	31·8	27·0
Sm	5·6	2·9	5·3	4·7
Eu	1·3	0·6	1·2	1·0
Gd	4·4	2·4	4·2	4·0
Tb	0·5	0·3	0·5	0·7
Dy	2·9	1·9	2·8	3·9
Ho	0·55	0·38	0·53	0·83
Er	1·5	1·1	1·5	2·3
Tm	0·2	0·2	0·2	0·3
Yb	1·4	1·3	1·4	2·0
Lu	0·21	0·20	0·21	0·31
Hf	4·2	3·5	4·1	5·3
Ta	0·9	0·8	0·9	0·9
Pb	17·4	26·5	18·3	17
Th	7·7	21·5	9·1	10·5
U	1·7	3·5	1·9	2·7

The composition of present-day upper continental crust is also listed for comparison (Rudnick & Gao, 2003).

Neoarchean magmatism and crustal growth in the NCC

Zircon U-Pb dating reveals that the TTG and potassic granitoids in the studied region were emplaced at 2595–2520 Ma; that is, over ~75 Myr towards the end of the Neoarchean. The age data statistics of the Archean basement rocks in the NCC also show that the Late Neoarchean (2·6–2·5 Ga) was an important period of magmatism (Yang *et al.*, 2009; Geng *et al.*, 2010; Nutman *et al.*, 2011; Sun *et al.*, 2012), with widespread TTG suites, ultramafic to mafic igneous rocks, charnockites and granites (Zhao *et al.*, 2001, 2005).

The TTG granitoids and potassic granites in the Xingcheng region have bulk-rock Nd and zircon Hf model ages ranging between 3·0 and 2·6 Ga (Tables 3 and 4; Figs 9–11), suggesting that no older (>3·0 Ga) sources were involved in their genesis. All zircons from these rocks have positive $\varepsilon_{Hf}(t)$ and fall between the evolution lines of the depleted mantle and CHUR in the $\varepsilon_{Hf}(t)$–t diagram (Fig. 11), distinct from those from the Early Archean rocks in the NCC (Wu *et al.*, 2005*a*), again pointing to more juvenile crustal sources compared with the Paleo- to Eoarchean crustal sources. Many studies have shown that the Archean basement rocks in

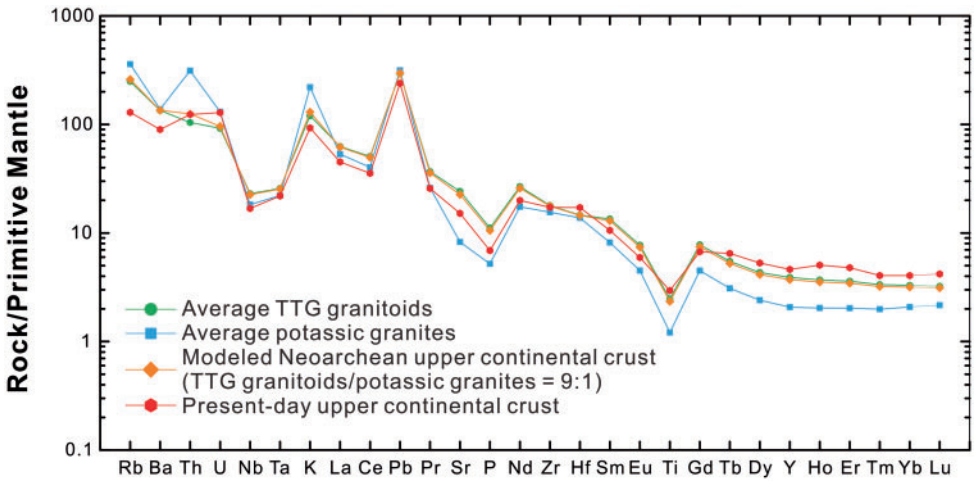

Fig. 14. Primitive mantle (PM)-normalized trace element patterns for the average composition of TTG granitoids and potassic granites and the calculated compositions of Archean upper continental crust in the Xingcheng (this study) and Qinhuangdao (Yang *et al.*, 2008) regions, assuming the ratio of TTG granitoids to potassic granites is 9:1. The composition of the present-day upper continental crust (Rudnick & Gao, 2003) is also plotted for comparison. The values of PM are from Sun & McDonough (1989).

the NCC are characterized by Nd and Hf model ages clustering at 3·0–2·6 Ga, indicating the timing of formation of the protoliths or segregation of the parental magma from the mantle (Wu *et al.*, 2005*b*; Yang *et al.*, 2008, 2009; Geng *et al.*, 2010; Jiang *et al.*, 2010; Wan *et al.*, 2011; Zhai & Santosh, 2011; Shi *et al.*, 2012; Wang & Liu, 2012, and references therein). We thus conclude that significant crustal growth occurred in the NCC during the Neoarchean, corresponding to the global growth of the Earth's crust recognized from other cratons (Condie & Aster, 2010; Condie *et al.*, 2011; Condie & Kröner, 2013; Condie, 2014, and references therein).

It is widely acknowledged that TTGs are the main components of Archean terranes and represent the primary felsic crust of the Earth (Martin *et al.*, 2005; Moyen, 2011), also that average Archean upper continental crust is essentially identical to the Archean TTGs (Condie, 1993, 2005*b*). However, as mentioned above, there are significant compositional discrepancies between the mature present-day felsic upper continental crust and the Archean TTGs, mainly in potassium, Y and the HREE (Table 5 and Fig. 14). These compositional discrepancies were gradually balanced by the addition of calc-alkaline granitoids with higher Y, HREE and potassium to the Archean upper continental crust throughout Earth's history, which is reflected by the fact that the volume ratio of TTGs relative to calc-alkaline granitoids has decreased since the end of the Archean (Condie, 2008).

Taken together with the Qinghuangdao granitoids reported by Yang *et al.* (2008), we calculated the compositions of the Neoarchean upper continental crust in the Xingcheng–Qinhuangdao region on the basis of the average compositions of TTG granitoids and potassic granites. We have found that a mix of TTG granitoids:potassic granites of 9:1 matches well the present-day upper continental crust with K_2O/Na_2O of 0·86, except that Y and HREE contents are ~20–30% lower than those of the present-day upper continental crust (Table 5 and Fig. 14). Therefore, the Neoarchean granitoids in the studied region can make at least 70–80% of the composition of the present-day upper continental continent crust, implying that the prototype upper continental crust of the NCC could have been formed at the end of the Archean. It should be noted that this scenario applies to the maturation of the continental crust of the NCC, but further study is needed if this is to be of general significance.

Tectonic implications: from micro-continental collision to post-collisional extension

The geodynamic setting of the Neoarchean blocks of the NCC, in which extensive magmatism and metamorphism occurred, has long been the subject of research and debate. The heat source for widespread regional metamorphism and large-scale partial melting of crustal materials is usually considered to be related to the intrusion and underplating of large volumes of mantle-derived magma. The emplacement of sufficient amounts of mantle-derived magma may occur in a variety of environments, including subduction-related tectonic settings (e.g. Liu *et al.*, 2010, 2011; Wan *et al.*, 2010, 2011; Nutman *et al.*, 2011; Wang *et al.*, 2011, 2012, 2013), hotspots driven by mantle plumes (e.g. Zhao *et al.*, 2001, 2005; Yang *et al.*, 2008; Zhai & Santosh, 2011; Zhao & Cawood, 2012), continental rift environments (e.g. Sandiford & Powell, 1986) and continental collisional belts (e.g. Niu *et al.*, 2013; Laurent *et al.*, 2014; Song *et al.*, 2014, 2015).

As discussed above, the Neoarchean TTG granitoids in the Xingcheng region have no obvious geochemical signatures indicating enhanced melt–peridotite interaction, such as elevated MgO contents and Mg# values, and Cr and Ni concentrations, which should be expected

if these TTG granitoids were produced through partial melting of subducting or subducted oceanic crust or oceanic plateau materials (Bédard, 2006; Moyen & Martin, 2012; Moyen & van Hunen, 2012; Bédard *et al.*, 2013; Martin *et al.*, 2014; Sizova *et al.*, 2015). However, the Neoarchean TTG and potassic granitoids are the reworking products of Mesoarchean crustal materials, instead of juvenile addition to the crust from the mantle as implied by their bulk-rock Nd and zircon Hf isotopic compositions. Their Mesoarchean source rocks include enriched mafic rocks and previously emplaced felsic TTG; thus they cannot be generated in subduction-related settings (continental or island arcs, thickened arc systems and accretionary orogens) where mainly juvenile mafic rocks act as source rocks (Bédard, 2006; Nagel *et al.*, 2012; Bédard *et al.*, 2013; Martin *et al.*, 2014). If these TTG were formed above hotspots driven by mantle plumes [i.e. melting at the base of a thick oceanic plateau crust heated by an upwelling mantle plume (Smithies *et al.*, 2009)], the resulting TTG rocks would be emplaced in a sequence of mantle-plume-related ultramafic to mafic rocks including komatiites, continental flood basalts, and the deep plumbing systems of dyke swarms and layered intrusions (Ernst *et al.*, 2008). But no such 2·6–2·5 Ga mantle-plume-related magmatism has been recognized in the study area, nor is there a global record of mantle plume activity at the end of the Archean (e.g. Ernst & Bleeker, 2010). Therefore, a mantle plume model may be inappropriate to account for the generation of the Neoarchean TTG and potassic granitoids in the Xingcheng region.

Bédard *et al.* (2013) proposed a model of cratonic drift in response to mantle convection currents and the resulting aggregation of Archean cratons and oceanic plateaux. The accretion between terranes led to thickening and delamination of mafic crust accompanied by the ascent of hot mantle, resulting in coeval basalt and TTG magmas. This scenario is highly unlikely for the Neoarchean TTG granitoids in the Xingcheng region as there are no coeval Neoarchean basaltic magmas. Furthermore, most of the TTG granitoids in the Xingcheng region formed at medium pressures along a geotherm (15–20°C km^{-1}; Moyen & Martin, 2012) that is too low for a plateau setting, but also too hot for a subduction situation, even considering the possibility that Archean subduction zones may have been hotter. A continental rift environment is also inappropriate because of the lack of alkali intrusive rocks, expected to be associated with rifting (Zhao *et al.*, 2001). Therefore, a continental collision setting is more likely to have produced the Neoarchean TTG and potassic granitoids in the Xingcheng region.

As shown in Fig. 1b, the Precambrian basement of the Eastern Block of the NCC is composed of two major kinds of terrane: a high-grade metamorphic terrane and a granitic terrane with no or only low-grade metamorphism. The high-grade metamorphic terrane contains tonalite, trondjhemite, charnockite and supracrustal rocks [ultramafic to mafic igneous rocks and sedimentary rocks with banded iron formations (BIF)], with diverse protoliths and varying ages of 3·8–2·6 Ga (e.g. Nutman *et al.*, 2011; Zhai & Santosh, 2011), all of which experienced granulite-facies metamorphism at ~2·6–2·5 Ga (Zhao *et al.* 2001, 2005). The contemporaneous high-grade metamorphism and plutonic magmatism indicate an intensive tectonothermal event in the Late Neoarchean (2·6–2·5 Ga) throughout the NCC; this event is most probably an orogenic event because the Neoarchean is an important period for the amalgamation of micro-continental blocks and cratonization of the eastern NCC and the Xingcheng region lies between micro-continental blocks with *c.* 3·8 Ga crustal nuclei (Fig. 1b; Caozhuang and Anshan; Zhai & Santosh, 2011). Recent reports of Neoarchean high-K calc-alkaline rocks in Western Liaoning (e.g. Wang *et al.*, 2012, 2013) also favor this possibility.

As mentioned above, the Neoarchean granitoids in the eastern NCC vary from sodic-to-potassic TTG granitoids, diorite–granodiorites and monzogranites to potassic-rich, peraluminous granites (Yang *et al.*, 2008; this study). This rock assemblage is comparable with that of magmatism in Phanerozoic continental collisional belts, which encompasses a series of adakitic, I-, S- and A-type granites and other igneous rocks and shows large compositional variation (e.g. Himalaya, North Qaidam and Caledonian orogens; Chung *et al.*, 2003; Niu *et al.*, 2013; Laurent *et al.*, 2014; Song *et al.*, 2014, 2015). The absence of S-type granites among the Neoarchean granitoids of the eastern NCC may reflect the fact that abundant sediments had not been developed until then. The Neoarchean TTG granitoids in the Xingcheng region were generated through partial melting of Mesoarchean enriched mafic crustal sources at different depths (up to 12 kbar or ~42 km) coupled with low-pressure crystal fractionation, which requires significant crustal thickening through micro-continental collision (e.g. Nutman & Friend, 2007). The potassic granites, with their intrusive contact with the TTG granitoids and younger age, represent the last pulse of Archean magmatism in the Xingcheng region and most probably formed by remelting of Mesoarchean TTGs or low-degree partial melting of Mesoarchean enriched mafic crustal materials in an extensional or non-compressional environment (i.e. a post-orogenic or post-collisional stage). These potassic granites can act as a marker for the end of an orogenic cycle and the final stabilization of the Archean proto-crust (Zhou *et al.*, 2011; Zhang *et al.*, 2012). The melting of the Mesoarchean mafic crust was triggered by melts rising from the upwelling mantle, which also modified the compositions of these melts by different degrees. The large variation of the initial zircon Hf isotopic compositions of the Neoarchean TTG and potassic granitoids in the Xingcheng region is also observed when a convergent (i.e. subduction) environment makes a transition to continental collision (Hawkesworth *et al.*, 2010; Laurent *et al.*, 2014), which is consistent with an increase in reworking processes associated with crustal thickening

during collision and melting of the mantle sources. Numerical modeling has suggested that Precambrian continental collisional belts are characterized by different tectonic styles compared with modern continental collisional belts, as they were formed over a hotter mantle and remained mechanically weak (Sizova, 2014). Thus shallow slab break-off often took place, limiting the occurrence of ultrahigh-pressure metamorphic complexes within Precambrian continental orogenic belts and allowing for frequent upwelling and subsequent melting of the mantle (Moyen & van Hunen, 2012; Sizova *et al.*, 2014). In fact, we cannot precisely constrain the details and configuration of the proposed continental collisional belt for the generation of the Neoarchean TTG and potassic granitoids in the Xingcheng region based on the available data. It should share some similarities with modern continental collisional belts in certain aspects and could be accommodated by various orogenic styles, such as retreating or advancing plate boundaries followed by collision, and evolve through various scenarios (e.g. slab retreat and break-off; Laurent *et al.*, 2014).

Together with the concurrent high-grade metamorphism widespread in the NCC, we conclude that the Neoarchean granitoids in the Xingcheng region were formed through an orogenic process involving transition from micro-continental collision to post-collisional extension at the late Neoarchean. The micro-continents formed during the Mesoarchean and at the end of Archean began to accrete and amalgamate, leading to significant crustal thickening, while also causing granulite-facies metamorphism and partial melting of Mesoarchean enriched mafic crustal materials at varying depths, caused by heating from mantle-derived mafic magmas and fractional crystallization. These micro-continental blocks have been intensively overprinted by a 2·6–2·5 Ga orogenic event and are difficult to define, as some ~3·8 Ga crustal remnants have been identified in some areas of the NCC. After collision, the amalgamated micro-continental blocks underwent extension. As a result, the mafic proto-crust experienced low-degree partial melting and the Mesoarchean TTGs may have also remelted, generating the potassic granites.

CONCLUSIONS

The Neoarchean crust in the Xingcheng region is made up of TTG granitoids and potassic granites. The TTG granitoids with MMEs formed through partial melting of Mesoarchean enriched mafic crustal sources at varying depths, combined with low-pressure fractional crystallization in a collisional environment at 2595–2558 Ma. The Taili gneisses were the products of low-pressure melting of Mesoarchean enriched mafic crust induced by Neoarchean juvenile mantle-derived mafic melts. Two kinds of potassic granite were produced by (1) low-degree partial melting of enriched mafic crustal sources at 2540 Ma and (2) remelting of Mesoarchean TTG in response to post-collisional extension at 2520 Ma. Upwelling of Neoarchean mantle-derived mafic magmas triggered the partial melting of their crustal source rocks and modified their compositions by different degrees.

The rock assemblages in the Suizhong granitic terrane resemble those of Phanerozoic orogens and record the evolution from collision of micro-continental blocks to post-collisional extension.

The major crustal growth in the eastern NCC took place during the Neoarchean. The prototype upper continental crust of the NCC, which makes up at least 70–80% of the composition of the present-day upper continental crust, might have been developed at the end of the Archean by mixing of TTG and potassic granitoids.

ACKNOWLEDGEMENTS

The authors are grateful to Jean-François Moyen, Tracy Rushmer and an anonymous reviewer for their detailed and constructive peer-review comments, which greatly improved the quality of this paper. Editorial handling by Simon Turner is also gratefully acknowledged. The authors wish to thank W. G. Liu and W. P. Zhu for the help during Nd isotope analyses.

FUNDING

This study was supported by the National Natural Science Foundation of China (grants 41430207, 41372060, 41572040 and 41130314).

REFERENCES

Adam, J., Rushmer, T., O'Neil, J. & Francis, D. (2012). Hadean greenstones from the Nuvvuagittuq fold belt and the origin of the Earth's early continental crust. *Geology* **40**, 363–366.

Andersen, T. (2002). Correction of common lead in U–Pb analyses that do not report ^{204}Pb. *Chemical Geology* **192**, 59–79.

Bai, X., Liu, S., Guo, R. & Wang, W. (2016). A Neoarchean arc–back-arc system in Eastern Hebei, North China Craton: Constraints from zircon U–Pb–Hf isotopes and geochemistry of dioritic–tonalitic–trondhjemitic–granodioritic (DTTG) gneisses and felsic paragneisses. *Precambrian Research* **273**, 90–111.

Barker, F. (1979). Trondhjemite: definition, environment and hypotheses of origin. In: Barker, F. (ed.) *Trondhjemites, Dacites, and Related Rocks*. Elsevier, pp. 1–12.

Bédard, J. H. (2006). A catalytic delamination-driven model for coupled genesis of Archaean crust and sub-continental lithospheric mantle. *Geochimica et Cosmochimica Acta* **70**, 1188–1214.

Bédard, J. H., Harris, L. B. & Thurston, P. C. (2013). The hunting of the snArc. *Precambrian Research* **229**, 20–48.

Belousova, E. A., Griffin, W. L. & O'Reilly, S. Y. (2006). Zircon crystal morphology, trace element signatures and Hf isotope composition as a tool for petrogenetic modelling: examples from eastern Australian granitoids. *Journal of Petrology* **47**, 329–353.

Black, L. P., Kamo, S. L., Allen, C. M., Aleinikoff, J. N., Davis, D. W., Korsch, R. J. & Foudoulis, C. (2003). TEMORA 1: a new

zircon standard for Phanerozoic U–Pb geochronology. *Chemical Geology* **200**, 155–170.
Bleeker, W. (2003). The late Archean record: a puzzle in *ca*. 35 pieces. *Lithos* **71**, 99–134.
Castillo, P. R. (2012). Adakite petrogenesis. *Lithos* **134–135**, 304–316.
Castro, A. (2003). The source of granites: inferences from the Lewisian complex. *Scottish Journal of Geology* **40**, 49–66.
Champion, D. C. & Smithies, R. H. (2007). Geochemistry of Paleoarchean granites of the east Pilbara Terrane, Pilbara Craton, Western Australia: implications for Early Archean crustal growth. In: Martin, R. H. S., van Kranendonk, J. & Vickie, C. B. (eds.) *Developments in Precambrian Geology, 15*. Elsevier, pp. 369–409.
Chappell, B. W. (1999). Aluminium saturation in I- and S-type granites and the characterization of fractionated haplogranites. *Lithos* **46**, 535–551.
Chappell, B. W., White, A. J. R. & Wyborn, D. (1987). The importance of residual source material (restite) in granite petrogenesis. *Journal of Petrology* **28**, 1111–1138.
Chen, B., Jahn, B.-m. & Wei, C. (2002). Petrogenesis of Mesozoic granitoids in the Dabie UHP complex, Central China: trace element and Nd–Sr isotope evidence. *Lithos* **60**, 67–88.
Chen, S., Niu, Y., Sun, W., Zhang, Y., Li, J., Guo, P. & Sun, P. (2015). On the origin of mafic magmatic enclaves (MMEs) in syn-collisional granitoids: evidence from the Baojishan pluton in the North Qilian Orogen, China. *Mineralogy and Petrology* **109**, 577–596.
Chen, S., Niu, Y. L., Li, J. Y., Sun, W. L., Zhang, Y., Hu, Y. & Shao, F. L. (2016). Syncollisional adakitic granodiorites formed by fractional crystallization: insights from their enclosed mafic magmatic enclaves (MMEs) in the Qumushan pluton, North Qilian Orogen at the northern margin of the Tibetan Plateau. *Lithos* **248–251**, 455–468.
Chen, Y., Song, S., Niu, Y. & Wei, C. (2014). Melting of continental crust during subduction initiation: A case study from the Chaidanuo peraluminous granite in the North Qilian suture zone. *Geochimica et Cosmochimica Acta* **132**, 311–336.
Chung, S. L., Liu, D. Y., Ji, J. Q., Chu, M. F., Lee, H. Y., Wen, D. J., Lo, C. H., Lee, T. Y., Qian, Q. & Zhang, Q. (2003). Adakites from continental collision zones: Melting of thickened lower crust beneath southern Tibet. *Geology* **31**, 1021–1024.
Compston, W., Zhong, F. D., Foster, J. J., Collerson, K. D., Bai, J. & Sun, D. C. (1983). Rubidium–strontium geochronology of Precambrian rocks from the Yenshan region, North China. *Precambrian Research* **22**, 175–202.
Condie, K. C. (1993). Chemical composition and evolution of the upper continental crust: Contrasting results from surface samples and shales. *Chemical Geology* **104**, 1–37.
Condie, K. C. (2005*a*). High field strength element ratios in Archean basalts: a window to evolving sources of mantle plumes? *Lithos* **79**, 491–504.
Condie, K. C. (2005*b*). TTGs and adakites: are they both slab melts? *Lithos* **80**, 33–44.
Condie, K. C. (2008). Did the character of subduction change at the end of the Archean? Constraints from convergent-margin granitoids. *Geology* **36**, 611–614.
Condie, K. C. (2014). How to Make a Continent: Thirty-fiveYears of TTG Research. In: Dilek, Y. & Furnes, H. (eds.) *Evolution of Archean Crust and Early Life, Modern Approaches in Solid Earth Sciences* **7**, 179–193.
Condie, K. C. & Aster, R. C. (2010). Episodic zircon age spectra of orogenic granitoids: The supercontinent connection and continental growth. *Precambrian Research* **180**, 227–236.
Condie, K. C. & Kröner, A. (2013). The building blocks of continental crust: Evidence for a major change in the tectonic setting of continental growth at the end of the Archean. *Gondwana Research* **23**, 394–402.
Condie, K. C., Bickford, M. E., Aster, R. C., Belousova, E. & Scholl, D. W. (2011). Episodic zircon ages, Hf isotopic composition, and the preservation rate of continental crust. *Geological Society of America Bulletin* **123**, 951–957.
Defant, M. J. & Drummond, M. S. (1990). Derivation of some modern arc magmas by melting of young subducted lithosphere. *Nature* **347**, 662–665.
Ernst, R. & Bleeker, W. (2010). Large igneous provinces (LIPs), giant dyke swarms, and mantle plumes: significance for breakup events within Canada and adjacent regions from 2·5 Ga to the Present. *Canadian Journal of Earth Sciences* **47**, 695–739.
Ernst, R. E., Wingate, M. T. D., Buchan, K. L. & Li, Z. X. (2008). Global record of 1600–700 Ma Large Igneous Provinces (LIPs): Implications for the reconstruction of the proposed Nuna (Columbia) and Rodinia supercontinents. *Precambrian Research* **160**, 159–178.
Foley, S., Tiepolo, M. & Vannucci, R. (2002). Growth of early continental crust controlled by melting of amphibolite in subduction zones. *Nature* **417**, 837–840.
Frost, C. D., Frost, B. R., Chamberlain, K. R. & Hulsebosch, T. P. (1998). The Late Archean history of the Wyoming province as recorded by granitic magmatism in the Wind River Range, Wyoming. *Precambrian Research* **89**, 145–173.
Geng, Y. S., Shen, Q. H. & Ren, L. D. (2010). Late Neoarchean to Early Paleoproterozoic magmatic events and tectonothermal systems in the North China Craton. *Acta Petrologica Sinica* **26**, 1945–1966 (in Chinese with English abstract).
Griffin, W. L., Wang, X., Jackson, S. E., Pearson, N. J., O'Reilly, S. Y., Xu, X. & Zhou, X. (2002). Zircon chemistry and magma mixing, SE China: *In-situ* analysis of Hf isotopes, Tonglu and Pingtan igneous complexes. *Lithos* **61**, 237–269.
Guo, J. H., O'Brien, P. J. & Zhai, M. (2002). High-pressure granulites in the Sanggan area, North China craton: metamorphic evolution, *P–T* paths and geotectonic significance. *Journal of Metamorphic Geology* **20**, 741–756.
Hawkesworth, C. J., Dhuime, B., Pietranik, A. B., Cawood, P. A., Kemp, A. I. S. & Storey, C. D. (2010). The generation and evolution of the continental crust. *Journal of the Geological Society, London* **167**, 229–248.
Hoffmann, J. E., Nagel, T. J., Münker, C., Næraa, T. & Rosing, M. T. (2014). Constraining the process of Eoarchean TTG formation in the Itsaq Gneiss Complex, southern West Greenland. *Earth and Planetary Science Letters* **388**, 374–386.
Holden, P., Halliday, A. N. & Stephens, W. E. (1987). Neodymium and strontium isotope content of microdiorite enclaves points to mantle input to granitoid production. *Nature* **330**, 53–56.
Hollings, P. & Kerrich, R. (2006). Light rare earth element depleted to enriched basaltic flows from 2·8 to 2·7 Ga greenstone belts of the Uchi Subprovince, Ontario, Canada. *Chemical Geology* **227**, 133–153.
Hou, K. J., Li, Y. H., Zou, T. R., Qu, X. M., Shi, Y. R. & Xie, G. Q. (2007). Laser ablation-MC-ICP-MS technique for Hf isotope microanalysis of zircon and its geological applications. *Acta Petrologica Sinica* **23**, 2595–2604 (in Chinese with English abstract).
Huang, H., Niu, Y., Nowell, G., Zhao, Z., Yu, X., Zhu, D.-C., Mo, X. & Ding, S. (2014). Geochemical constraints on the petrogenesis of granitoids in the East Kunlun orogenic belt, northern Tibetan Plateau: Implications for continental crust growth through syn-collisional felsic magmatism. *Chemical Geology* **370**, 1–18.

Jahn, B.-M. & Ernst, W. G. (1990). Late Archean Sm–Nd isochron age for mafic–ultramafic supracrustal amphibolites from the Northeastern Sino-Korean Craton, China. *Precambrian Research* **46**, 295–306.

Jahn, B.-M., Auvray, B., Blais, S., Capdevila, R., Cornichet, J., Vidal, F. & Hameurt, J. (1980). Trace element geochemistry and petrogenesis of Finnish greenstone belts. *Journal of Petrology* **21**, 201–244.

Jahn, B. M., Glikson, A. Y., Peucat, J. J. & Hickman, A. H. (1981). REE geochemistry and isotopic data of Archean silicic volcanics and granitoids from the Pilbara Block, Western Australia: implications for the early crustal evolution. *Geochimica et Cosmochimica Acta* **45**, 1633–1652.

Jayananda, M., Chardon, D., Peucat, J. J. & Capdevila, R. (2006). **2**·61 Ga potassic granites and crustal reworking in the western Dharwar craton, southern India: Tectonic, geochronologic and geochemical constraints. *Precambrian Research* **150**, 1–26.

Jiang, N., Guo, J. H., Zhai, M. G. & Zhang, S. Q. (2010). ~2·7 Ga crust growth in the North China craton. *Precambrian Research* **179**, 37–49.

Kröner, A., Cui, W.-Y., Wang, S.-Q., Wang, C.-Q. & Nemchin, A. A. (1998). Single zircon ages from high-grade rocks of the Jianping Complex, Liaoning Province, NE China. *Journal of Asian Earth Sciences* **16**, 519–532.

Laurent, O., Martin, H., Moyen, J. F. & Doucelance, R. (2014). The diversity and evolution of late-Archean granitoids: Evidence for the onset of 'modern-style' plate tectonics between 3·0 and 2·50 Ga. *Lithos* **205**, 208–235.

Li, S. & Zhao, G. (2007). SHRIMP U–Pb zircon geochronology of the Liaoji granitoids: Constraints on the evolution of the Paleoproterozoic Jiao–Liao–Ji belt in the Eastern Block of the North China Craton. *Precambrian Research* **158**, 1–16.

Liu, D. Y., Nutman, A. P., Compston, W., Wu, J. S. & Shen, Q. H. (1992). Remnants of ≥3800 Ma crust in the Chinese part of the Sino-Korean craton. *Geology* **20**, 339–342.

Liu, J., Liu, F., Ding, Z., Liu, C., Yang, H., Liu, P., Wang, F. & Meng, E. (2013a). The growth, reworking and metamorphism of early Precambrian crust in the Jiaobei terrane, the North China Craton: Constraints from U–Th–Pb and Lu–Hf isotopic systematics, and REE concentrations of zircon from Archean granitoid gneisses. *Precambrian Research* **224**, 287–303.

Liu, S., Wan, Y., Sun, H., Nutman, A. P., Xie, H., Dong, C., Ma, M., Liu, D. & Jahn, B.-m. (2013b). Paleo- to Eoarchean crustal evolution in eastern Hebei, North China Craton: New evidence from SHRIMP U–Pb dating and *in-situ* Hf isotopic study of detrital zircons from paragneisses. *Journal of Asian Earth Sciences* **78**, 4–17.

Liu, S. W., Wang, W., Bai, X., Zhang, F. & Yang, P. T. (2010). Geological events of Early Precambrian complex in North Chaoyang Area, Liaoning Province. *Acta Petrologica Sinica* **26**, 1993–2004 (in Chinese with English abstract).

Liu, S. W., Santosh, M., Wang, W., Bai, X. & Yang, P. T. (2011). Zircon U–Pb chronology of the Jianping Complex: Implications for the Precambrian crustal evolution history of the northern margin of North China Craton. *Gondwana Research* **20**, 48–63.

Ludwig, K. R. (2003). *User's Manual for Isoplot 3.0: a Geochronological Toolkit for Microsoft Excel. Berkeley Geochronology Centre, Special Publication* **4**.

Macpherson, C. G., Dreher, S. T. & Thirlwall, M. F. (2006). Adakites without slab melting: High pressure differentiation of island arc magma, Mindanao, the Philippines. *Earth and Planetary Science Letters* **243**, 581–593.

Martin, H. (1999). Adakitic magmas: modern analogues of Archaean granitoids. *Lithos* **46**, 411–429.

Martin, H., Smithies, R. H., Rapp, R., Moyen, J. F. & Champion, D. (2005). An overview of adakite, tonalite–trondhjemite–granodiorite (TTG), and sanukitoid: relationships and some implications for crustal evolution. *Lithos* **79**, 1–24.

Martin, H., Moyen, J.-F., Guitreau, M., Blichert-Toft, J., Le Pennec, J.-L. (2014). Why Archaean TTG cannot be generated by MORB melting in subduction zones. *Lithos* **198–199**, 1–13.

Miller, J., Moyen, J.-F. & Benn, K. (2008). The 2·74–2·66 Ga Kenogamissi complex (Abitibi): Evolving sources of plutons mirroring geodynamics. *Geochimica et Cosmochimica Acta, Supplement* **72**, 629.

Morel, M. L. A., Nebel, O., Nebel-Jacobsen, Y. J., Miller, J. S. & Vroon, P. Z. (2008). Hafnium isotope characterization of the GJ-1 zircon reference material by solution and laser-ablation MC-ICPMS. *Chemical Geology* **255**, 231–235.

Moyen, J.-F. (2011). The composite Archaean grey gneisses: Petrological significance, and evidence for a non-unique tectonic setting for Archaean crustal growth. *Lithos* **123**, 21–36.

Moyen, J.-F. & Martin, H. (2012). Forty years of TTG research. *Lithos* **148**, 312–336.

Moyen, J.-F. & van Hunen, J. (2012). Short-term episodicity of Archaean plate tectonics. *Geology* **40**, 451–454.

Moyen, J.-F., Martin, H. & Jayananda, M. (2001). Multi-element geochemical modelling of crust–mantle interactions during late-Archaean crustal growth: the Closepet granite (South India). *Precambrian Research* **112**, 87–105.

Moyen, J. F., Martin, H., Jayananda, M. & Auvray, B. (2003). Late Archaean granites: a typology based on the Dharwar Craton (India). *Precambrian Research* **127**, 103–123.

Moyen, J.-F., Stevens, G., Kisters, A. F. M. & Belcher, R. W. (2007). TTG plutons of the Barberton Granitoid–Greenstone Terrain, South Africa. In: Martin, J., van Kranendonk, R. H. S. & Vickie, C. B. (eds) *Developments in Precambrian Geology, 15*. Elsevier, pp. 607–667.

Moyen, J.-F., Champion, D. & Smithies, R. H. (2010). The geochemistry of Archaean plagioclase-rich granites as a marker of source enrichment and depth of melting. *Geological Society of America Special Papers* **472**, 35–50.

Nagel, T. J., Hoffmann, J. E. & Münker, C. (2012). Generation of Eoarchean tonalite–trondhjemite–granodiorite series from thickened mafic arc crust. *Geology* **40**, 375–378.

Niu, Y., Zhao, Z., Zhu, D.-C. & Mo, X. (2013). Continental collision zones are primary sites for net continental crust growth—a testable hypothesis. *Earth-Science Reviews* **127**, 96–110.

Nutman, A. P. & Friend, C. R. L. (2007). Adjacent terranes with *ca.* 2715 and 2650 Ma high-pressure metamorphic assemblages in the Nuuk region of the North Atlantic Craton, southern West Greenland: Complexities of Neoarchaean collisional orogeny. *Precambrian Research* **155**, 159–203.

Nutman, A. P., Wan, Y., Du, L., Friend, C. R. L., Dong, C., Xie, H., Wang, W., Sun, H. & Liu, D. (2011). Multistage late Neoarchaean crustal evolution of the North China Craton, eastern Hebei. *Precambrian Research* **189**, 43–65.

Patiño Douce, A. E. (2005). Vapor-absent melting of tonalite at 15–32 kbar. *Journal of Petrology* **46**, 275–290.

Patiño Douce, A. E. & Beard, J. S. (1995). Dehydration-melting of biotite gneiss and quartz amphibolite from 3 to 15 kbar. *Journal of Petrology* **36**, 707–738.

Qian, J., Wei, C., Zhou, X. & Zhang, Y. (2013). Metamorphic *P–T* paths and new zircon U–Pb age data for garnet–mica schist from the Wutai Group, North China Craton. *Precambrian Research* **233**, 282–296.

Qian, Q. & Hermann, J. (2013). Partial melting of lower crust at 10–15 kbar: constraints on adakite and TTG formation. *Contributions to Mineralogy and Petrology* **165**, 1195–1224.

Rapp, R. P. & Watson, E. B. (1995). Dehydration melting of metabasalt at 8–32 kbar: implications for continental growth and crust–mantle recycling. *Journal of Petrology* **36**, 891–931.

Rapp, R. P., Watson, E. B. & Miller, C. F. (1991). Partial melting of amphibolite/eclogite and the origin of Archean trondhjemites and tonalites. *Precambrian Research* **51**, 1–25.

Rapp, R. P., Shimizu, N., Norman, M. D. & Applegate, G. S. (1999). Reaction between slab-derived melts and peridotite in the mantle wedge: experimental constraints at 3·8 GPa. *Chemical Geology* **160**, 335–356.

Rapp, R. P., Xiao, L. & Shimizu, N. (2002). Experimental contraints on the origin of potassium-rich adakites in eastern China. *Acta Petrologica Sinica*, 293–302.

Rapp, R. P., Shimizu, N. & Norman, M. D. (2003). Growth of early continental crust by partial melting of eclogite. *Nature* **425**, 605–609.

Rudnick, R. L. & Gao, S. (2003). Composition of the continental crust. In: Rudnick, R. L. (ed.) *The Crust*. vol. **3**, Elsevier, pp. 1–64.

Samsonov, A. V., Bogina, M. M., Bibikova, E. V., Petrova, A. Y. & Shchipansky, A. A. (2005). The relationship between adakitic, calc-alkaline volcanic rocks and TTGs: implications for the tectonic setting of the Karelian greenstone belts, Baltic Shield. *Lithos* **79**, 83–106.

Sandiford, M. & Powell, R. (1986). Deep crustal metamorphism during continental extension: modern and ancient examples. *Earth and Planetary Science Letters* **79**, 151–158.

Santosh, M., Tsunogae, T., Li, J. H. & Liu, S. J. (2007a). Discovery of sapphirine-bearing Mg–Al granulites in the North China Craton: Implications for Paleoproterozoic ultrahigh temperature metamorphism. *Gondwana Research* **11**, 263–285.

Santosh, M., Wilde, S. A. & Li, J. H. (2007b). Timing of Paleoproterozoic ultrahigh-temperature metamorphism in the North China Craton: Evidence from SHRIMP U–Pb zircon geochronology. *Precambrian Research* **159**, 178–196.

Sen, C. & Dunn, T. (1994). Dehydration melting of a basaltic composition amphibolite at 1·5 and 2·0 GPa: implications for the origin of adakites. *Contributions to Mineralogy and Petrology* **117**, 394–409.

Shi, Y. R., Wilde, S. A., Zhao, X. T., Ma, Y. S., Du, L. L. & Liu, D. Y. (2012). Late Neoarchean magmatic and subsequent metamorphic events in the northern North China Craton: SHRIMP zircon dating and Hf isotopes of Archean rocks from Yunmengshan Geopark, Miyun, Beijing. *Gondwana Research* **21**, 785–800.

Sisson, T., Ratajeski, K., Hankins, W. & Glazner, A. (2005). Voluminous granitic magmas from common basaltic sources. *Contributions to Mineralogy and Petrology* **148**, 635–661.

Sizova, E., Gerya, T. & Brown, M. (2014). Contrasting styles of Phanerozoic and Precambrian continental collision. *Gondwana Research* **25**, 522–545.

Sizova, E., Gerya, T., Stüwe, K. & Brown, M. (2015). Generation of felsic crust in the Archean: A geodynamic modeling perspective. *Precambrian Research* **271**, 198–224.

Skjerlie, K. P. & Johnston, A. D. (1996). Vapour-absent melting from 10 to 20 kbar of crustal rocks that contain multiple hydrous phases: implications for anatexis in the deep to very deep continental crust and active continental margins. *Journal of Petrology* **37**, 661–691.

Skjerlie, K. P. & Patiño Douce, A. E. (2002). The fluid-absent partial melting of a zoisite-bearing quartz eclogite from 1·0 to 3·2 GPa; implications for melting in thickened continental crust and for subduction-zone processes. *Journal of Petrology* **43**, 291–314.

Smithies, R. H. (2000). The Archaean tonalite–trondhjemite–granodiorite (TTG) series is not an analogue of Cenozoic adakite. *Earth and Planetary Science Letters* **182**, 115–125.

Smithies, R. H., Champion, D. C. & Van Kranendonk, M. J. (2009). Formation of Paleoarchean continental crust through infracrustal melting of enriched basalt. *Earth and Planetary Science Letters* **281**, 298–306.

Song, B., Nutman, A. P., Liu, D. Y. & Wu, J. S. (1996). 3800 to 2500 Ma crustal evolution in the Anshan area of Liaoning Province, northeastern China. *Precambrian Research* **78**, 79–94.

Song, S., Niu, Y., Su, L., Wei, C. & Zhang, L. (2014). Adakitic (tonalitic–trondhjemitic) magmas resulting from eclogite decompression and dehydration melting during exhumation in response to continental collision. *Geochimica et Cosmochimica Acta* **130**, 42–62.

Song, S., Wang, M., Wang, C. & Niu, Y. (2015). Magmatism during continental collision, subduction, exhumation and mountain collapse in collisional orogenic belts and continental net growth: A perspective. *Science China Earth Sciences* **58**, 1284–1304.

Song, S. G., Niu, Y. L., Wei, C. J., Ji, J. Q. & Su, L. (2010a). Metamorphism, anatexis, zircon ages and tectonic evolution of the Gongshan block in the northern Indochina continent—An eastern extension of the Lhasa Block. *Lithos* **120**, 327–346.

Song, S. G., Su, L., Li, X. H., Zhang, G. B., Niu, Y. L. & Zhang, L. F. (2010b). Tracing the 850-Ma continental flood basalts from a piece of subducted continental crust in the North Qaidam UHPM belt, NW China. *Precambrian Research* **183**, 805–816.

Sun, J. F., Yang, J. H., Wu, F. Y. & Wilde, S. A. (2012). Precambrian crustal evolution of the eastern North China Craton as revealed by U–Pb ages and Hf isotopes of detrital zircons from the Proterozoic Jing'eryu Formation. *Precambrian Research* **200–203**, 184–208.

Sun, S. S. & McDonough, W. F. (1989). Chemical and isotopic systematics of oceanic basalts: implications for mantle composition and processes. In: Saunders, A. D. & Norry, M. J. (eds) *Magmatism in the Ocean Basins.Geological Society, London, Special Publications* **42**, 313–345.

Sylvester, P. J. (1994). Archaean granite plutons. Condie, K. C. (ed.) *Archaean Crustal Evolution*. Elsevier, pp. 261–314.

Tam, P. Y., Zhao, G., Liu, F., Zhou, X., Sun, M. & Li, S. (2011). Timing of metamorphism in the Paleoproterozoic Jiao–Liao–Ji Belt: New SHRIMP U–Pb zircon dating of granulites, gneisses and marbles of the Jiaobei massif in the North China Craton. *Gondwana Research* **19**, 150–162.

van Hunen, J. & Moyen, J.-F. (2012). Archean subduction: fact or fiction? *Annual Review of Earth and Planetary Sciences* **40**, 195–219.

Vernon, R. H. (1984). Microgranitoid enclaves in granites—globules of hybrid magma quenched in a plutonic environment. *Nature* **309**, 438–439.

Wall, V. J., Clemens, J. D. & Clarke, D. B. (1987). Models for granitoid evolution and source compositions. *Journal of Geology* **95**, 731–749.

Wan, Y., Liu, D., Yin, X., Simon A, W., Xie, L., Yang, Y., Zhou, H. & Wu, J. (2007). SHRIMP geochronology and Hf isotope composition of zircons from the Tiejiashan granite and supracrustal rocks in the Anshan area, Liaoning Province. *Acta Petrologica Sinica* **23**, 241–252 (in Chinese with English abastract).

Wan, Y., Liu, D., Wang, S., Dong, C., Yang, E., Wang, W., Zhou, H., Ning, Z., Du, L., Yin, X., Xie, H. & Ma, M. (2010). Juvenile magmatism and crustal recycling at the end of the Neoarchean in Western Shandong Province, North China

Craton: Evidence from SHRIMP zircon dating. *American Journal of Science* **310**, 1503–1552.

Wan, Y., Liu, D., Wang, W., Song, T., Kröner, A., Dong, C., Zhou, H. & Yin, X. (2011). Provenance of Meso- to Neoproterozoic cover sediments at the Ming Tombs, Beijing, North China Craton: An integrated study of U–Pb dating and Hf isotopic measurement of detrital zircons and whole-rock geochemistry. *Gondwana Research* **20**, 219–242.

Wan, Y., Ma, M., Dong, C., Xie, H., Xie, S., Ren, P. & Liu, D. (2015). Widespread late Neoarchean reworking of Meso- to Paleoarchean continental crust in the Anshan–Benxi area, North China Craton, as documented by U–Pb–Nd–Hf–O isotopes. *American Journal of Science* **315**, 620–670.

Wan, Y. S., Liu, D. Y., Song, B., Wu, J. S., Yang, C. H., Zhang, Z. Q. & Geng, Y. S. (2005). Geochemical and Nd isotopic compositions of 3·8 Ga meta-quartz dioritic and trondhjemitic rocks from the Anshan area and their geological significance. *Journal of Asian Earth Sciences* **24**, 563–575.

Wang, A. D. & Liu, Y. C. (2012). Neoarchean (2·5–2·8 Ga) crustal growth of the North China Craton revealed by zircon Hf isotope: A synthesis. *Geoscience Frontiers* **3**, 147–173.

Wang, C., Song, S., Niu, Y. & Su, L. (2015a). Late Triassic adakitic plutons within the Archean terrane of the North China Craton: Melting of the ancient lower crust at the onset of the lithospheric destruction. *Lithos* **212–215**, 353–367.

Wang, M., Song, S., Niu, Y. & Su, L. (2014a). Post-collisional magmatism: Consequences of UHPM terrane exhumation and orogen collapse, N. Qaidam UHPM belt, NW China. *Lithos* **210–211**, 181–198.

Wang, Q., Xu, J. F., Jian, P., Bao, Z. W., Zhao, Z. H., Li, C. F., Xiong, X. L. & Ma, J. L. (2006). Petrogenesis of adakitic porphyries in an extensional tectonic setting, Dexing, South China: implications for the genesis of porphyry copper mineralization. *Journal of Petrology* **47**, 119–144.

Wang, W., Liu, S. W., Bai, X., Yang, P. T., Li, Q. G. & Zhang, L. F. (2011). Geochemistry and zircon U–Pb–Hf isotopic systematics of the Neoarchean Yixian–Fuxin greenstone belt, northern margin of the North China Craton: Implications for petrogenesis and tectonic setting. *Gondwana Research* **20**, 64–81.

Wang, W., Liu, S., Wilde, S. A., Li, Q., Zhang, J., Bai, X., Yang, P. & Guo, R. (2012). Petrogenesis and geochronology of Precambrian granitoid gneisses in Western Liaoning Province: Constraints on Neoarchean to early Paleoproterozoic crustal evolution of the North China Craton. *Precambrian Research* **222–223**, 290–311.

Wang, W., Liu, S., Santosh, M., Bai, X., Li, Q., Yang, P. & Guo, R. (2013). Zircon U–Pb–Hf isotopes and whole-rock geochemistry of granitoid gneisses in the Jianping gneissic terrane, Western Liaoning Province: Constraints on the Neoarchean crustal evolution of the North China Craton. *Precambrian Research* **224**, 184–221.

Wang, W., Zhai, M., Li, T., Santosh, M., Zhao, L. & Wang, H. (2014b). Archean–Paleoproterozoic crustal evolution in the eastern North China Craton: Zircon U–Th–Pb and Lu–Hf evidence from the Jiaobei terrane. *Precambrian Research* **241**, 146–160.

Wang, W., Liu, S., Santosh, M., Wang, G., Bai, X. & Guo, R. (2015b). Neoarchean intra-oceanic arc system in the Western Liaoning Province: Implications for Early Precambrian crustal evolution in the Eastern Block of the North China Craton. *Earth-Science Reviews* **150**, 329–364.

Watkins, J., Clemens, J. & Treloar, P. (2007). Archaean TTGs as sources of younger granitic magmas: melting of sodic metatonalites at 0·6–1·2 GPa. *Contributions to Mineralogy and Petrology* **154**, 91–110.

Wei, C., Qian, J. & Zhou, X. (2014). Paleoproterozoic crustal evolution of the Hengshan–Wutai–Fuping region, North China Craton. *Geoscience Frontiers* **5**, 485–497.

Whalen, J. B., Percival, J. A., McNicoll, V. J. & Longstaffe, F. J. (2004). Geochemical and isotopic (Nd–O) evidence bearing on the origin of late- to post-orogenic high-K granitoid rocks in the Western Superior Province: implications for late Archean tectonomagmatic processes. *Precambrian Research* **132**, 303–326.

Wiedenbeck, M., Allé, P., Corfu, F., Griffin, W. L., Meier, M., Oberli, F., Quadt, A. V., Roddick, J. C. & Spiegel, W. (1995). Three natural zircon standards for U–Th–Pb, Lu–Hf, trace element and REE analyses. *Geostandards Newsletter* **19**, 1–23.

Wu, F., Yang, J., Liu, X., Li, T., Xie, L. & Yang, Y. (2005a). Hf isotopes of the 3·8 Ga zircons in eastern Hebei Province, China: Implications for early crustal evolution of the North China Craton. *Chinese Science Bulletin* **50**, 2473–2480.

Wu, F., Li, X., Zheng, Y. & Gao, S. (2007). Lu–Hf isotopic systematics and their application in petrology. *Acta Petrologica Sinica* **23**, 185–220.

Wu, F. Y., Zhao, G. C., Wilde, S. A. & Sun, D. Y. (2005b). Nd isotopic constraints on crustal formation in the North China Craton. *Journal of Asian Earth Sciences* **24**, 523–545.

Wu, F.-Y., Yang, Y.-H., Xie, L.-W., Yang, J.-H. & Xu, P. (2006). Hf isotopic compositions of the standard zircons and baddeleyites used in U–Pb geochronology. *Chemical Geology* **234**, 105–126.

Wu, M., Zhao, G., Sun, M., Li, S., Bao, Z., Tam, P. Y., Eizenhöefer, P. R. & He, Y. (2014). Zircon U–Pb geochronology and Hf isotopes of major lithologies from the Jiaodong Terrane: Implications for the crustal evolution of the Eastern Block of the North China Craton. *Lithos* **190–191**, 71–84.

Xiao, L. & Clemens, J. D. (2007). Origin of potassic (C-type) adakite magmas: Experimental and field constraints. *Lithos* **95**, 399–414.

Xie, S., Xie, H., Wang, S., Kröner, A., Liu, S., Zhou, H., Ma, M., Dong, C., Liu, D. & Wan, Y. (2014). *Ca.* 2·9 Ga granitoid magmatism in eastern Shandong, North China Craton: Zircon dating, Hf-in-zircon isotopic analysis and whole-rock geochemistry. *Precambrian Research* ***255****(Part 2)*, 538–562.

Yang, J., Gao, S., Chen, C., Tang, Y. Y., Yuan, H. L., Gong, H. J., Xie, S. W. & Wang, J. Q. (2009). Episodic crustal growth of North China as revealed by U–Pb age and Hf isotopes of detrital zircons from modern rivers. *Geochimica et Cosmochimica Acta* **73**, 2660–2673.

Yang, J. H., Wu, F. Y., Wilde, S., Xie, L. W., Yang, Y. H. & Liu, X. M. (2007). Tracing magma mixing in granite genesis: *in situ* U–Pb dating and Hf-isotope analysis of zircons. *Contributions to Mineralogy and Petrology* **153**, 177–190.

Yang, J. H., Wu, F. Y., Wilde, S. A. & Zhao, G. C. (2008). Petrogenesis and geodynamics of Late Archean magmatism in eastern Hebei, eastern North China Craton: Geochronological, geochemical and Nd–Hf isotopic evidence. *Precambrian Research* **167**, 125–149.

Zeh, A., Gerdes, A. & Barton, J. M. (2009). Archean accretion and crustal evolution of the Kalahari Craton—the zircon age and Hf isotope record of granitic rocks from Barberton/Swaziland to the Francistown arc. *Journal of Petrology* **50**, 933–966.

Zhai, M., Li, T. S., Peng, P., Hu, B., Liu, F. & Zhang, Y. (2010). Precambrian key tectonic events and evolution of the North China craton. In: Kusky, T. M., Zhai, M.-G. & Xiao, W. (eds) *The Evolving Continents: Understanding Processes of Continental Growth.Geological Society, London, Special Publications* **338**, 235–262.

Zhai, M. G. & Santosh, M. (2011). The early Precambrian odyssey of the North China Craton: A synoptic overview. *Gondwana Research* **20**, 6–25.

Zhang, C.-L., Li, H.-K., Santosh, M., Li, Z.-X., Zou, H.-B., Wang, H. & Ye, H. (2012). Precambrian evolution and cratonization of the Tarim Block, NW China: Petrology, geochemistry, Nd-isotopes and U–Pb zircon geochronology from Archaean gabbro–TTG–potassic granite suite and Paleoproterozoic metamorphic belt. *Journal of Asian Earth Sciences* **47**, 5–20.

Zhang, Y., Wei, C., Tian, W. & Zhou, X. (2013). Reinterpretation of metamorphic age of the Hengshan Complex, North China Craton. *Chinese Science Bulletin* **58**, 4300–4307.

Zhao, G. & Cawood, P. A. (2012). Precambrian geology of China. *Precambrian Research* **222–223**, 13–54.

Zhao, G., Wilde, S. A., Cawood, P. A. & Lu, L. (1999). Thermal evolution of two textural types of mafic granulites in the North China Craton; evidence for both mantle plume and collisional tectonics. *Geological Magazine* **136**, 223–240.

Zhao, G., Wilde, S. A., Guo, J., Cawood, P. A., Sun, M. & Li, X. (2010). Single zircon grains record two Paleoproterozoic collisional events in the North China Craton. *Precambrian Research* **177**, 266–276.

Zhao, G. C., Wilde, S. A., Cawood, P. A. & Lu, L. Z. (1998). Thermal evolution of Archean basement rocks from the eastern part of the North China Craton and its bearing on tectonic setting. *International Geology Review* **40**, 706–721.

Zhao, G. C., Wilde, S. A., Cawood, P. A. & Sun, M. (2001). Archean blocks and their boundaries in the North China Craton: lithological, geochemical, structural and *P*–*T* path constraints and tectonic evolution. *Precambrian Research* **107**, 45–73.

Zhao, G. C., Sun, M., Wilde, S. A. & Li, S. Z. (2005). Late Archean to Paleoproterozoic evolution of the North China Craton: key issues revisited. *Precambrian Research* **136**, 177–202.

Zhou, Y.-Y., Zhao, T.-P., Wang, C. Y. & Hu, G.-H. (2011). Geochronology and geochemistry of 2·5 to 2·4 Ga granitic plutons from the southern margin of the North China Craton: Implications for a tectonic transition from arc to post-collisional setting. *Gondwana Research* **20**, 171–183.